Printed Organic Light Emitting Diodes for Biomedical Applications

Claire Lochner

Electrical Engineering and Computer Sciences
University of California at Berkeley

May 1, 2020

Printed Organic Light Emitting Diodes for Biomedical Applications

by

Claire Meyer Lochner

A dissertation submitted in partial satisfaction of the
requirements for the degree of
Doctor of Philosophy

in

Engineering - Electrical Engineering and Computer Sciences

in the

Graduate Division

of the

University of California, Berkeley

Committee in charge:

Professor Ana Claudia Arias, Chair
Professor Jan Rabaey
Professor Liwei Lin

Summer 2018

The dissertation of Claire Meyer Lochner, titled Printed Organic Light Emitting Diodes for Biomedical Applications, is approved:

Chair _____   Date _____

_____   Date _____

_____   Date _____

University of California, Berkeley

Printed Organic Light Emitting Diodes for Biomedical Applications

Abstract

Printed Organic Light Emitting Diodes for Biomedical Applications

by

Claire Meyer Lochner

Doctor of Philosophy in Engineering - Electrical Engineering and Computer Sciences

University of California, Berkeley

Professor Ana Claudia Arias, Chair

Organic light-emitting diodes (OLEDs) are made from a growing library of man-made semiconductor materials. Unlike inorganic LEDs, OLED materials can be custom-designed and synthesized for desired emission characteristics. The bulk of OLED development to date has been for display and lighting applications, leveraging their tunable color characteristics and high efficiencies. Within display and lighting development, there has been a push to fabricate OLEDs over large areas of flexible substrates compatible with low-cost, high-throughput roll-to-roll printing technology. It is this flexibility and scalable processing that has more recently garnered attention for using OLEDs in wearable optoelectronic biomedical devices. This work focuses on the development of solution-processed, printed OLEDs specifically for biomedical applications.

As a proof of concept that solution processed polymer OLEDs can perform in a wearable biomedical device, green and red OLEDs spin-coated on glass substrates were implmented in an all-organic otoelectronic pulse oximeter to measure heart rate and arterial oxygen saturation. These OLEDs were able to generate a clear photoplethysmogram (PPG), the signal from which heart rate and oxygenation are derived, in conjunction with both inorganic and organic photodiodes. The fully organic opto-electronic sensor was able to accurately measure heart rate and oxygenation within 2% error of a commercially available hospital-grade pulse oximeter.

The next step from a proof of concept device was to develop OLED structures and processing more in line with fabricating flexible and scalable devices. Structurally, most OLEDs employ indium-tin oxide (ITO) as a transparent anode. However, ITO is brittle, and therefore not an ideal material for a flexible device meant to be worn flush with the human body. In this work an ITO-free near-infrared (NIR) OLED was fabricated on a flexible polyethylene napthalate (PEN) substrate. In place of ITO, the anode was thermally evaporated $WO_3/Ag/WO_3$. To improve scalability and increase through-put (compared to spin-coating), all polymer layers were printed via blade coating. These OLEDs exhibited a 735 nm emission peak and 2.17% external quantum efficiency (EQE) at 100 $mAcm^{-2}$.

To maximize OLED scalability and reduce manufacturing costs for inexpensive optical biomedical devices, the entire device structure should be printed and high vacuum evaporation processes should be eliminated. Here, efforts were made to replicate the thermally evaporated $WO_3/Ag/WO_3$ anode with blade coated layers. Partially printed $WO_3/Ag/WO_3$ anode OLEDs with WO_3 layers printed from a WO_3 nanoparticle ink and thermally evaporated Ag were achieved. The OLEDs had a red, 617 nm emission peak and exhibited 1-10 $mW\,cm^{-2}$ forward flux per pixel area, values compatible with the wavelength and irradiance requirements of optical biomedical devices. Further Ag ink development out of the scope of this work is necessary in order to achieve a fully printed $WO_3/Ag/WO_3$ electrode, however a step towards fully printed OLEDs suitable for biomedical applications has been made.

In addition to scalability and flexibility, OLEDs for biomedical applications should have optimzied emission spectra. NIR light has the highest penetration depth in human tissue compared to visible light wavelengths. However, the development of solution-processable organic emitters with emission peaks beyond 800 nm has been slow. Here, a printed ITO-free 745 nm NIR OLED with a secondary emission peak at 815 nm is achieved by increasing the thickness of the emissive layer from 150 to 250 nm, affecting the optical interference within the device to alter the emission spectrum.

To show the importance and impact of deeper NIR emission in an optical biomedical device, PPG signals acquired from a subject's forefinger using a NIR OLED with the secondary 815 nm peak and an NIR OLED with only a 745 nm emission peak were compared. The calibrated strength (magnitude) of the PPG acquired with the NIR-shifted OLED was 32.87% higher than the PPG acquired with the 745 nm OLED. What's more, the better PPG was acquired with less light: the 745 nm OLEDs had a maximum 1 $mW\,cm^{-2}$ irradiance on the subject's forefinger, while the NIR-shifted OLED's irradiance was only .33 $mW\,cm^{-2}$. This underscores the value of developing NIR OLEDs with deeper NIR emission for biomedical applications.

For printed and flexible OLEDs to catch on in biomedicine on a wide scale, their improved utility over currently available devices needs to be demonstrated. Flexible organic optoelectronic pulse oximeter patch prototypes developed and fabricated by Cambridge Display Technology and the Arias Group were shown to physicians from a variety of specialties. The physicians provided feedback on how the organic optoelectronic oximeters could aide their practice in ambulatory emergency care, chronic respiratory disease management, intraoperative monitoring, and pediatrics. Strategies for where and how to best interface the sensors with the human body were also developed from the physicians' input. PPG signals were acquired from flexible organic optoelectronic oximeters secured to the abdomen and back, both novel locations for pulse oximetry.

To Zora and Archie

Contents

List of Figures

List of Tables

Acknowledgments

A lot of people in different parts of my life have spurred me to where I am now, writing a doctoral dissertation at UC Berkeley. The list is long, so I'm going with chronological(ish) order.

"Thank you!"

...to my family, who have loved me and encouraged my intellectual growth since day one. Especially my brother Zac, who is the only one who understands what it means to live the life of an experimentalist. Thanks for showing me the way and for always having my back.
...to my seventh grade science teacher Ms. D'Angelo at Transit Middle School back home in Buffalo, NY. You advocated for me to be put on the advanced science track, even when my guidance counselor thought it was a bad idea because I wasn't on the advanced math track yet. If it weren't for Ms. D'Angelo's advocacy, I wouldn't have received the science education that got me here.
...to my high school math teacher Mr. Sondel at Williamsville East High School. I didn't find math fun or interesting until I was sitting in your class. The pure joy you have for mathematics was contagious, and gave me an enthusiasm for the subject that I'd never thought I'd have. Without that love of math instilled in me, I wouldn't have become an electrical engineering major.
...to the lifelong friends that I gained in high school. Maleeha Haroon, Becky Ruan, Jackie Wong, Jake Silverberg, and Mike Maley. Thank you for your continued love, laughter, and cheer leading. I am blessed to have friendships like ours that have stood the test of time and distance. No matter how far apart we are, our bond is forever.
...to Janice Li, another lifelonger from Williamsville East. I count myself lucky to have you in my city. I've always valued your wisdom and your support these last couple years has meant a lot to me. Grabbing a catch-up drink with you is a highlight on my social calendar. Now that my dissertation is done I hope that they happen often enough to not be catch-ups, I think I owe you a few.
...to Profs. Jennifer Zirnheld and Kevin Burke of SUNY Buffalo. Thank you for your unending support even after I've left UB. And for the amazing meals. You exposed me to the world of fine dining and tasting menus, and my life will never be the same.
...to my Arias Lab family - Prof. Ana Claudia Arias has given me the freedom to pursue my interests and complete my PhD in my own way. With the rest of the "Fantastic Four" we built a lab where mutual respect, collaboration, and friendship can thrive.
...to Yasser Khan, Adrien Pierre, Jonathan Ting, and Donggeon Han, my flexible organic optoelectronic pulse oximeter teammates.
...to Nir Yaacobi-Gross and our collaborators at CDT for supplying materials, funding, and research support.
...to my dissertation committee members, Prof. Jan Rabey and Prof. Liwei Lin, for your time and support of this thesis.
...to the people that have kept me fed and caffeinated during my PhD. Abe of Abe's Cafe -

your food is delicious, your cold brew is the best on Euclid, and your kindness is legendary. Janet, my daily barista for many years at Yali's, I still feel guilty that I stopped buying lattes once my office started having free coffee. I always enjoyed our brief conversations.

...to my dear friend Rachel Traylor. Your friendship has been one of the highlights of grad school. I'm looking forward to many more days spent in your garden watching your pumpkins grow and Hampton and Archie play. I know I can always count on you, thank you.

...to my office mates turned buddies: Daniel Contreras, Dan Drew, David Burnett, Filip Maksimovic, and Joey Greenspun. NWPs forever.

...to Archibald Harris Jr., Deeba, Wacunda, Kody, and Sneg. May you all live out strong, happy, and healthy lives full of adventure.

...to my sister-in-law Marija Mandic, you are one of the kindest and coolest people I've ever met.

...to Des and Harold Scott, the best "in-laws" a person could ask for. Thank you for welcoming me so warmly into your family. I love you guys and am grateful to have you in my life.

...to Archer Rufio Roland, the sweetest and softest writing buddy. And yet my harshest critic; you literally peed on the first draft of this thesis. It's ok, I still love you.

...to Simon, you've been a source of endless support. Thank you for seeing this through with me.

Chapter 1

Introduction

Organic light emitting diodes (OLEDs) are a family of LEDs made with carbon compound semiconductors [1, 2]. Unlike their inorganic counterparts, OLEDs can be fabricated using high-throughput roll-to-roll manufacturing methods at temperatures compatible with flexible plastic substrates [3, 4]. Organic semiconductors can be custom synthesized for a desired emission spectrum, and the devices made from them can be scaled up to cover large areas, or down to sub-mm pixels. Inorganic light sources which include LEDs, fluorescent lamps, and laser diodes, are currently being used for biomedical applications, including pulse oximetry, optogenetics, phototherapy, and near infrared spectroscopy. Originally developed and studied for lighting and displays, OLEDs have recently begun to be demonstrated in some of these optoelectronic medical devices too. This thesis explores how OLEDs can be used in wearable devices with an emphasis on pulse oximetry, and how OLED structures and manufacturing can be tailored to wearable biomedical applications.

1.1   Thesis organization

Chapter 2 reviews optical biomedical devices. The metrics for medical light sources are discussed and summarized for pre-existing OLED devices as well as inorganic light sources in applications where OLEDs haven't yet been employed.

Chapter 3 will leave the reader with an introductory understanding of the OLED materials, fabrication techniques, and characterization methods use throughout the rest of thhis thesis.

Chapter 4 takes a deep dive into the development of solution processed polymer blend OLEDs for an all-organic optoelectronic pulse oximeter, a device used ubiquitously in medicine to measure heart rate and arterial oxygen saturation. (All optical sensor experiments performed on human subjects in this thesis were carried out with informed consent under the approval of the University of California, Berkeley Institutional Review Board, protocol ID number 2014-03-0681.)

Chapter 5 presents and ITO-free, 100% additively processed printed polymer NIR OLED.

In these devices, ITO is replaced with a flexible $WO_3/Ag/WO_3$ anode. The optical and electrical characteristics of the NIR OLED printed on $WO_3/Ag/WO_3$ are compared to an identical NIR OLED printed on ITO.

Chapter 6 explores an OLED structure with a fully printed anode and polymer layers. The structure developed in Chapter 5 is attempted to be re-created via printing. Printing the WO_3 portions of the anode is successfully implemented with an evaporated Ag layer, and the limitations of implementing OLEDs with a printed Ag layer are described.

Chapter 7 focuses on the human-machine interface of OLEDs in a flexible pulse oximeter. Deeper NIR emission is achieved by altering the emission layer thickness in a printed NIR OLED. The benefit of this deeper NIR emission for a biomedical device is demonstrated with a photoplethysmogram (PPG) measurement performed on a human subject. Additionally, feed back from practicing physicians that consulted on flexible pulse oximeter design and applications is presented. Physician input was used to improve the interface between the sensor and the human body and to guide how and where it can best be applied.

Chapter 8 concludes this thesis. Future work will be suggested and several wearable OLED-based biomedical systems will be proposed.

Chapter 2

A Review of OLEDs in wearable biomedical devices

Organic light-emitting diodes (OLEDs) are LEDs made from organic semiconductors instead of inorganic materials such GaAs [5] or GaN [6]. Because they use organic small molecules and polymers, OLEDs can be fabricated via thermal evaporation [7], spin-coating [2], or printing [8, 9, 10] at temperatures that are compatible with plastic substrates ($<$ 200°C), unlike their inorganic counterparts which require high temperature processing. Flexible OLEDs are commonly made on the plastics polyethylene naphthalene (PEN) and polyethylene terephthalate (PET), with finished devices less than 500 μm thick. The bounds of OLED technology's flexibility are being pushed with even thinner and more flexible substrates. For example, Yokota et al. fabricated flexible OLED displays on ultra-thin (1.5 μm) parylene and polyimide substrates that can be worn on the body like a temporary tattoo, as shown in Figure 2.1(a) and (b) [11]. OLEDs have even been crafted into flexible 3D structures, as demonstrated by Kim et al., who fabricated OLEDs on 25-60 μm thick polyimide substrates that were cut and folded into the 3D shapes shown in Figure 2.1(c) and (d) [12].

Over the last thirty years, organic light emitting diodes (OLEDs) have been developed for display and lighting applications. Part of what makes OLEDs attractive for displays and novel light fixtures is that can be thin, light-weight, large-area scalable, and flexible. At the same time, there has been a push to make biomedical devices smaller, more portable, and easier to use in daily life, as evidenced by the commercial success of wrist-worn fitness monitoring wearables. Among these biomedical devices, both currently on the market and in research, are those whose operating principles rely on an artificial light source. The same characteristics that make OLEDs attractive for novel displays and light fixtures make them ideal candidates for wearables. OLEDs' thin and flexible form factor have the potential to enable the long-term and comfortable wear of optoelectronic biomedical devices beyond the wrist. This review outlines a selection of biomedical devices that employ light, and the efforts and opportunities for the implementation of OLEDs to enable or improve their physical interface with the human body.

Inorganic LEDs are currently used in biomedicine to measure heart rate and blood oxy-
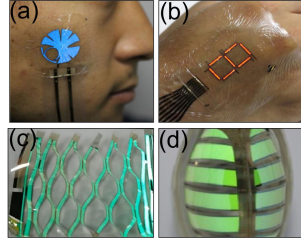
Figure 2.1: **Flexible OLEDs**. **(a)** Yokota et al. spin-cast polymer OLEDs on 1.5 μm thick parylene/polyimide substrates creating optoelectronic skins that can be adhered conformally to the human body in the shape of the University of Tokyo logo worn on the cheek and a **(b)** seven-segment display worn on a hand [11]. **(c)** Kim et al. thermally evaporated OLEDs on spin-cast polyimide substrates. Using traditional kirigami techniques the substrates of the finished OLEDs were cut and folded into a window blind-like panel and **(d)** globe lamp shape [12].

genation with pulse oximetry, to monitor hemodynamics with near-infrared spectroscopy (NIRS), to study and control brain function with optogenetics, and to treat wounds, acne, and cancer with phototherapy. The rigid inorganic optoelectronics used in commercial biomedical devices limit their fit, tissue coverage, portability, and physical location. As illustrated in Figure 2.2, the wearable pulse oximetry (Figure 2.2(a)), optogenetic (Figure 2.2(b)), phototherapy (Figure 2.2(c)), and NIRS (Figure 2.2(d)) devices that use inorganic light sources are bulky and obtrusive on the user's body. In contrast, a more conformal and comfortable fit is afforded by flexible OLEDs, which are also more scalable in terms of surface area than inorganic LEDs [13], thus enabling light-emitting biomedical devices with improved tissue coverage. The improved tissue coverage and conformal fit of flexible biomedical devices has been shown to lead to higher SNR than inflexible alternatives [14]. Herein we review biomedical applications of light in which OLEDs have already been implemented: pulse oximetry, near infrared spectroscopy (NIRS), optogenetics, and phototherapy. For each application, a summary of its general operating principles is presented, followed by discussions of specific use cases and the metrics of the light sources that have been employed.

2.1 OLED metrics for biomedical applications

The OLED performance characteristics most relevant to biomedical applications are flux, irradiance (the amount of flux incident per unit area of illuminated tissue), and emission spectrum. An OLED's emission spectrum can be characterized by its peak wavelength and full width at half-maximum (FWHM, the difference between the wavelengths at which the OLED's spectral radiant flux is one half of its peak value). OLEDs generally have larger FWHM than inorganic LEDs, which must be taken into consideration for applications such as fNIRS (functional NIRs) and optogenetics, which use multiple light sources whose
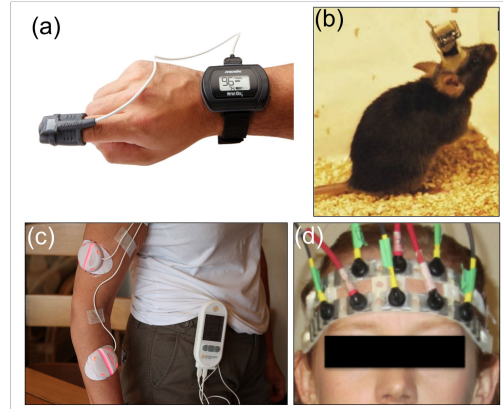
Figure 2.2: **Optoelectronic biomedical devices with inorganic light-emitting devices**. **(a)** Nonin's mobile WristOx$_2$ pulse oximetry system has a sensor probe on the finger containing two LEDs and a photodetector, connected via wire to wrist-worn electronics and display [15]. **(b)** A mobile optogenetic apparatus with an inorganic LED worn by a mouse [16]. **(c)** The Ambulight PDT photodynamic therapy device uses red LEDs to treat non-melanoma skin cancer [17]. **(d)** An array of optical fibers connected to a laser diode light source and photodetector comprises an apparatus for cranial near-infrared spectroscopy (NIRS) [18].

spectral overlap should be minimized. The requirements for an OLED's flux, irradiance, peak emission wavelength, and FWHM is dictated by its application. Table 2.6 summarizes these metrics of the light sources reviewed herein, as well as the bodily location and time scale of the treatment, the size of the light source, and, where applicable, the sampling rate and/or treatment dosage (irradiance multiplied by exposure time).

2.2   Pulse oximetry

Pulse oximeters are used ubiquitously in the medical profession to monitor a patient's general cardiovascular and respiratory health. Pulse oximetry is an optical measurement of heart rate and oxygenation, based on the known absorptivities of oxygenated and deoxygenated hemoglobin in the blood as a function of incident light wavelength [19, 20, 21]. In a standard pulse oximeter, two different colored LEDs with peak wavelengths coinciding with a difference in oxygenated and deoxygenated hemoglobin absorptivity alternately emit light into the user's forefinger. Some light is absorbed within the finger, where hemoglobin accounts for the majority of absorption. The remaining unabsorbed light is measured by a photodetector on the opposite side of the finger, as shown in Figure 2.3(a)). As the heart beats, the blood volume flowing through the user's arteries decreases during diastole and increases during systole. The amount of light absorbed by the blood and thus transmitted to the photodetector therefore fluctuates with the heart's systolic and diastolic phases, as

illustrated in Figure 2.3(b). The photodetector signal increases during diastole and decreases during systole, as shown for red and green LEDs in Figure 2.3(c). This signal is called the photoplethysmogram, or PPG. A persons heart rate is extracted from the distance between the diastolic peaks in the PPG and their oxygen saturation (SpO_2) is calculated using a modified version of Beer Lambert's Law from the ratio between the PPG signals generated by each LED[19, 22]. Clinical pulse oximeters use red and near infrared (NIR) LEDs and generally operate in transmission mode on a person's finger, earlobe, or, in the case of infants, the foot. Pulse oximeters can also operate in reflection mode, where the LEDs and photodetector are adjacent to each other. In this configuration, the photodetector senses the light that is reflected back from the blood to the tissue's surface [23, 24, 25]. Reflection mode pulse oximetry is an attractive alternative to transmission mode because it is not limited to the few locations on the body that are thin enough for optical transmission [26, 27].

Pulse oximetry with OLEDs

The first all-organic optoelectronic pulse oximeter was demonstrated by Lochner et al. with a transmission-mode probe composed of red and green OLEDs spin-cast on ITO glass and a organic photodetector (OPD) printed on PEN (shown in Figure 2.3(d)) [22]. In this oximeter, the red OLED had a 626 nm peak wavelength and the green OLED had a 532 nm peak wavelength. An green OLED was used instead of NIR because visible spectrum solution-processable organic emitters were further along in development (for lighting and display applications) at the time of the work's completion. A 532 nm OLED was a viable NIR alternative because the difference in oxygenated and deoxygenated hemoglobin absorptivity is comparable at 532 nm and NIR wavelengths. The red and green OLEDs measured 2 mm x 2 mm and were both operated at approximately 350 $mAcm^{-2}$, 9 V, and 1 kHz. The red and green OLED's irradiance was 5.83 and 20.1 $mWcm^{-2}$, respectively. The magnitude of the PPG signal acquired by the photodetector was 3 mV for the green OLED and 2.5 mV for the green OLED. The combination of solution processed red and green OLEDs with a printed OPD successfully demonstrated the transmission mode measurement of human heart rate and SpO_2 oxygen saturation from a user's finger, with less than 2% error compared to the heart rate and SpO_2 values acquired simultaneously by a commercial red and NIR LED finger probe pulse oximeter. This work will be discussed in more detail in Chapter 4 of this thesis.

Yokota et al. and Han et al. further the developed OLEDs for pulse oximetry, employing flexible OLEDs fabricated on plastic substrates in reflection mode pulse oximeters [8, 11]. Yokota et al. used green (517 nm) and red (609 nm) OLEDs spin-coated on an ultra-flexible parylene and polyimide substrate to perform reflectance oximetry on a person's fingertip (Figure 2.3(e)). The OLEDs were operated with at 6 V, .2 Hz. The magnitude of the PPG acquired by a single OPD pixel located in between the OLEDs ranged from 100 - 200 μV. This oximeter was demonstrated to detect both optimal and sub-optimal SpO_2 levels at 99 and 90%, in agreement with a commercial transmission mode finger probe oximeter. Han et al. printed red, green, and NIR OLEDs (peak wavelengths at 520, 611, and 725
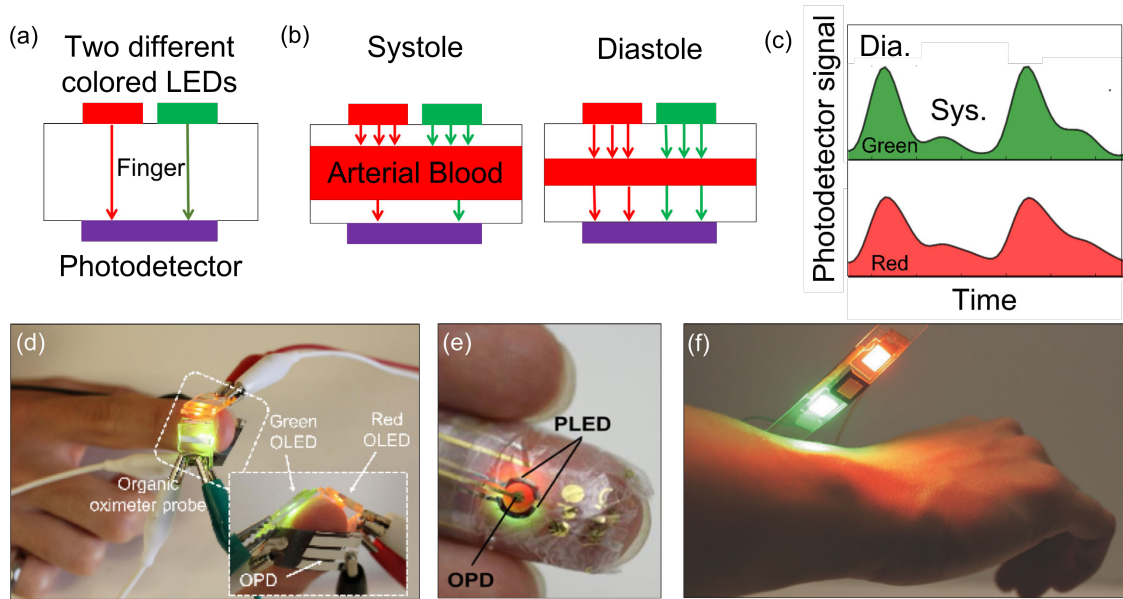
Figure 2.3: **Pulse oximetry**. **(a)** A transmission mode pulse oximeter sensor is composed of two different colored LEDs placed on one side of the finger and a photodetector on the other. Only one color LED is on at a time, both flashing on and off at a rate of approximately 1 kHz. **(b)** The largest absorber of light in the finger is blood, the amount of which fluctuates during the systole and diastole phases of the heart, meaning more or less light reaches the photodetector depending on the phase of the heartbeat. **(c)** The fluctuation of the photodetector signal thus increases and decreases with the heartbeat, known as the photoplethysmogram (PPG). The heart rate is measured from the time interval between the diastolic peaks in the PPG. The arterial oxygenation value is derived from the ratio of the PPG generated by each wavelength. **(d)** A transmission mode pulse oximeter assembled from spin-coated red and green OLEDs and a printed organic photodetector (OPD) worn the finger [22]. **(e)** A flexible reflection mode pulse oximeter made with spin-coated red and green polymer OLEDs (PLED) and an OPD worn on the pad of the finger [11]. **(f)** A flexible reflection mode pulse oximeter worn on the outer wrist assembled from printed red and green OLEDs and an inorganic photodetector [8].

nm) on a patterned ITO PEN substrate for reflection mode PPG measurements. Each pixel was 7 mm x 7 mm. The green, red, and NIR OLED's irradiance was 1.39, 1.82, and .4 $mWcm^{-2}$, respectively, when operated at 10 $mAcm^{-2}$.The OLEDs were integrated with an inflexible inorganic silicon photodetector and worn on the backside of the user's wrist, as shown with red and green OLEDs in Figure 2.3(f)). The PPG signal was measured from reflected light incident on the photodetector positioned between the OLEDs. Clear 1.2, 1.1, and 1.0 mV PPG signals were acquired using the NIR, green, and red OLEDs. A 98.77% oxygen saturation was measured using the red and green devices and verified by a commercial transmission mode pulse oximeter.

Continuous heart rate and oxygenation monitoring may be beneficial to chronically ill patients [28, 29], but accurate ambulatory pulse oximetry is challenging because the accuracy of commercially available pulse oximeters is limited by motion artifacts and ambient light interference if the sensor isn't fitted properly on the user [30]. Additionally, there an unmet need to easily and reliably detect regional perfusion and oxygenation at the organ level in critically ill patients [31]. With their closer fit to the human body, flexible OLEDs have the potential to enable more accurate ambulatory and regional pulse oximetry, pending studies of long-term organic optoelectronic pulse oximeter use under varying levels of user locomotion and on various bodily locations.

Pulse oximetry for endodontic diagnostics

In addition to monitoring the state of a person's general circulatory system, a pulse oximeter has been used to asses the health of dental pulp, the central part of a tooth comprised of blood vessels and living tissue [32, 33, 34]. Traditional dental pulp health assessments employ electrical or thermal tests to gauge a patient's level of sensation experienced upon a suspect tooth's exposure to stimulation. These tests are uncomfortable for the patient and subject to his or her tolerance for pain and discomfort. In contrast, Schnettler et al. demonstrated pulp health diagnosis using pulse oximetry [32]. A transmission mode pulse oximeter placed over a tooth was used to measure its SpO_2. The oral SpO_2 value was compared to the SpO_2 measured by a finger probe oximeter that was also worn by the patient to determine that it was giving an accurate value. This gave an objective and painless indication of the state of the tooth's vasculature and whether or not intervention (ie. a root canal) was required. Gopikrishna et al. validated using pulse oximetry in lieu of thermal or electrical stimulation on recently traumatized teeth, which may experience temporary paresthesia that render them unresponsive to electrical or thermal stimulation for at least a month after injury [33]. The pulse oximeter was able to diagnose pulp vitality on the first day of reported tooth trauma, enabling treatment at least 28 days sooner than would have been possible with the physical methods. A limitation to using pulse oximetry for endodontic diagnosis lies in the form factor of available transmission mode pulse oximeter probes. So far pulse oximetry has only been used to study pulp vitality in the anterior teeth. A new oximetry probe form factor is needed to perform dental pulp oximetry on molar and wisdom teeth.

This is an example of an opportunity for flexible OLEDs to meet a biomedical device need that is currently unmet.

2.3 Near-infrared spectroscopy (NIRS)

Near-infrared spectroscopy (NIRS) is a screening technique used to monitor the presence (or lack thereof) of blood and its flow in living tissue, also known as hemodynamics [35, 36]. To monitor hemodynamics, a NIRS device irradiates a person's tissue over the area of interest. The absorption spectra of various chromophores in human tissue are shown in Figure 2.4(a). While collagen, melanin, and fat have larger absorption coefficients than oxygenated and deoxygenated hemoglobin in the NIR optical window, hemoglobin still accounts the majority light absorption because it is present in higher concentrations [37]. Similarly to reflection mode pulse oximetry, some of the light is absorbed within the body and the reflected light is measured by a photodetector, as shown in Figure 2.4(b). Because blood accounts for the majority of light absorption in human tissue at NIR wavelengths, the more blood present in the underlying organ or tissue, the higher the absorption of light and the the lower the photodetector signal. The useful wavelengths for NIRS lie between 700 nm and 1300 nm, known as the optical window in human tissue. The penetration depth of wavelengths shorter than 700 nm is limited by higher levels of scattering in organic tissues, while wavelengths longer than 1300 nm are primarily absorbed by water molecules [38]. The specific application of NIRS to brain activity monitoring and intracranial hematoma detection present opportunities for OLED application, and will be discussed herein, as well as preliminary OLED NIRS work.

Brain activity monitoring with functional near infrared spectroscopy (fNIRS)

Functional NIRS (fNIRS, also known as functional near infrared imgaing, or fNIRI) is a non-invasive technique that uses optical signals to monitor brain function. fNIRS devices use NIR light to sense changes in oxygenated and deoxygenated hemoglobin concentrations in the brain. The sensing portion of an fNIRS device is made up of an array of light sources and detectors placed on the skull, as shown in Figure 2.4c [37, 40, 41]. Mental activity changes the concentration of oxygenated and deoxygenated hemoglobin in different areas of the brain [18], triggering a change in the amount of light absorbed in the brain tissue and thus detector signals in the fNIRS system. The typical fNIRS device uses an array of optical fiber leads to make contact with the subject's skull [18]. Light is generated by an externally housed laser diode and transmitted through the optical fibers to the skull. Similarly, light reflected from the brain to the skull is transferred through the optical fibers to an external photodetector.

One specific application of fNIRS is the noninvasive detection of impaired cerebrovascular function in neonatal infants [42]. Infants born with congenital heart disease and/or under-
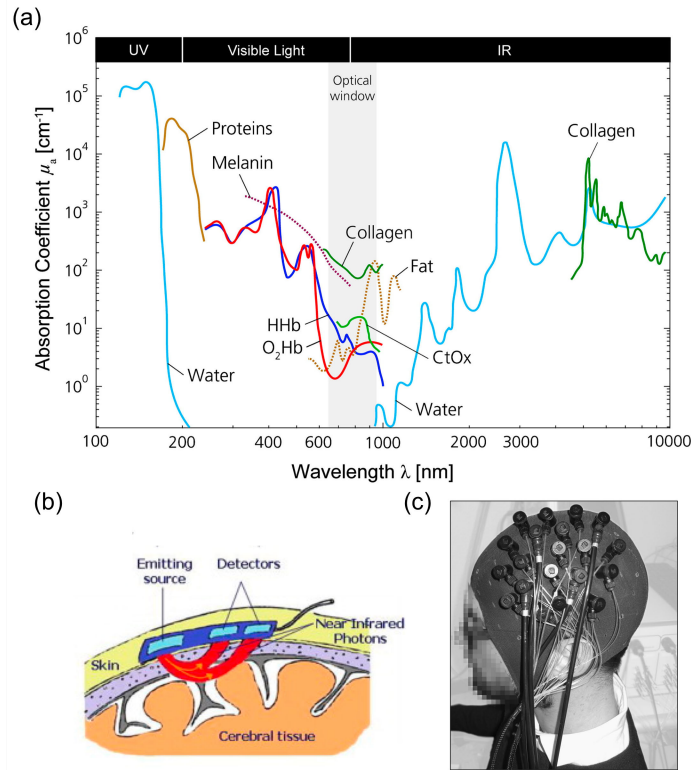
Figure 2.4: **Near infrared spectrscopy (NIRS)**. **(a)** The absorption coefficient of chromophores in biological tissue (water, protein, melanin, collagen, fat, cytochrome oxidase, and oxygenated and deoxygenated hemoglobin) as a function of wavelength. The NIR optical window between 650-950 nm (shaded in grey) is where light has the deepest penetration depth in biological tissue and hemoglobin accounts for the majority of light absorption because hemoglobin is present in higher concentrations than the other chromophores with larger absorption coefficients [37]. **(b)** Schematic of the path of photons for an NIRS device worn on the skull [39]. **(c)** An experimental cranial fNIRS probe with optical fibers carrying optical signals. [37].

going cardiovascular surgery may not have adequate blood supply to the brain, which can result in neurological injuries [43]. fNIRS devices applied to the forehead over the prefontal cortex are used to monitor brain activity in these at-risk infants. The application of fNIRS on the prefrontal cortex is additionally being studied for indications of future developmental and psychological disorders such as ADHD, and as a research tool to study psychopathology in children [44, 45]. fNIRS devices are also used in older populations to study Alzheimer's disease, depression, epilepsy, Parkinson's disease, stroke recovery, psychiatric disorders, and brain computer interfaces [40].

The current trend in fNIRS device design is to make systems portable and more comfortable to wear while increasing the number of light sources and detectors they contain [37, 40]. For example, Kim et al. demonstrated a portable 12-channel fNIRS headband with inorganic LEDs and photodiodes integrated into a flexible printed circuit board (flexPCB) worn across the user's forehead [46]. Muehlemann et al. similarly demonstrated a flexPCB NIRS device with four inorganic LED/photodetector pairs [47]. However, a greater number of channels are needed for high resolution fNIRS imaging of brain activity [48]. Furthermore, in order to have a 3D mapping of brain activity, there must be a variety of spacing distances between emitters and detectors in order to measure hemodynamics at multiple depths [49]. OLEDs have the scalability and flexibility to potentially enable portable fNIRS devices containing many channels with a variety of emitter-detector spacings that can be worn flush with the user's head, eliminating the need for arrays of protruding optical fibers.

Intracranial hematoma detection

Another clinical application of NIRS is intracranial hematoma detection [50]. Delayed intracranial hematomas can cause secondary brain injury in patients who have suffered head trauma. If diagnosed early, they are treatable and secondary brain injury can be prevented or minimized. In a high-resource hospital setting, CT scans and MRIs are primarily used to detect hematomas. However, CT scanners and MRI machines are not ubiquitously available. Portable hand-held NIRS devices can be used to detect hematomas in the field or in a low-resource setting [51, 52]. The hand-held NIRS device consists of an NIR light source and a detector in a single enclosure that it is manually moved across a person's skull. If there is no hematoma, the detected signal should be similar at symmetric locations on the skull. If there is a hematoma, more light from the NIRS device will be absorbed by the excess of blood, so less light will be reflected back out of the skull and the photodetector signal above it will decrease [52]. Riley et al.'s portable NIRS device was equipped with inorganic LEDs operating at 100 Hz that emitted 10 mW of flux at 750, 800, or 850 nm [52]. It was manually moved over an optical phantom at a rate of 500 mms^{-2} in order to detect spatial changes in reflected light intensity due to hematoma models within the phantom.

Similarly to fNIRS, the potential implementation of a wearable 2D array of OLEDs for intracranial hematoma could enable continuous monitoring for delayed hematomas while removing the opportunity for human error present in a hand-held manually scanning device.

NIRS with OLEDs

A NIRS device using an OLED as its light source has been demonstrated by Bansal et al. to measure changes in blood flow and oxygenation in a person's forearm [53], as shown in Figure 2.5(a). The OLED had a broad emission spectrum with a peak in the red at 615 nm and a tail in the NIR (Figure 2.5(b)). It was placed in between two OPDs, each covered with a different filter to allow the OPD to detect light with a peak wavelength of either 610 or 700 nm (Figure 2.5(b)). The OLED and OPD pixels were placed onto a subjects forearm with 20 mm spacing between them in order to probe the oxygen saturation of the underlying muscle tissue (the larger the spacing between light emitter and detector, the deeper the penetration depth of the measurement). Figure 2.5(c)) shows the recorded change in the OPD signal upon exciton by 610 nm and 700 nm as ischemia was induced in the arm by a blood pressure cuff. The 700 nm signal had a larger slope because the difference between oxy- and deoxygenated hemoglobin absorptivity is greater at 700 nm than at 610 nm, indicating that NIR wavelengths are better than red for hemodynamics monitoring.

As mentioned in the pulse oximetry discussion, the development of NIR OLEDs has lagged behind that of visible light OLEDs. However, as the interest in wearables has grown, so too has the development of high-efficiency NIR OLED materials [54]. More recently Yamanaka et al. demonstrated a NIRS measurement on a subject's forearm using an organic small molecule OLED with a 780 nm emission peak [55]. The OLED, 4 mm^2 in size, was fabricated on an ITO glass substrate. It was placed 3 cm away from a photodiode on the subject's forearm and driven at 100 $mAcm^{-2}$ for 3.5 $mWcm^{-2}$ irradiance. Pressure was repeatedly applied and released on the subject's arm in order to impede and enable blood flow, and the photodiode signal fluctuated correspondingly.

While NIR OLEDs, have become more efficient, their peak wavelengths are still in the shorter end of the full NIR spectrum. The optical window in tissue goes up to 1300 nm; in order to take full advantage of it, NIR OLEDs need further development to efficiently emit light at longer wavelengths. It is also worth noting that the longer the wavelength, the less the light is scattered within human tissue, and the higher its penetration depth [56].

2.4 Optogenetics

Optogenetics is a technique to activate or deactivate living cells using the light-induced excitation or inhibition of light-sensitive proteins to control ion flow across neural cell membranes [57, 58]. Two light-sensitive proteins used in optogenetics are channelrhodopsin-2 (ChR2), which absorbs blue light, and halorhodopsin (NpHR), which absorbs yellow light. As shown in Figure 2.6(a), when blue light s absorbed by ChR2, it depolarizes the ion channel across a neuron's membrane, causing a transient voltage spike. Conversely, when yellow light is absorbed by NpHR, the neuronal membrane's ion channel is hyperpolarized, inhibiting electrical signal, which is detected as a lack of a voltage spike. The ChR2 and NpHR proteins, characterized as opsins, must be introduced into mammals through artificial
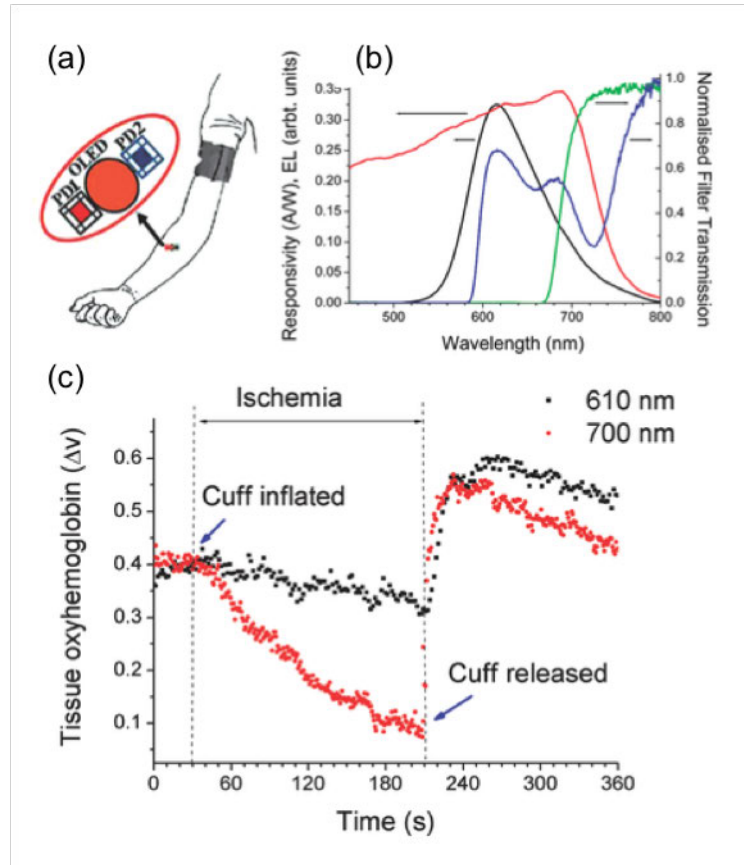
Figure 2.5: **NIRS with an OLED** [53]. **(a)** Bansal et al.'s NIRS device was an OLED flanked by two OPDs placed on a user's forearm. **(b)** The OLED had a broad emission spectrum (black line) and the OPD had a broad absorption spectrum (red line). A filter was placed over each OPD, one for 610 nm peak absorption (blue line), and the other for 700 nm peak absorption (green line). **(c)** The OPD responses to 610 nm and 700 nm light were altered during the inflation and relaxation of a blood pressure cuff on the arm, showing a change in tissue oxygenation.

means, so most optogenetic experiments involving opsins are performed on cell cultures, microorganisms, and mice [59]. The goal of optogenetic research is to better understand neural function and one day be able to use optical stimulation for human brain machine interfaces.

Optogenetics with OLEDs

Optogenetics experiments were first conducted on mice using a single LED or optical fibre for opsin activation, which limited resolution and test subject mobility. Because of their light weight, flexiblity, and ability to be fabricated in high-resolution 2D arrays, OLEDs have been investigated as an alternate light source for optogenetic experiments. Morton et al. performed optogenetics experiments on Drosophila larvae with ChR2 using blue (464 nm), green (515 nm), and orange (606 nm)OLEDs [60]. The OLEDs were thermally evaporated on ITO glass substrates and powered by a 5 V, .2 Hz square wave. The blue, green, and orange OLED irradiance values were 2.5, 3, and 4 $mWcm^{-2}$, respectively. Upon optical stimulation, activated ChR2 causes the larvae to contract. The larvae responded strongest to the blue OLEDs, followed by the green, with no response to the orange OLEDs, as expected from ChR2's photoresponse spectrum, whose peak is at 450 nm with half-maximum at 515 nm.

Steude et al. demonstrated a 230,000 pixel blue OLED array thermally evaporated on a CMOS backplane (for individual pixel addressability) that selectively trigged individual photoresponsive cells in culture [61, 62]. Each OLED pixel measured 6 μm x 9 μm and emitted .11 $mWcm^{-2}$ at 60 Hz. The OLED's with had 477 nm peak wavelength and 44 nm FWHM, overlapping the absorption spectrum of the ChR2 ion channels in the genetically modified cells (HEK-293) under test. The OLED array was able to address individual cells, inducing localized currents that were controlled by illuminating various patterns in the array.

Smith et al. have proposed a fully flexible blue (455 nm peak emission) OLED array integrated with an active matrix thin-film transistor array [64]. OLED test structures with 4 mm^{-2} pixels were thermally evaporated on an ITO PEN substrate. Each pixel was driven by a 13 V, 20 Hz pulse with 10 ms pulse for 100 $mWcm^{-2}$ irradiance. As shown in Figure 2.6b, Smith et al. propose that these OLEDs could be integrated into fully flexible and addressable OLED array and implanted against the cortical surface of the brain for long-term targeted optogenetic neural control. For a less invasive device, Smith et al. also proposed an OLED array worn externally on the outer the ear to stimulate neurons associated with the vegas nerve (shown in Figure 2.6(c))[65], the stimulation of which has been investigated as a treatment for epileptic seizures [66] and mental health disorders that do not respond to pharmacological therapies [67].

2.5 Photo- and photodynamic therapy

Photo- and photodynamic therapies harness the effects of light interacting with tissue on a cellular chemistry level to treat various ailments [68]. Phototherapy (PT) uses light alone, and photodynamic therapy (PDT) employs a substance that sensitizes target cells in
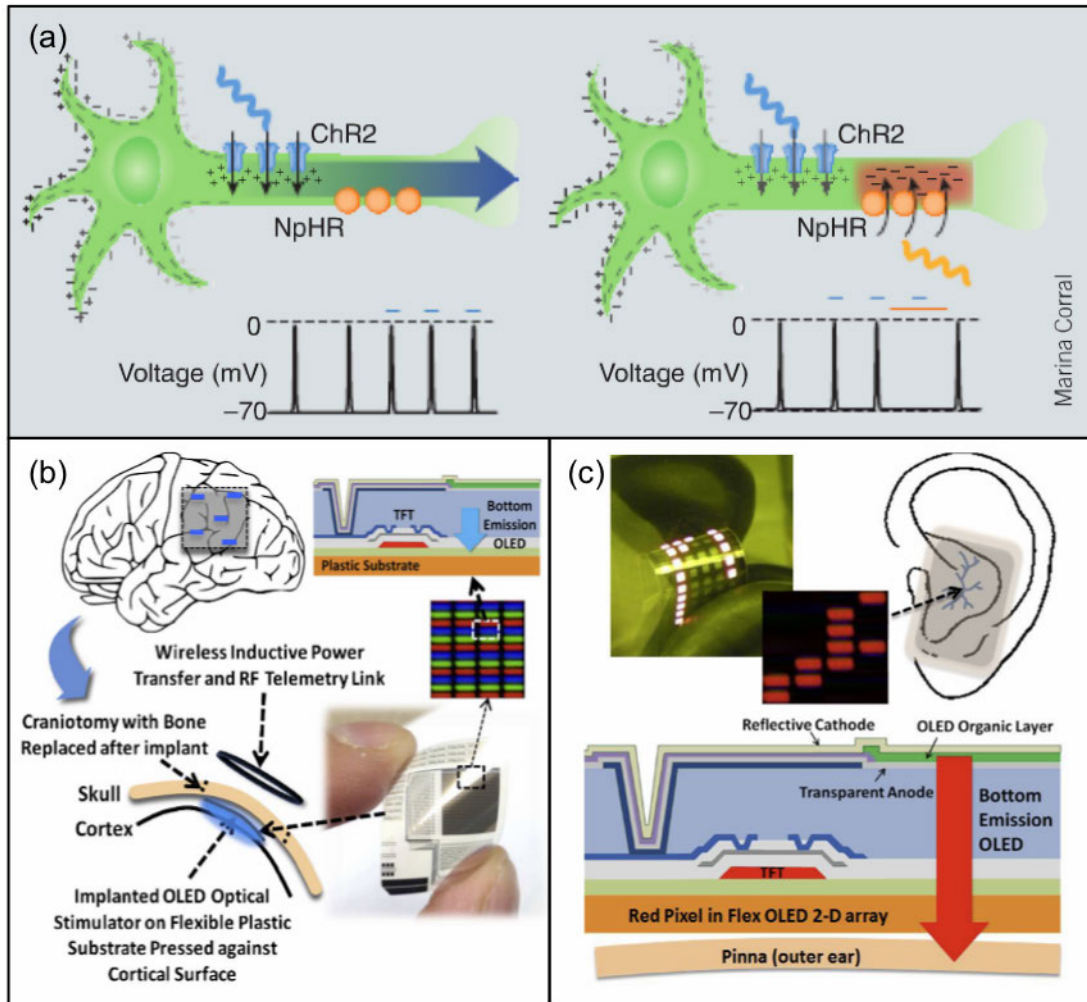
Figure 2.6: **Optogenetics**. **(a)** Nuerons containing light-sensitive proteins are activated or inhibited when exposed to a particular wavelength of light. Blue light triggers the protein channelrhodopsin-2 (ChR2) to depolarize the neuronal membrane, causing electrical flow. Yellow light triggers halorhodopsin (NpHR) to hyperpolarize the neuronal membrane, inhibiting the cell's electrical signal. The electrical signals generated by an activated neuron are sensed as a voltage spike, while the deactivated neuron is sensed by a lack of voltage spikes. The blue and yellow lines above the voltage plots indicate when the neuron is exposed to blue and/or yellow light [63]. **(b)** A proposed flexible array composed of thin-film transistor (TFT)-controlled multi-color OLEDs to selectively stimulate and/or inhibit select groups of neurons in the brain [64]. **(c)** A flexible TFT-controlled OLED array proposed to be applied to the outer ear, targeting the vegas nerve's auricular branches for mental health treatment [65].

tissue to react with incident photons of a particular wavelength. PT and PDT have been used to treat a variety of medical conditions including depression [69], sleep disorders [70], jaundice [71], acne [72, 73, 74, 75, 76], some cancers [77], and to support wound healing [78, 79]. Phototherapeutic light sources have been developed over time to be more user friendly and to have controllable settings. The first PT light source was the sun, followed by low level lasers, to the fluorescent lamps and inorganic LEDs used today [80]. Flexible OLEDs have the potential to be the next step in phototherapy's evolution.

Wound healing with inorganic light sources

Phototherapy with red and NIR light is used for wound healing, encouraging new tissue growth while easing pain [78, 79]. Red and NIR light absorbed by mammalian cells stimulate mitochondrial respiration, which in turn increases the cell's metabolism [81]. With higher functioning cells, the irradiated tissue heals faster than it would on its own [78, 79].

For example, phototherapy is used to treat oral mucositis in cancer patients, a condition where the mucus lining in the mouth atrophies because of chemotherapy and causes painful ulcers [82]. Oral mucositis can prevent patients from eating and has at times been treated with addictive narcotic pain killers. Corti et al. demonstrated phototherapy with a red inorganic LED to treat oral mucositis [83]. The LED was integrated into a hand-held plastic wand. It had a peak wavelength at 645 nm, a 30 nm FWHM, and 7.8 mW flux. It was applied to the mouth to deliver a .99 Jcm^{-2} dose in three five-minute phototherapy sessions per day over the course of one week. The healing rate of the damaged tissue was accelerated between 117% and 164 % compared to the control group [83].

Similarly, Hodgson et al. used a red inorganic LED (670 nm, 20 nm FWHM) to treat oral mucositis, but applied the light extra-orally [84]. A Warp 75 red LED array from Quantum Devices (Barneveld, WI) was used to apply phototherapy to each of the subject's cheeks and anterior throat tissue. The LED array had a 50 $mWcm^{-2}$ irradiance and was held within 2 cm of each area for 80 s, providing a 4 Jcm^{-2} dose per area once per day for 14 days. For comparison, subjects in the control group underwent a placebo phototherapy that used the same Warp 75 LED device but with less than 5 $mWcm^{-2}$ irradiance. Hodgson et al. found that there was a statistically significant improvement in patient pain according to the World Health Organization pain assessment scale, but failed to show statistically significant improvement using other pain assessment scales (NCI-CTCAE and OMAS). It was hypothesized that the phototherapy was less effective because the actual dosage received by the damaged mucosal membranes (the applied dosage less light absorbed by non-target tissue) was too low. The Warp 75 LED device itself is a large hand-held block containing an array of LEDs, and cannot be applied flush to mucosal membrane. The LED wand used by Corti et al. was more effective and could be applied directly to the mucous membrane in the mouth, underscoring the importance of conformal contact between the light source and the target area for effective phototherapy.

Wound healing with OLEDs

X. Wu et al. have shown that red OLEDs improve wound healing in vitro and in vivo diabetic models[85]. The OLEDs were thermally evaporated on ITO glass substrates, each pixel having a 1.8 cm^2 area and 623 nm emission peak. For in vivo testing, Zucker Diabetic Fatty rats were given two wounds, one on either side of its flank. The wounds on the right side were irradiated with either an OLED or a 635 nm laser (both operating at 10 $mW\,cm^{-2}$ irradiance) for 8 minutes and 20 seconds immediately after wounding, and then once daily for a week. Wounds treated with OLED and laser light both showed higher percentages of healing than the non-irradiated wounds: OLED treated wounds had 45+/-4.61 % closure, laser treated wounds had 50.50+/-4.90 % closure, and control wounds had 29.88+/-5.08 % closure six days after injury. This improvement in wound closure was attributed to the photonic activation of cytochrome c oxidase (CCO), which in turn increases adenosine triphosphate (ATP) levels, mitochondrial metabolism, and cell proliferation.

Cancer treatment with inorganic light sources

Photodynamic therapy is being investigated as a non-invasive treatment for both internal organ and non-melanoma skin cancers [77]. Most oncological photodynamic therapy is conducted with lasers, incandescent lamps, or inorganic LEDs [77]. During therapy, the light source targets a photosensitizer that is in close proximity to cancerous tissue. The photosensitizer reacts with oxygen to create reactive oxygen species that in turn damage cancerous tumor cells [77, 86].

PDT has been shown to successfully treat the non-melanoma skin cancers artinic keratosises (AK), basal cell carcinoma (BCC), and Bowens disease (BD) [87]. Figure 2.7(a) illustrates the PDT treatment process for basal cell carcinoma [88]. First, the photosensitizer cream 5-aminolevulinic acid (ALA) is applied to the cancerous lesion (Figure. 2.7(a)i-ii). A bandage is applied over the cream while it is absorbed into the skin, where the ALA generates the molecule protpohyrin IX (PpIX) that reacts with the PDT light (Figure. 2.7(a)iii-iv). Reactive oxygen species result from the reaction between PpIX and the photons it absorbs. The reactive oxygen species in turn trigger cell death in the surrounding cancerous tissue (Figure. 2.7(a)v-vi). While more comfortable and less invasive than the physical extraction of the cancerous tissue, limitations for this PDT treatment include mild to severe pain during therapeutic irradiation and the time necessary for patients to visit their doctor's office for prolonged treatments [87].

When designing a light source for PDT, both the absorption spectrum of the photosensitizer and penetration depth of tissue should be considered. For example, the photosensitizer ALA is converted into protpohyrin IX (PpIX) in cancerous epidermal cells, and the PpIX produces the cancer-killing reactive oxygen species upon photoexcitation [76]. PpIX's maximum absorption peak is at 410 nm, with smaller peaks at 505, 540, 580, and 635 nm [87]. While blue light would be best for activating PpIX, longer wavelengths have larger penetration depths in human tissue [89], which makes red a better choice for treating cancerous

tissue below the epidermal surface. One of the limitations to treating internal tumors with PDT is the rate of the of the photosensitizer/photon/oxygen reaction. If the light-triggered chain of reactions occurs at too high a rate, the local oxygen concentration will be depleted, meaning that reactive oxygen species will no longer be produced to attack the cancer cells [90]. This renders any continued PDT ineffective [91]. Metronomic photodynamic therapy (mPDT) is being investigated as a solution to this scenario: a lower light intensity is used over a longer period of time with multiple doses of photosensitizer so that the local oxygen isnt depleted during treatment, and more tumor-killing reactive species are produced.

Cancer treatment with OLEDs

Guo et al. have demonstrated mPDT using a red OLED on a mouse with a brain tumor (aka glioma) [92]. The OLED had a 626 nm emission peak, was 7 mm in diameter, weighed 5 g, and was powered by 7.5 V and 15 mA to output 3 $mWcm^{-2}$. Figure 2.7(b) shows the schematic of the OLED, it's electroluminescence spectrum, and how it was mounted on the skull of a glioma mouse model. The tumor area was dosed with ALA and illuminated for 3.7 hours, giving a of 40 Jcm^{-2} phototherapuetic dose. When compared to the control group, the mice that underwent OLED photodynamic therapy had a significantly higher average total survival time (the mPDT treated mice survived for an of average 40.5 ± 9.2 days, while the control group survived for an average of 26 ± 2 days). Guo et al. chose to investigate OLEDs for photodynamic therapy because their lightweight and flexible form factor make them more practical for mPDT trials in mice than other lighting apparati, successfully demonstrating the advantages of OLEDs in this use case.

Attili et al. have demonstrated PDT for non-melanoma skin cancer treatment using a red OLED (manufactured by Osram Opto Semiconductors) to treat 12 patients with either Bowen's Disease or basal cell carcinoma [93]. The red OLED had an emission peak at 620 nm (the total emission spectrum ranged from 550-750 nm) and 5 $mWcm^{-2}$ irradiance. Each patient received one 45-60 Jcm^{-2} dose treatment per month for two months. The study showed a significant decrease in pain experienced by the patient during treatment with the OLED compared to treatment with an inorganic LED, which had both a higher irradiance (80 $mWcm^{-2}$) and dose (75 Jcm^{-2}). Both the OLED and the inorganic LED cleared the targeted tissue of cancerous cells. Figure 2.7(c) shows a cancerous lesion before photodynamic therapy (top left) and after 12 months of treatment (top right), as well as the OLED used for treatment and a portable box containing its power supply and control circuitry (bottom).

Acne treatment

Phototherapy is also used to treat acne vulgaris [72, 73, 74, 75, 76]. Standard acne treatment involves the application of various creams that have undesirable side effects including dermal dryness and bleached clothing[]. The orally ingested medication isotretinoin can also be prescribed, but extra care must be taken during its use because it can cause severe
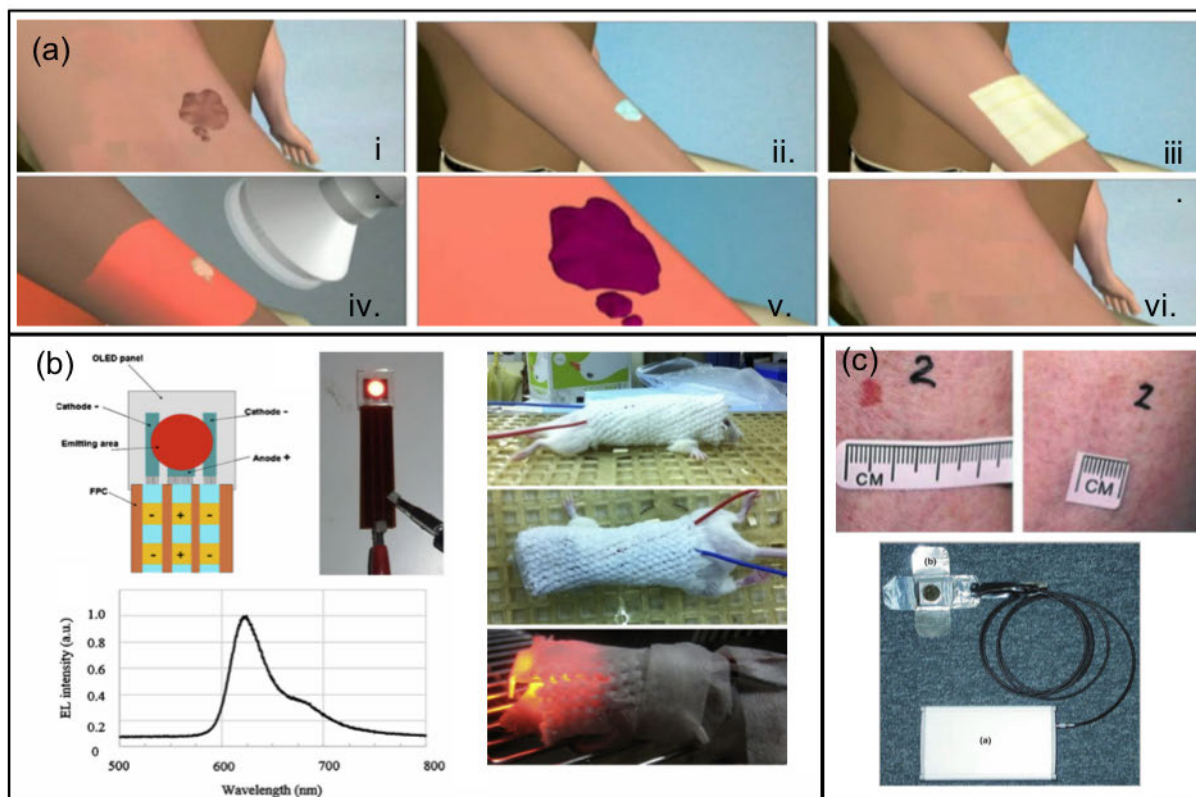
Figure 2.7: **Photodynamic therapy**. **(a)** The topical PDT process for basal cell carcinoma: first the (i) cancerous lesion on the arm (ii) is covered with a cream containing a photosensitizer. (iii) A bandage is applied to the treatment site for a period of time until the photosensitizer concentration builds in the tissue. (iv) The lesion is then illuminated, triggering (v) the cell death process. If successful, (vi) the lesion will be reduced or eradicated [88]. **(b)** Guo et al. performed PDT on a mouse model of human glioblastoma with an OLED. The OLED's peak wavelength was 626 nm and it was light enough to be worn by a mouse for an extended period of time [92]. **(c)** Attili et al. used a red OLED (bottom photo) to perform PDT on BCC and Bowen's Disease lesions (top left photo before treatment, top right photo 12 months after treatment). Patients treated with the OLED reported less pain than patients treated with a higher inorganic LED with a higher irradiance but similar dose [93].

birth defects if used while pregnant [94, 95]. Photodynamic therapy on the other hand is non-invasive with minimal side-effects when used as prescribed.

Acne treatment phototherapy is conducted with blue and red light. The blue light kills acne-causing bacteria (propinoibacterium acnes), and the red light reduces pain caused by blue light irradiation and heals damaged skin [72, 74, 79]. When irradiated with 415 nm light, porphyrin molecules produced by propinoibacterium acnes generate singlet oxygen species. These singlet oxygen species then react with the bacteria to trigger cell death [75]. The red light is applied after blue light treatment to repair damaged skin cells.

Papageorgiou et al. studied phototherapy's effect on 107 patients with mild to moderate acne vulgaris [72]. Patients were given either blue and red, only blue, or white fluorescent lamps for daily 15 minute phototherapy sessions. Other patients used standard benzoyl peroxide cream over twelve weeks. The blue lamps had a 415 nm peak wavelength and 4.23 $mWcm^{-2}$ irradiance for a 3.8 Jcm^{-2} dose per session. The red lamps had a 660 nm peak wavelength and 2.67 $mWcm^{-2}$ irradiance for a 2.4 Jcm^{-2} dose per session. Patients that were given blue and red light sources saw a larger decrease in inflammatory acne lesions (76% improvement) than those given only blue ($\approx$60%) or white ($\approx$25%) light sources or benzoyl peroxide cream ($\approx$58%) after 12 weeks of treatment.

Blue and red light phototherapy acne treatment devices are currently commercially available for at-home use [96, 97, 98]. The light sources in these devices are inorganic LEDs. The LEDs are built into a face mask, or a pen for spot-treatments of individual lesions. However, acne affects large surface areas of the body other than the face. An opportunity for OLEDs lies in the fact that similarly easy at-home phototherapeutic treatment for acne on the chest or back, for example, will require a large area conformally fitting device with more LEDs than what is currently available with inorganic light sources.

2.6 Conclusion

In this review we presented opportunities for OLEDs in pulse oximetry, NIRS, optogenetics, and phototherapy. We hope that it encourages continued development of OLEDs for a variety of biomedical applications. For example, NIR materials with peak emission beyond 800 nm would enable further application of OLEDS for fNIRS, and would be able to fight more types of cancer with a deeper penetration depth in tissue if paired with an NIR absorbing photosensitizer for PDT [99, 100, 101]. For applications like fNIRS and optogenetics, where multiple light sources may be used, it is important to take into account the fact that OLEDs generally have wider emission spectra than inorganic LEDs. In order to prevent spectral overlap, filters may need to be implemented or the OLEDs' emission spectra could be narrowed with a microcavity structure [102]. In order to enable a fully wearable device, OLED integration with small scale driver and communication electronics and flexible light-weight energy storage will be required. These components have been demonstrated separately [103, 104, 105, 106, 107], but challenges remain in integrating the parts into a whole system. In particular, the OLEDs in this review required over 3.3 or even 5 V (the standard

microcontroller output voltages) in order to generate enough flux. As progress continues to be made in developing OLED materials with high brightness at lower voltages [108, 109, 110], this challenge will be mitigated. Overall, based on the works reviewed herein, we believe that flexible OLEDs have a demonstrated potential to be an essential part of biomedical wearables that will improve patient care.

Application	Light Source	Wavelength (nm)	FWHM (nm)	Dose (J/cm²)	Samp. Rate (Hz)	Flux (mW)	Irradiance (mW/cm²)	Pixel Size (cm²)	Area of App.	App. Time	Ref.
Pulse Oximetry	OLED	532, 626	75, 80	N/A	1 k	8.04, 2.33	20.1, 5.83	.4	Finger	Continuous	[22]
Pulse Oximetry	OLED	520, 611, 725	75, 80, 100	N/A	-	.68, .89, .19	1.39, 1.82, .39	.49	Wrist	Continuous	[8]
Pulse Oximetry	OLED	517, 609	80, 90	N/A	.2	-	-	-	Finger	Continuous	[11]
NIRS	OLED	615	90	N/A	1	-	-	1.44	Forearm	Continuous	[53]
NIRS	OLED	780	-	N/A	-	.14	3.5	.04	Forearm	Continuous	[55]
NIRS Hematoma Detection	LED	750, 800, 850	-	N/A	100	10	-	-	Head	2 mins	[52]
fNIRS	LED	780, 850	-	N/A	14	-	-	-	Forehead, Arm	-	[46]
fNIRS	LED	760, 870	25, 40	N/A	100	3.5, 5	-	-	Head, Arm	-	[47]
fNIRS	Laser Diode	690-780, 830-887	$\leq$ 50	N/A	2-100	2-10	-	-	Head	-	[37, 111, 40]
Optogenetics	OLED	464, 515, 606	-	N/A	.2	.156, .188, .25	2.5, 3, 4	.0625	Cell Culture	-	[60]
Optogenetics	OLED	477	44	N/A	60	$5.94x10^{-7}$-.11	-	$5.4x10^{-7}$	Cell Culture	-	[62]
Optogenetics	OLED	455	55	N/A	20	4	100	.04	-	-	[64]
PT (Wound Healing)	OLED	623	65	5	-	18	10	1.8	Rat Body	Daily over 7 days	[85]
PT (Wound Healing)	LED	645	30	.99	-	7.8	-	-	Intra-oral	3 x5 min. daily for 1 week	[83]
PT (Wound Healing)	LED	670	20	4	-	50	-	-	Cheek, anterior throat	80 s daily for 2 weeks	[84]
PT (Acne Treatment)	Fluorescent Lamp	415, 660	35, 20	3.8, 2.4	-	-	4.23, 2.67	-	Face	15 mins, daily	[72]
PDT (Mouse Glioma)	OLED	626	50	40	-	6.75	3	2.25	Mouse Skull	3.7 hrs	[92]
PDT (BCC and Bowen's Disease)	OLED	620	120	45-60	-	15.7	5	3.14	Leg, Torso	Hourly over 4 hrs	[93]

Table 2.1: **Summary of reviewed biomedical light sources.** The application, type of light source, and the light-source's wavelength, FWHM, light dosage, sampling rate, flux, irradiance, pixel size, area of application, and application duration.

Chapter 3

Solution processed organic light-emitting diodes: materials, fabrication, and characterization

This chapter is an introduction to solution processed OLEDs and the fabrication and characterization methods used in this thesis. It is meant to be a general reference for those unfamiliar with solution processed OLEDs. The specific processing and characterization parameters implemented in this work will be presented in more detail in the following chapters.

3.1 Materials

The organic semiconductor materials used in OLEDs can be divided into two main categories: small molecules and polymers. Small molecule OLEDs were first demonstrated in 1987 by Ching W. Tang and Steven Van Slyke, engineers at Eastman Kodak [7]. The emissive material used was the small molecule 8-hydroxyquinoline aluminum (Alq_3),and it was thermally evaporated on a glass substrate with a patterned ITO anode. The first polymer OLED was demonstrated by Burroughes et al. in 1990 [2]. In this case the emissive layer was a film of poly(p-phenylene vinylene) (PPV), spin-coated from solution on a glass substrate with a patterned ITO anode. An important distinction between these two devices is the way that the active layer was processed - the small molecule was vacuum deposited and the polymer was spin-cast from solution. Small molecules are naturally insoluble and are therefore not compatible with solution processing, including printing. Printed electronics, specifically roll-to-roll printed electronics, is an area of rapid research because it has the potential to enable highly scalable, customizable, high-throughput, and low-cost electronic and optoelectronic devices [112, 13, 3].

The vast majority of commercial OLED displays are made from thermally evaporated small molecule OLEDs. Research is undergoing to make small molecule emitters soluble [113], but at present there is a wide selection of solution processable polymer emitters to

choose from. One of the main goals of this work was to fabricate printed OLEDs, so the OLEDs herein were made from soluble polymer emitters.

Both polymer and small molecule OLED device stacks have become more complex over time in order to improve performance [114]. Electron and hole blocking layers have been employed to improve even carrier injection into the emissive layer and prevent exciton quenching at the electrodes. Another efficiency boosting development has been the implementation of phosphorescent emitters [115]. When an exciton (a bound electron/hole pair) is formed in an organic semiconductor, it is either a single exciton or a triplet exciton. In a singlet exciton, the electron and hole have opposite spins and are processing in opposite directions. A singlet exciton can directly relax and release a photon. Statistically, 25% of each exciton formed in an OLED's emissive layer will be a singlet. Alq_3 and PPV are both fluorescent emitters, meaning that only singlet excitons (only 25% of excitons formed) in the emissive layer release a photon upon relaxation. In fluorescent materials, triplet excitons (75% of excitons formed) do not emit photons upon relaxation [116], limiting efficiency. However, exciton spin-orbit coupling in phosphorescent emitters doped with high atomic number elements (such as platinum and iridium) does provide a radiative pathway for triplet exciton relaxation [115]. Thus OLEDs made with these heavy metal phosphorescent materials have higher internal quantum efficiencies (the percentage of photons emitted per electron/hole pairs injected) than fluorescent emitters.

The organic semiconductors used in this thesis were provided by Cambridge Display Technology. The emissive materials used in Chapter 4 and 6 were fluorescent conjugated polymers. The emitters used in Chapter 5 and 7 were proprietary phosphorescent materials.

3.2 Device structure

A very basic OLED structure is pictured in Figure3.1. The bottom layer of the OLED is a transparent anode, the most common anode material being indium tin oxide (ITO). Both glass and flexible plastic substrates can be purchased with ITO coatings or ITO can be deposited in the lab via physical vapor deposition (PVD). Commercially available plastic/ITO substrates vary in quality in terms of surface roughness and conductivity and can cost upwards of $300 per A4-sized sheet. It is also worth noting that while it is used throughout the flexible electronics field, ITO in itself is a brittle material. However, ITO films are stable, transparent, conductive, and have a work function compatible with favorable hole injection into organic semiconductors. These are the characteristics necessary for a good OLED anode, which will be explored in further detail in Chapters 5 and 6 of this thesis with an ITO replacement.

PEDOT:PSS is commonly used as a hole injection and planarization layer solution on top of the anode. PEDOT:PSS is a commercially available water-soluble conductive polymer that comes in a variety of formulations for varying levels of conductivity, work function, and deposition methods (all PEDOT:PSS used in this work was purchased from the Heraeus Group). In different types of PEDOT:PSS solutions, there is a tradeoff between conductivity

(a)
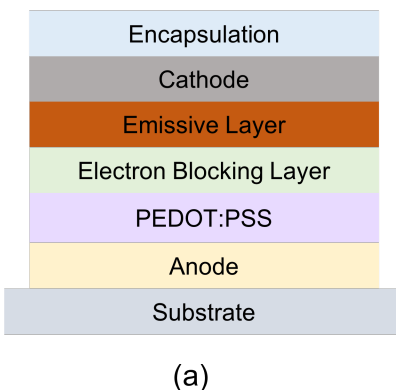
Figure 3.1: **The standard polymer OLED structure** consists of a substrate, anode (for hole injection), PEDOT:PSS layer (for anode smoothing and hole transport), an electron blocking layer (to prevent exciton quenching at the anode), an emissive layer, a cathode (for electron injection), and encapsulation.

and work function. The higher the conductivity, the lower the work function (worse for hole injection). Aside from assisting with hole injection, PEDOT:PSS serves as a smoothing layer, decreasing the effective surface roughness of the anode. It is very important for the bottom OLED layers to be smooth in order to prevent shorting in the device.

The next layer that may be included is an electron blocking/hole transporting layer. The electron blocking layer is a semiconductor with HOMO and LUMO levels that favor hole transport from the hole injection layer into the emissive layer while preventing excitons from travelling to the anode where quenching occurs (exciton quenching is when when an exciton transfers its energy to the electrode instead of emitting a photon)[117, 118, 119]. While most organic semiconductors for electron blocking layers and emissive layers have similar solubilities[120], a thermally cross-linked electron blocking layer can resist dissolution during emission layer deposition once it has been heated beyond its glass transition temperature (typically 180°C for at least 30 minutes) [121, 122, 123, 124].

Next is the emission layer. A polymer emission layer may consist of a single material or may be a blend of two or more semiconductors. Within the emissive layer, electrons and holes form an exciton. When exciton relaxation emits a photon, the photon's wavelength corresponding to the emissive molecule's bandgap. The general carrier injection, transport, and recombination process will be shown in more detail for polymer blends in Chapter 4. If using a blend, it is important to consider the effect of solvent and fabrication conditions on the morphology of the finished film. This is because polymer blend morpohology effects charge transport, exciton formation, and recombination [125, 126]. Again, this will be covered in more detail in Chapter 4.

Next up, most OLED cathodes are composed of a thin low work-function material capped by a thicker layer of conductive and air-stable metal. Commonly used low work-function materials are LiF, Ca, and NaF [127, 128]. None of these materials are printable; they

are deposited via thermal or electron-beam evaporation. LiF and NaF must be precisely deposited to thicknesses on the order of 1 nm - they are insulators and will inhibit electron transport between the conductive metal and the emissive layer if they are too thick for electrons to tunnel through. Ca on the other hand is more conductive and can be deposited at higher thicknesses (5-15 nm). Unfortunately, most low work function materials degrade when exposed to oxygen and/or moisture. Thus the final layer in a standard OLED is encapsulation.

Thin film encapsulation for flexible printed OLEDs needs a low water vapor transmission rate (WVTR) and high degree of flexibility [129]. Organic/inorganic layers alternately deposited directly onto an OLED provide this [130, 131]. Because an OLED's cathode degrades in air, OLEDs must be encapsulated after cathode deposition in a controlled nitrogen or argon environment, before they are exposed to ambient air. If an integrated thermal evaporation/PVD/glovebox system isn't available, pre-coated barrier plastics, such as DuPonts Teonex, can be purchased and applied with an encapsulation epoxy. Epoxies for electronics encapsulation are commercially available (the epoxies used in this work are DELO Katiobond and DELO Photobond products). OLED encapsulation can be enhanced by including a getter material to absorb moisture that does penetrate the encapsulation, and by including a metal layer in the encapsulation stack [132]. Recently, companies have advertised flexible and self-adhesive encapsulation tapes [133]. These encapsulation tapes remain elusive for purchase on an academic scale in the United States at this point in time, but will hopefully become available in the future.

3.3   OLED fabrication

This section outlines the general practices for solution processed OLED material preparation and device fabrication used in this thesis. Specific fabrication procedures will be described in more detail in the following chapters. This section it meant to be used as a reference guide for basic OLED fabrication.

Solution preparation

Organic solvents commonly used to process organic semiconductors include chloroform, dichlorobenze, toluene, xylenes, and tetrahydrofuran. The performance of the finished OLED is dependent on the solvent used in its fabrication, in part because the solvent boiling point/evaporation rate can affect the quality of film formation with regards to morphology[126]. This will be discussed further in Chapter 4. The first step in making a solution is to prepare a glass scintillation vial with a solvent-compatible cap by cleaning it, preferably with the same solvent to be used for the solution. The vial can be air-dried with a N_2 gun before it is filled with measured polymer. If the polymer is sensitive to moisture and oxygen, move the vial into a glovebox before using a pipette to add an anhydrous solvent to the vial. For best dissolution, place a micro stir bar in the solution and heat stir it on a hot plate

with a stir function for at least two hours, preferably overnight. Depending on the solvent, the hot plate temperature is usually set between 40 and 60 (it should be warm enough to encourage dissolution but not too hot the evaporate the solvent). Once the solution is thoroughly dissolved, it should be left to cool to room temperature before it is filtered into a new clean vial in order to remove any undissolved material. A .45 um PTFE filter is commonly used for organic solvent solutions.For particular high molecular weight polymers, glass filters can be used instead of PTFE. In order to maximize the final amount of solution, a blunt needle can be used to extract the solution from the original vial into a syringe before passing it through the filter. It is also recommended that clean solvent is passed through the syringe and filter before the solution in order to ensure that the solution isn't contaminated with stray particulates.

Substrate preparation

The first and most important step in any fabrication process it to thoroughly clean the substrate. Whether the substrate is PEN, PET, or glass, it should be subjected to a sonication bath in a series of cleaning solutions. Different labs have different sonication procedures, but a good staple is 15 minutes sonication in soapy DI water followed by rinsing and then 15 minutes sonication in DI water, followed by 15 minutes sonication in acetone (before putting any substrate in acetone, check to make sure that acetone won't dissolve it. For example, PET and acetone are not compatible) and then 15 minutes sonication in isopropyl alochol (IPA, 2-propanol). Not everyone finds the first two sonication steps necessary but the soapy water soak can help remove static particles from the substrate's surface. If cleaning a substrate in acetone, it should be cleaned in IPA after, as acetone can leave a film behind. Once the substrate has been cleaned in the sonication bath, it should be treated with O_2 plasma for at least 15 seconds at 50 W in order to remove any remaining organic contaminants and to increase its hydrophilicity.

If using a flexible substrate and any heating steps in the fabrication process, the substrate should be placed on an inflexible carrier in order to prevent substrate deformation. An effective carrier is glass coated with Gel Pak. Gel Pak is available in varying levels of adhesiveness and temperature stability. The OLEDs in this work require processing at 180°C, and GelPak DGL-X4 was used. DGL-X4 is a double-sided Gel Pak film with thermal stability up to 225°C. A hand-held print roller was used to apply the GelPak to the glass carrier in order to prevent any air pockets from forming between the two. The clean plastic substrate was then applied to the glass carrier/GelPak stack. This entire stack should be baked in a vacuum oven at the maximum temperature of the process for at least 2 hours in order to fully dehydrate the materials and allow any substrate deformation to occur (which should be minimal if the substrate is attached securely to the GelPak) before device layers are deposited.

	Speed (rpm)	Acceleration (rpm/s)	Film Thickness (nm)
	3500	500	65
	3500	1000	65
Green-2	2500	1000	65
	2500	500	75
	2500	258	95
	2500	86	120
	5500	1000	50
	4000	1000	60
	4000	774	60
Red-2	4000	350	70
	4000	258	80
	4000	172	85
	2500	1000	60

Table 3.1: **Spin-cast thin-film thickness as a function of spin-speed and accelera-tion** for Green-2 and Red-2 polymers.

Spin-coating

The original method for fabricating solution-processed OLEDs was spin-coating, the same method used for applying photoresist to silicon wafers in inorganic semiconductor processing [134]. During spin-coating, the substrate is placed on the spin-coater chuck, a specified ink volume is dispensed onto the substrate (enough for the entire surface to be covered), and the spin-coater chuck is accelerated at a set rate to a set speed for a set amount of time. The ink is whisked over the surface of the substrate, some sticking to the substrate to form a uniform film while the excess is thrown off onto the walls of the spin-coater. If using an ink made with a high boiling point solvent such water or o-xylene, it is very likely that some solvent remains in your film after spin-coating, so the sample should be annealed before the next processing step in order to evaporate remaining solvent.

Controllable variables that affect the thickness of spin-coated films are ink concentration, spin acceleration, and spin velocity. The higher the polymer concentration, the thicker the film. The higher the acceleration rate and velocity, the thinner the film. Changing the spin-coater's acceleration rate has a greater affect on film thickness than changing the velocity. Table 3.1 shows the spin-coated film thickness as a function of acceleration and speed for two different polymer solutions (Red-2 (20 mg/ml in toluene) and Green -2 (15 mg/mL in o-xylene), both proprietary materials provided by CDT).

In OLEDs, the thickness of the the emissive layer impacts device performance. Because the emissive layer materials have low electron and hole mobilities, the thicker the layer, the higher its resistance. This is shown for OLEDs made with a Red-2 emissive layer in Figure 3.2. Each OLED had an identicle structure except for the thickness of its active layer, which was varied between 110 nm, 80 nm, 70 nm, and 60 nm. At 10 V, the OLED with a 110 nm thick emissive layer had a 48.7 $mAcm^{-2}$ current density and 8.8 $mWcm^{-2}$ light output. Both the current density and light output increased with decreasing film thickness to 70.4 $mAcm^{-2}$ and 9.8 $mWcm^{-2}$ at 80 nm, 115 $mAcm^{-2}$ and 13 $mWcm^{-2}$ at 70 nm, and 325
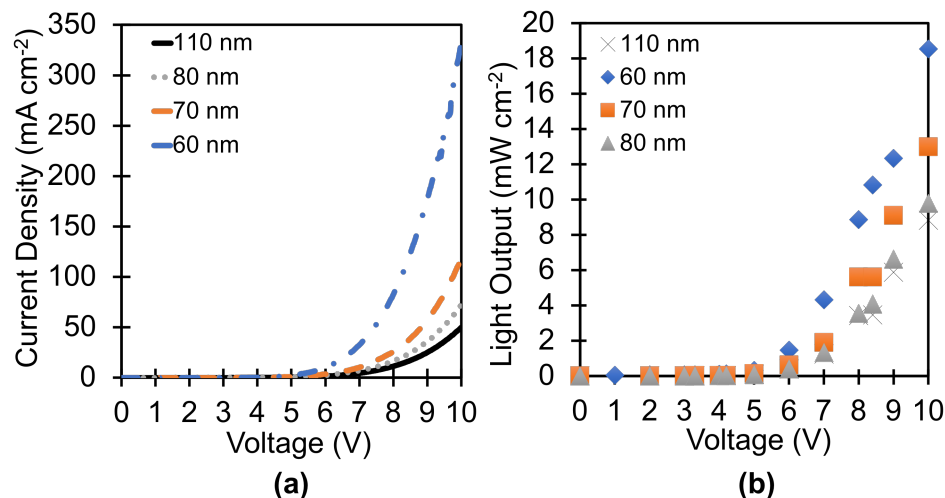
Figure 3.2: **Active layer thickness effect on Red-2 OLED performance.** (a) Current density and (b) light output as a function of voltage for Red-2 OLEDs with 110 nm, 80 nm, 70 nm, and 60 nm emissive layer thicknesses.

$mAcm^{-2}$ and 18.5 $mWcm^{-2}$ at 60 nm. From this data it can be concluded that the thinner the active the layer, the better the OLED's performance. However, if the emissive layer is too thin, shorts will be present in the device.

Blade coating

Blade coating is the printing method used for printed in Chapters 5, 6, and 7 of this work. Blade coating was selected because it has high throughput and low ink consumption. While not necessary for the OLEDs in this work, 2-D patterns can be blade coated by patterning the hydrophobicity of the substrate to control where printed ink wets the substrate[135, 8].

The blade coater used in this work is the Zehtner GMBH ZUA 2000.8 Universal Applicator. Ink is pipetted onto the substrate in front of the blade coater, and a linear actuator pushes the blade over the ink to the end of the printing area, as shown in Figure 3.3. Semi-conducting and conductive polymer, metal oxide nanoparticle, and organo-metallic inks were all printed with this method in this work. The adjustable variables for blade coating are substrate temperature (the substrate can be attached to a hot plate during printing), blade height, coating speed, ink volume, and ink concentration.

Printed film thickness is most affected by blade height, ink concentration, and printing speed. The higher the ink concentration, blade height, and print speed, the thicker the film. For inks made form high-boiling point solvents, the quality of the printed film is improved by elevating the substrate temperature. If the ink takes too long to dry, the resulting film could be mottled. Speeding the drying time ensures that the ink dries where it is deposited and the final film uniformity will be improved. On the other hand, if the substrate temperature
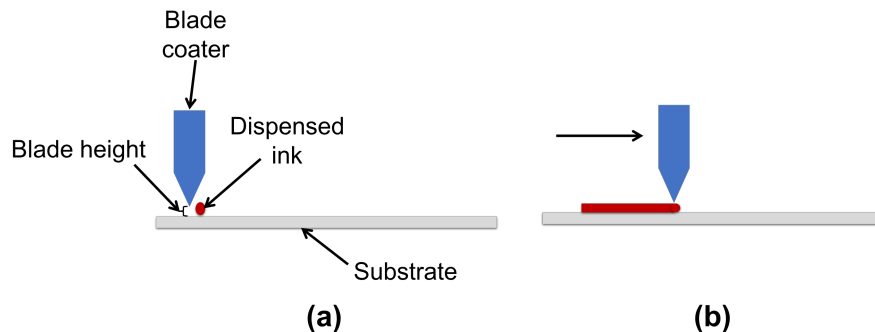
Figure 3.3: **Side view of the blade coating process.** **(a)** Ink is dispensed onto the substrate in front of the blade coater. The blade height is set as the distance between edge of the blade and the substrate. **(b)** The blade is pushed forward over the substrate at a uniform speed, spreading the ink into a film.

is set too high, the ink will dry at the top of the print before it can be spread over the substrate.

Table 3.2 at the end of this chapter presents the effects of printing parameters on print quality for different OLED materials. More detailed information on the printing parameters and procedures for devices in this thesis are presented in Chapters 5, 6, and 7.

Thermal evaporation

Thermal evaporation the most common method of OLED cathode deposition. In a thermal evaporator, the material to be deposited (the evaporation source) is placed on a tungsten boat that is suspended between two electrodes. The substrate is secured to a patterned steel shadow mask that defines the electrode pattern and placed inside the evaporator above the evaporation source. The shadow masks used in this work were designed in AutoCad and purchased from Photo Etch Technology. Once the source and substrate are in place, the evaporators bell jar is closed and put under vacuum. Once under sufficient vacuum ($4x10^{-6}$ Torr in this work), a current is applied across the boat, heating the source material so that it evaporates and re-solidifies on the substrate through the shadow mask.

Care needs to be taken while evaporating a cathode so as not to create shorts in the device. If the evaporation rate is too high, the evaporated material will impact the target with too much energy and short through to the anode. In this work, Ca was evaporated with a rate between .5-2 Å/s and Al was evaporated with a rate between 2-4 Å/s. The evaporation rate is affected by the amount of material used, the chamber pressure, and the amount of current supplied to the evaporation source. If there is an extended evaporation procedure, such as for a 100 nm Al film, the procedure should be broken up into multiple stages with a cool down time in between in order to decrease thermal stress, which in turn decreases the probability of shorts and leakage current. Figure 3.4 shows the current density
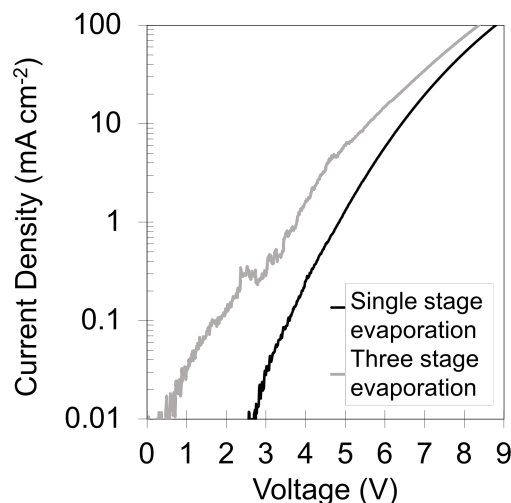
Figure 3.4: **OLED current density vs. voltage as a function of cathode evaporation procedure.** An OLED whose 10 nm Ca/100 nm Al cathode was evaporated in one stage (grey line) had a higher leakage current than an OLED whose cathode evaporation was split into 3 stages (black line): the 10 nm Ca layer was evaporated, then the system was allowed to cool for 15 minutes before evaporating 50 nm Al, then allowed to cool again for 15 minutes, and then the final 50 nm Al was evaporated.

vs. voltage characteristic for two OLEDs made with the same evaporated cathode structure (Ca (5 nm)/Al (100 nm)). The OLED whose cathode was evaporated in one setting had significant leakage current, while the OLED whose cathode was evaporated in three stages (10 nm Ca, 50 nm Al, and 50 nm Al) with 15 minute cool-down breaks in between did not.

Encapsulation

In this work, a UV-curable epoxy (Delo Katiobond and Delo Photobond) and a barrier-coated PEN coverslip (PQA1 from Dupont Teijin Films) were applied over OLED pixels, leaving portions of the electrodes exposed for electrical contact as shown in Figure 3.5(c). A 30 W UV lamp (inexpensive nail polish curing lamps are a viable alternative to expensive UV lamps marketed for electronics curing) was used to cure the epoxy for 10 minutes. After encapsulation, Ag paste (Ted Paella) was applied to the exposed contacts so that they weren't inadvertently scratched during testing.

Encapsulation materials can be evaluated with a calcium test. For a calcium test, calcium is evaporated onto a substrate, encapsulated, and observed the film is optically observed over time in atmosphere. Freshly evaporated Ca appears to be a reflective metallic film. Once Ca is exposed to oxygen and moisture in the air, it becomes transparent. The longer it takes for encapsulated Ca to disappear, the better the encapsulation. Figure 3.5(b) shows
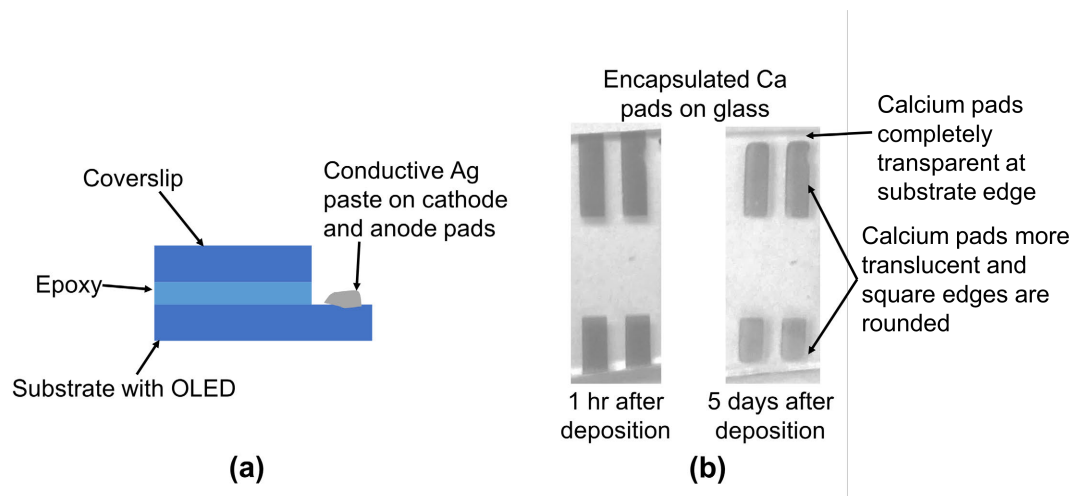
Figure 3.5: **OLED encapsulation**. **(a)** An encapsulated OLED ready for test has cured encapsulation epoxy beneath a coverslip over the active pixels. Conductive Ag epoxy is applied to the exposed anode and cathode contacts to prevent damaging them during testing. **(b)** Ca pads thermally evaporated on a glass substrate encapsulated with epoxy and a cover slip 1 hour after deposition (left) and 5 days after deposition (right). After 5 days, the calcium pads are more translucent and completely transparent at the substrate edge, evidence of degradation caused by exposure to oxygen and moisture.

encapsulated Ca pixels 1 hour after deposition with no visible decay, and 5 days after deposition where decay is visible. After 5 days, the encapsulated Ca pads became completely transparent at the edge of the substrate (where oxygen and moisture diffusion through the encapsulation is greatest), their rectangular edges appeared to be rounded, and the entire pad became more translucent than the pristine Ca pads.

3.4 Characterization

This section introduces the characterization methods used to evaluate the OLEDs and their constituent parts in this thesis.

Goniometry

Goniometry is used to measure the contact angle between a solution and the surface on which it is to be deposited. A very small volume of ink (in the 1's of μL range) is dispensed onto a substrate and a camera is used to capture the image of the ink drop, as shown in 3.6. The inside angle made between the tangent of the droplet and the substrate is the contact angle. If the contact angle is less than 90 the ink should wet the substrate; the lower the contact angle, the better the wetting. If the contact angle is greater than 90 then
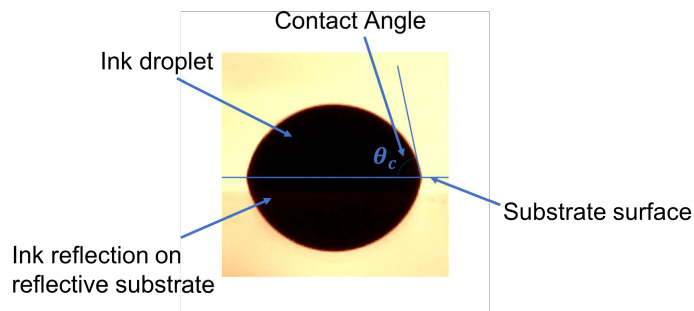
Figure 3.6: **Contact angle measurement image.** The contact angle is measured as the
angle between the substrate surface and the tangent of the ink droplet's curve.

the ink will not wet the substrate. The contact angle can be decreased by changing the ink
composition or treating the substrate's surface. Ink additives to improve wetting include
surfactants [136], and surface treatments include O_2 plasma and UV ozone to increase the
number of hydrophillic -OH groups on the substrate's surface [137].

UV-Vis-NIR spectroscopy

A UV-Vis-NIR spectrometer can be used to measure the transmittance or absorption of
a film or solution across a selected spectrum. Transmittance is commonly measured to char-
acterize the transparency of electrode and charge transport layers. Absorption is measured
to give insight into a material's energy structure ($E = hc/\lambda$). When performing UV-Vis-
NIR spectroscopy on thin films, it is best to deposit the thin film on a glass substrate, as
plastic substrates or substrates with barrier coatings have non-linear or non-polar absorption
properties that cause aberrations in their measured spectra.

Fluorescence Spectroscopy

Fluorescence spectroscopy is used to measure light that fluoresces from a material upon
excitation with a monochromatic light source. The excitation wavelength should be at a
peak in the material's absorption spectrum. By looking at the absorption and fluorescence
spectra of multi-material solutions or thin films, one can gain an understanding of energy
transfer processes between the materials. For example, if a film made with two different
materials is illuminated with the peak absorption of Material A but only fluoresces the
fluorescence spectrum of Material B, than you can deduce that energy from the incident
photons is transferred from Material A to Material B, and the film's output photons originate
in Material B. This will be described in more detail in Chapter 4.

Surface profilometry

Surface profilometry is used to measure the thickness and surface roughness of thin films ranging from 10s of nanometers to 100s of microns. A surface profilometer moves a stylus over a sample with variable force, distance, and time. The stylus will move up and down with hills and valleys in the film, from which thickness and surface roughness is measured. In order to measure the thickness of a film, part of the film needs to be scratched or etched away to create a step to measure between the substrate and the top of the film. Care must be taken not to damage the substrate if scratching the film, or else the measurement will be inaccurate. If etching the film, one must be aware that the etchant might not leave a clean step - the part of the film adjacent to the desired step location could be partially dissolved, giving an inaccurate measurement. Thus it is recommended that the film be physically scratched with a smooth, straight edge (like a square edged tweezer) with enough force to remove the thin film but not enough force to damage the substrate.

Four-point probe

The four-point probe is used to measure sheet resistance of conductive thin films. Current is supplied through the sample via the two outer probe tips, and the subsequent voltage generated in the sample is measured between the inner two probe tips. A geometry factor for the specific test probe is multiplied by the resulting measured resistance in order to give the sheet resistance in the units Ohms/square. Four-point probe measurements were conducted in this work to compare the conductivities of various electrode materials processed with various fabrication methods and parameters.

Fluorescence microscopy

Fluorescence microscopy can be used to observe the morphology of a film with at least one fluorescent component. It can be performed with a specialized fluorescence microscope or with a color filter placed over the light aperture in a standard bench-top optical microscope. The high energy microscopic light (usually green or blue) will excite the fluorescent component of the thin film, making it visible, while the non-fluorescent portion will remain dark, allowing the user to observe a more detailed film morphology than with a white light optical microscope alone.

Atomic force microscopy

Atomic force microscopy (AFM) is used to investigate thin film surface features that are too small for optical microscopy or surface profilometry. AFM can quantify the surface roughness and thickness of a film, as well as show its surface morphology.

Electrical and optical OLED characterization

The OLEDs in this work were characterized with a Keithley 2601 sourcemeter and Orb Optronix Integrating Sphere 6" LMS system equipped with a SP-75 spectrometer.

Current density vs. voltage sweeps were conducted from -3 V to the voltage at which the set current limit was reached (typically 7-12 V, depending on the OLED). The voltage sweep started below 0 V in order to observe leakage current. By plotting the absolute value of current density on a log scale vs. voltage, one can observe leakage current and turn-on voltage. On a non-log plot, the current density should increase with a steep slope after turn-on if the device structure is fully optimized for good charge carrier injection and transport.

For optical characterization, the OLED was measured in the integrating sphere. Sweeping the voltage (from 0 to the maximum desired voltage), the Orb Optronix system measures spectral flux (the amount of flux per wavelength, which when plotted gives the emission spectrum, in Wnm^{-1}), and total flux (W), from which irradiance ($mWcm^{-2}$) and external quantum efficiency can be derived.

Irradiance is the total flux (mW in this work) per unit area of illumination, which in this work is considered to be the OLED pixel's area (in cm^2) because the OLEDs are intended to be flush against the user's skin in a biomedical device.

$$Radiance = \frac{Flux}{\pi \cdot Area}$$

External Quantum Efficiency (EQE) is a measure of the number of photons emitted from an OLED as a percentage of the number of electrons injected into the device. EQE is calculated by:

$$EQE(\%) = 100 \cdot \frac{photons\ out}{electrons\ in}$$

where

$$photons\ out = \frac{flux}{hc/\frac{\int \lambda \cdot S(\lambda)d\lambda}{\int S(\lambda)d\lambda}}$$

and

$$electrons\ in = I/q$$

so

$$EQE(\%) = 100 \cdot \frac{flux}{hc/\frac{\int \lambda \cdot S(\lambda)d\lambda}{\int S(\lambda)d\lambda}} \cdot \frac{q}{I}$$

$S(\lambda)$ is the spectral flux at a given wavelength, h is Planck's Constant ($6.626 \times 10^{-34}\ m^2 kg s^{-1}$), c is the speed of light ($3 \times 10^8\ ms^{-1}$), q is the charge of an electron ($1.602 \times 10^{-19}\ coulombs$), and I is the current at a given voltage (EQE must be calculated for each voltage point).

Full Width at Half Maximum (FWHM) is the width (in nm) of the two points on an emission spectrum where the spectral flux is half of the maximum spectral flux value at the peak wavelength. FWHM is used to characterize spectral width.

This concludes the introduction to the materials and methods used throughout this thesis. Next up in Chapter 3, polymer blend OLEDs and their application in an organic-optoelectronic pulse oximeter will be presented in detail.

Table 3.2: Doctor blade coating conditions for various materials.

Ink Composition	Solvent	Ink Conc. (mg/mL)	Blade Height (μm)	Blade Speed (cm/s)	Subs. Temp. (°C)	Ink Vol. (μL)	Substrate	Film Quality	Film Thickness (nm)
TFB:F8BT (1:9) pinholed film	o-xylene	5	200	2.5	24	80	PEN	too thin	
TFB:F8BT (1:9)	o-xylene	20	500	1.5	60	10	PEN/TFB film	Non-uniform	
TFB:F8BT (1:9)	o-xylene	15	500	1.5	90	80	Glass	Good	35
TFB:F8BT (1:9)	o-xylene	15	1000	1.5	90	200	Glass	Good	130
TFB:F8BT (1:9) ink	o-xylene	20	450	2.5	60	20	PEN/Cr/Ag/PEDOT:PSS	Not enough	
TFB:F8BT (1:9)	o-xylene	20	450	2.5	60	40	PEN/Cr/Ag/PEDOT:PSS	Non-uniform	
TFB:F8BT (1:9)	o-xylene	20	450	2.5	80	40	PEN/Cr/Ag/PEDOT:PSS	Good	150
TFB	o-xylene	5	500	1.5	50	15	PEN	Good	
Red-1	o-xylene	20	450	2.5	80	40	PEN/Cr/Ag/PEDOT:PSS	Good	
Red-1	chloroform	20	450	2.5	24	10	PEN	Non-uniform	
Red-1	chloroform	20	450	2.5	40	10	PEN	Good	
Red-1	toluene	20	450	2.5	80	40	PEN	OK	75
Red-1	toluene	20	600	2.5	80	40	PEN	Poor	
Red-1 ink doesn't spread enough	toluene	20	650	2.5	80	40	PEN	Poor	
Red-1 ink doesn't spread enough (spread better but ridges in film)	toluene	20	550	2.5	90	40	PEN	Blade too low	
Green-1	chloroform	15	450	2.5	24	10	PEN	Non-uniform	
Green-1	chloroform	15	450	2.5	40	10	PEN	Good	
Green-1	toluene	15	450	2.5	80	40	PEN	OK	
Green-1	o-xylene	15	450	2.5	90	60	PEN	Good	
Green-1	o-xylene	15	450	3	90	50	PEN	Poor - too fast	
Green-1	o-xylene	15	350	2.5	90	50	PEN	Good	130
TFB:F8BT:TBT (25:70:5)	o-xylene	10	250	2.5	60	20	Glass/Ag Ink/PEDOT:PSS	Good	70
TFB:F8BT:TBT (25:70:5)	o-xylene	20	550	3	60	20	PEN/WO$_3$/Ag/PEDOT:PSS	Good	
TFB:F8BT:TBT (25:70:5)	o-xylene	20	550	2.5	60	30	PEN/PEDOT:PSS	Good	130

Table 3.2 continued from previous page

Ink Composition	Solvent	Ink Conc. (mg/mL)	Blade Height (μm)	Blade Speed (cm/s)	Subs. Temp. (°C)	Ink Vol. (μL)	Substrate	Film Quality	Film Thickness (nm)
(25:70:5) TFB:F8BT:TBT	o-xylene	15	500	2	90	80	PEN	Not enough ink	
(25:70:5) TFB:F8BT:TBT	o-xylene	15	500	2	90	100	PEN	Not enough ink	
(25:70:5) TFB:F8BT:TBT	o-xylene	15	500	2	90	200	PEN	Good	90
(25:70:5) TFB:F8BT:TBT	o-xylene	15	1000	1.5	90	200	Glass	Good	95
(25:70:5) TFB:F8BT:TBT	o-xylene	15	100	1.5	90	100	PEN in glovebox	Good	215
(25:70:5) TFB:F8BT:TBT	o-xylene	10	100	1.5	90	100	PEN in glovebox	Good	75
Red-2AB (95:5)	o-xylene	22	200	2.5	65	60	PEN in glovebox	Good	70
NIR-2AB (92.5:97.5)	toluene	15	200	2.5	65	60	PEN in glovebox	Good	40
NIR-2AB (92.5:97.5)	toluene	15	200	2.5	65	120	PEN in glovebox	Good	100
InkTec PR-010	-		250	2.5	24	25	Glass	Good	70
InkTec PR-010	-		400	2.5	24	25	Glass	Good	150
InkTec PR-010	-		300	2.5	120	5	PEN/WO$_3$	Good	40
InkTec PR-010	-		225	2.5	120	5	PEN/WO$_3$	Good	35
InkTec PR-010	-		550	3	120	20	PEN/WO$_3$		
InkTec PR-010	-		200	2.5	120	5	Glass	Good	35
InkTec PR-010	-		50	2.5	120	5	Glass	Good	15
InkTec PR-010	-		50	2.5	24	5	Glass	Pinholed	20
InkTec PR-010	-		100	2.5	24	5	Glass	Pinholed	50
InkTec PR-010	-		50	2.5	120	5	Glass	Good	15
InkTec PR-010	-		75	2.5	120	3	Glass	Good	25
InkTec PR-010	-		50	2.5	120	3	Glass	Blade too low	
PEDOT:PSS PVP AI4083			250	1.5	90	35	Glass/Ag Ink	Poor wetting	
PEDOT:PSS .65 wt% zonyl surfactant			350	2.5	40	15	PEN/Cr/Ag	Good	
PEDOT:PSS .65 wt% zonyl surfactant	-		250	1.5	90	35	Glass/Ag Ink	Good	50
PEDOT:PSS .1 wt% zonyl surfactant	-		500	3	90	150	PEN/WO$_3$/Ag	Good	
PEDOT:PSS .01 wt% zonyl surfactant	-		350	2	90	80	PEN	Good	60

Table 3.2 continued from previous page

Ink Composition	Solvent	Ink Conc. (mg/mL)	Blade Height (μm)	Blade Speed (cm/s)	Subs. Temp. (°C)	Ink Vol. (μL)	Substrate	Film Quality	Film Thickness (nm)
.01 wt% zonyl surfactant PEDOT:PSS	-	-	300	2	90	100	PEN	Good	200
.01 wt% zonyl surfactant PEDOT:PSS	-	-	100	2	90	100	PEN	Good	115
.01 wt% zonyl surfactant PEDOT:PSS	-	-	75	2	90	100	PEN	Good	80
.01 wt% zonyl surfactant PEDOT:PSS	-	-	50	2	90	100	PEN	Good	80
.05 wt% zonyl surfactant PEDOT:PSS	-	-	75	1.5	90	80	Glass	Good	120
.05 wt% zonyl surfactant	-	-	75	3	100	80	PEN/WO$_3$/Ag/WO$_3$	Good	70
WO$_3$	-	-	250	3	24	80	PEN	Good	55
WO$_3$	-	-	500	3	24	20	PEN	Good	

Chapter 4

Transmission mode pulse oximetry with spin-coated polyfluorene blend OLEDs

4.1   Red and green polyfluorene OLED operation

The first goal of this work was to determine whether or not polymer OLEDs could be used in a transmission mode pulse oximeter. Two different colored OLEDs had to be created, one with a peak wavelength at which oxyhemoglobin has a higher absorptivity than deoxyhemoglobin, and the other with a peak wavelength at which oxyhemoglobin has a lower absorptivity than deoxyhemoglobin. Such two wavelengths are in the red and green portions of the optical spectrum. In this work, red and green OLEDs were made using the semiconducting conjugated polymers poly[(9,9-dioctylfluorenyl-2,7-diyl)-co-(4,4-(N-(4-sec-butylphenyl)diphenylamine)] (TFB), Poly[(9,9-di-n-octylfluorenyl-2,7-diyl)-alt-(benzo[2,1,3] thiadiazol-4,8-diyl)] (F8BT), and poly[(9,9-diocty luorene)-2,7-diyl-alt-(4,7-bis(3-hexylthien-5-yl)-2,1,3-benzothia- diazole)-2,2-diyl] (TBT), whose structures are shown in Figure 4.1. All three polymers are members of the polyfluorene family, a set of materials that has been thoroughly studied in organic optoelectronic applications [126, 125, 138, 139, 140, 141]. Polyfluorenes are attractive OLED materials because they are soluble in non-chlorinated organic solvents (for fewer manufacturing restrictions), commercially available (note that when purchasing polymers, some companies have higher quality materials than others), and stable in air.

Multiple polyfluorenes are often blended together in order to boost device efficiency [126, 125]. In an ideal OLED, electrons and holes will form excitons that will relax in the middle of the emissive layer, away from the electrodes where non-emissive recombination (or quenching) occurs. For this to happen, electrons and holes need to be injected into the emissive layer at the same rate and travel through it with the same mobility. While the rate of carrier injection is controlled by the energy barriers between emissive layer and the
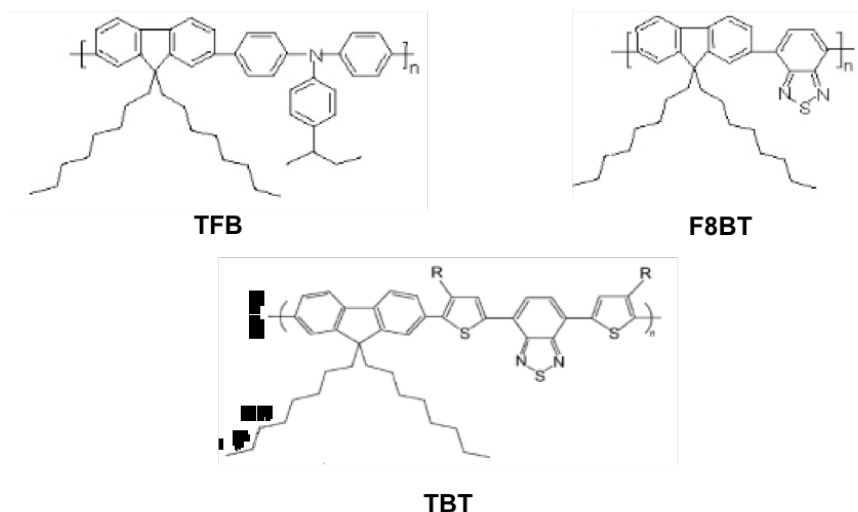
Figure 4.1: **TFB, F8BT, and TBT chemical structures.**

electrodes, the carrier mobility is subject to the electron and hole mobilities of the emissive layer polymer. In polyfluorenes, there is a disparity between electron and hole mobilities [142, 143]. This causes an imbalance of charge carries in the emissive layer, lowering the OLED's efficiency. And so F8BT (a green emitter), a polyfluorene with higher electron mobility, is blended with TFB (a blue emitter), a polyfluorene with higher hole mobility, for a green OLED in order to achieve more balanced charge carrier transport in the emissive layer and higher efficiency than a green emitting device made from F8BT alone. The ideal path (neglecting quenching and trapping) of electrons and holes in a polymer blend consisting of a hole transporting material and an electron transporting material is depicted and described in Figure 4.2.

Electrons are injected into lowest unoccupied molecular orbital (LUMO, analogous to the conduction band of an inorganic semiconductor) of the electron transport material, in this case F8BT, and holes are injected into the highest occupied molecular orbital (HOMO, analogous to the valence band of an inorganic semiconductor) of the hole transporting material, in this case TFB (Figure 4.2(a)). Electrons travel through the F8BT and holes travel through the TFB (Figure 4.2(b). At an interface between F8BT and TFB, the electron and hole form an exciton [141](Figure 4.2(c)).

When an exciton relaxes to emit a photon in a polyfluorene OLED, it does so by fluorescence. Excitons in the singlet state can relax directly, the electron falling from the LUMO to the HOMO and releasing energy in the form of a photon with a wavelength set by the energy gap between the polymer's HOMO and LUMO levels. If there is another polymer with a smaller band gap present (F8BT in the case of a TFB:F8BT blend), Forster resonance energy transfer (FRET) will occur: the smaller bandgap polymer will absorb the photon (Figure 4.2(d)), the energy of which excites an electron from the HOMO of the small
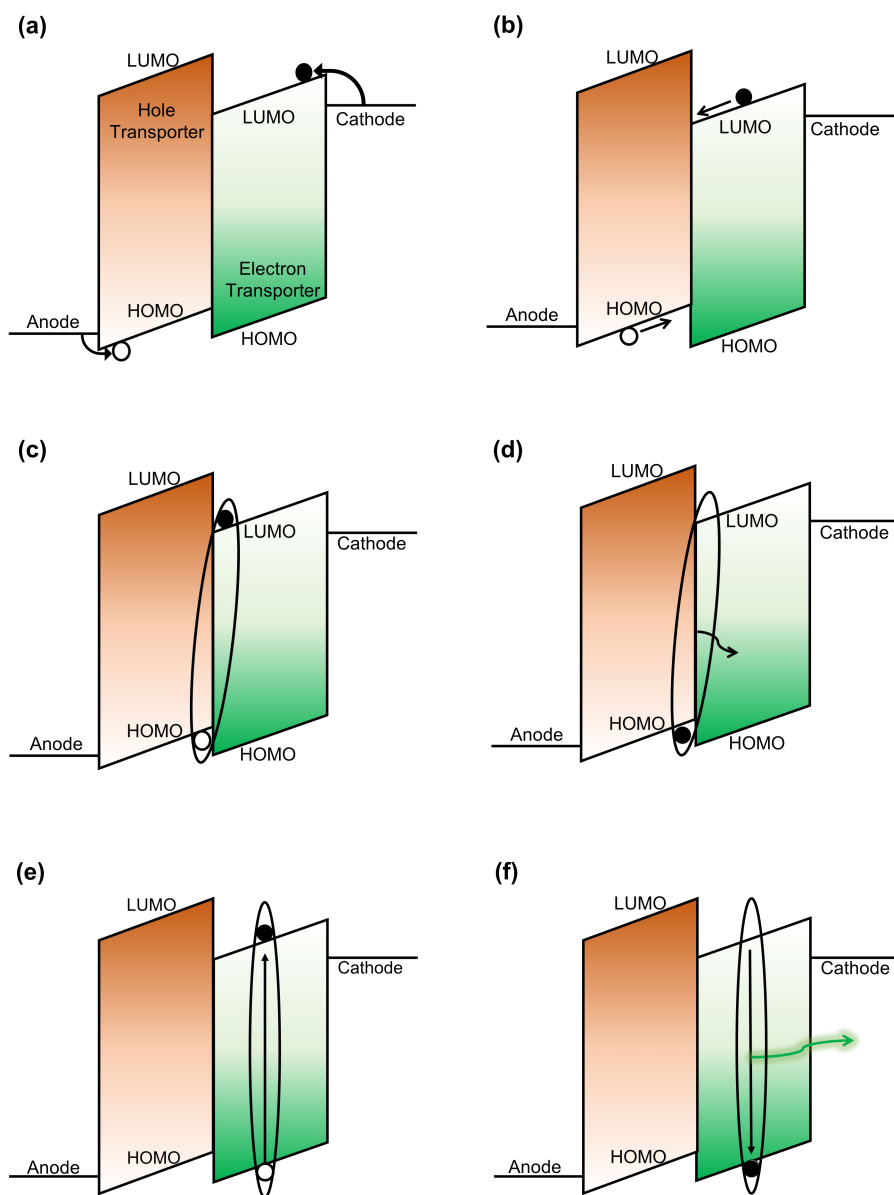
Figure 4.2: **Polyfluorene blend OLED operation scheme**. **(a)**, Electrons are injected into the electron transporting polymer (eg. F8BT) from the cathode while holes are injected into the hole transporting polymer (eg. TFB) from the anode. **(b)**, Electrons and holes travel through their respective polymers. **(c)**, At the interface between the electron and hole transporters, a bound electron/hole pair forms an exciton. **(d)**, When the exciton relaxes, its energy is transferred to the smallest band gap material, in this case the electron transporter. **(e)**, This transferred energy excites a new exciton within the small band gap material. **(f)**, When a singlet exciton relaxes in the smallest band gap material, a photon is emitted.

bandgap polymer to its LUMO, forming an exciton (Figure 4.2(e)). If that exciton is a singlet it will produce a photon upon relaxation (Figure 4.2(f)). If there is no other smaller bandgap polymer, then the photon will not be re-absorbed and may exit the film [144]. This is what happens in a TFB:F8BT film, whose electroluminesence spectrum is dominated by green emission from F8BT. For red emission, a small amount of TBT is added to the blend (TFB:F8BT:TBT, at a ratio of 25:70:5). TBT has a bandgap smaller than F8BT, so the photons omitted by the tri-blend OLED come from the TBT. TBT is a small fraction of the blend because it has poor charge transport properties, its sole function being red emission.

FRET can be experimentally observed by characterizing the absorption and photoluminescence spectra of polymer films. As shown in Figure 4.3(a), the photoluminescence spectrum of TFB overlaps the absorption spectrum of F8BT, indicating that FRET will occur and any singlet excitons at the TFB:F8BT interface (an exciton formed between two molecules is also called an exciplex) will transfer its energy to F8BT upon relaxation. The photoluminesence spectrum of F8BT overlaps with that of TFB:F8BT, proving that the emission is from the blend's F8BT dominates. Similarly in Figure 4.3(b), the photoluminescence spectrum of TFB:F8BT aligns with the absorption spectrum of TBT and the photoluminescence of the TFB:F8BT:TBT blend matches that of TBT.

Charge transport, exciton formation, and recombination in polyfluorenes is also dependent on film morphology, which in turn has been studied to be dependent on the film's processing conditions including solution concentration, solvent, molecular weight, and substrate surface energy [126, 145, 146, 147, 148]. Figure 4.4 is a tapping-mode AFM height image that shows the surface morphology of a TFB:F8BT blend thin film made from a 20 mg/mL o-xylene solution. As shown, the TFB and F8BT components of the polymer blend phase separate under these solution conditions. The dark, low-height regimes are primarily TFB and the light, taller height regimes are primarily F8BT. The TFB and F8BT regimes were determined by comparing the AFM image with a photoluminescence image taken under blue illumination in an optical microscope equipped with a filter for fluorescence imaging. As shown in the photoluminescence image of TFB:F8BT in Figure 4.5, the bright regimes are primarily F8BT and the dark regimes are primarily TFB. This multitude of separated TFB- and F8BT-rich phase domains aids in localized charge carrier confinement, promoting exciplex formation at TFB/F8BT interfaces [148].

4.2 Spin-coated red and green polyfluorene OLED fabrication

As discussed in Chapter 3, an OLED requires more than just an emissive polymer thin film - it needs electrodes to inject electrons and holes and single carrier layers to improve efficiency. The OLEDs in this chapter have a LiF/Al cathode, an ITO anode, a PEDOT:PSS PVP AI4083 hole injection layer (HIL), and a TFB electron blocking layer (EBL). As shown in the energy structure diagrams for TFB:F8BT and TFB:F8BT:TBT devices in Figure
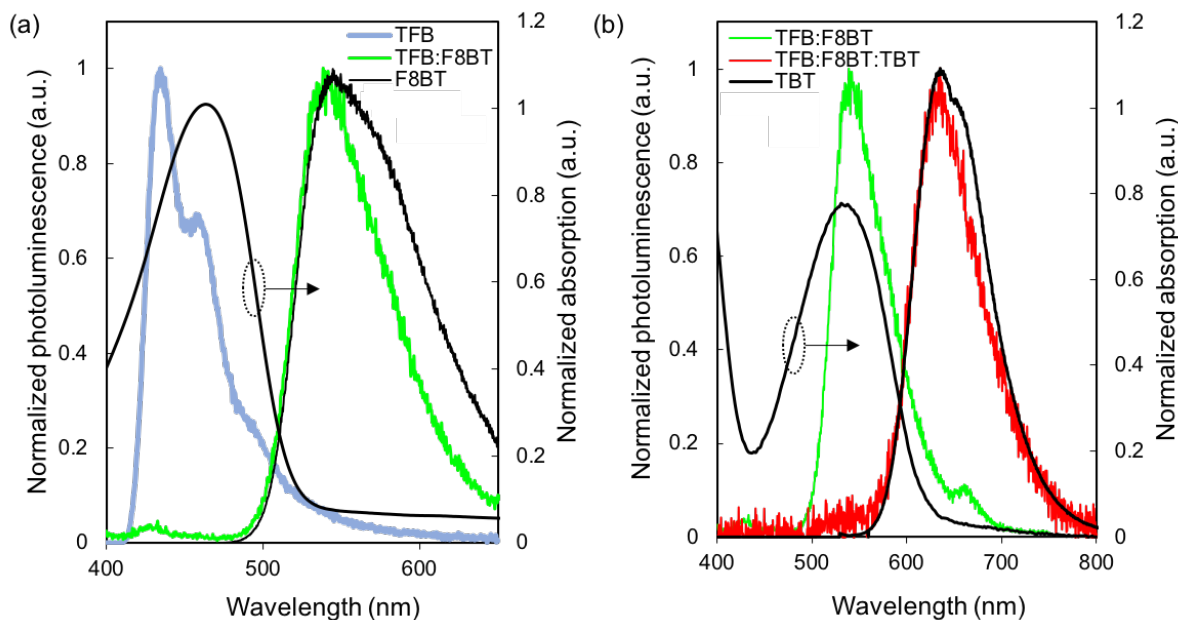
Figure 4.3: **Polyfluorene blend thin film optical characteristics**. **(a)**, The absorption
spectrum of F8BT (black line, secondary axis) overlaps the photoluminescence spectrum
of TFB (blue line), and the photoluminescence spectrum of TFB:F8BT (green line) over-
laps that of F8BT (black line, primary axis), indicating FRET occurs in the TFB:F8BT
blend. **(b)**, The absorption spectrum of TBT (black line, secondary axis) overlaps the pho-
toluminescence spectrum of TFB:F8BT (green line), and the photoluminescence spectrum
of TFB:F8BT:TBT (red line) overlaps that of TBT (black line, primary axis), indicating
FRET occurs in the TFB:F8BT:TBT blend.
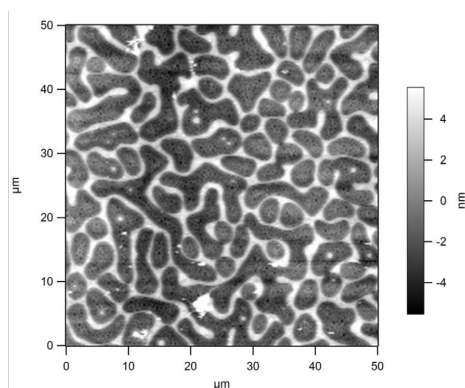
Figure 4.4: **AFM height image of a TFB:F8BT film.** The film was spin-cast from a 20
mg/mL o-xylene solution. TFB and F8BT phase separate in dried films made from o-xylene
solutions.
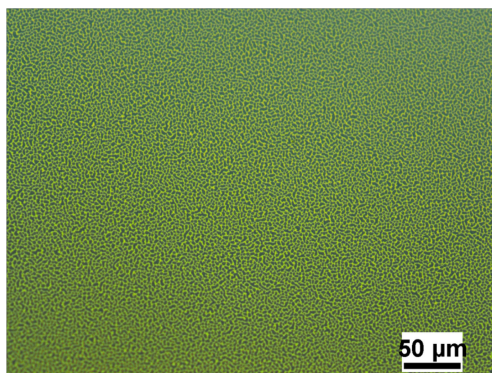
Figure 4.5: **Photoluminescence image of a TFB:F8BT film under blue excitation.**
The film was fabricated from a 20 mg/mL o-xylene solution. Dark phases are TFB and light
phases are F8BT.

4.6, the work function of the LiF/Al cathode is 3.4 eV, so there is no energetic barrier for
electron injection in to the 3.5 eV LUMO of F8BT. At the anode, the PEDOT:PSS hole
injection layer (HIL) reduces the energy barrier for hole injection from the ITO into the
HOMO of TFB, the electron blocking layer and the hole transport material in the emissive
layer. The TFB electron blocking layer between the emissive layer and the HIL prevents
exciton quenching at the electrode [121], decreasing non-radiative recombination and thus
increasing device efficiency.

Both green (TFB:F8BT, mixed at a 1:9 weight ratio) and red (TFB:F8BT:TBT, mixed
at a 25:70:5 weight ratio) OLEDs were spin-coated from 10 mg/mL o-xyelen solution on
glass substrates patterned with four 2 mm ITO strips. Pixels were defined by the overlap
between the 2 mm wide LiF/Al cathode and the ITO strips, with four 2 mm x 2 mm pixels
per substrate, as shown in Figures 4.7 and 4.8. The patterned ITO-substrates were cleaned
via sonication in acetone and then isopropyl alcohol. The substrate surfaces were made
hydrophilic with a 2 minute 50 W plasma treatment prior to spincoating a 40 nm layer of
Clevios PEDOT:PSS PVP AI4083. Any remaining moisture was evaporated in a 10 minute
annealing step at 120°C before moving the samples into a controlled nitrogen environment
for the remainder of the fabrication procedure. TFB was spin-coated from a 10 mg/mL
o-xylene solution and then annealed at 180°C for 45 minutes before cooling the sample to
room temperature and spin-rinsing the surface with 200 $/mu$L o-xylene, resulting in a 10-20
nm thick electron blocking layer. The active layer was then spun at 4500 rpm (with 1000
rps acceleration) for a 100 nm film thickness. The LiF (1 nm)/Al (100 nm) cathode was
thermally evaporated under vacuum at 4×10^{-6} Torr. Finished devices were encapsulated
with UV-curable Delo Katiobond LP612 epoxy and a clean quartz glass coverslip.

The OLEDs' irradiance and current density (J) as a function of voltage (V) are shown
in Figure 4.9. While both the red and green OLEDs have a similar J-V characteristic
(approximately 350 $mAcm^{-2}$ at 9 V), the irradiance of the green OLED is approximately
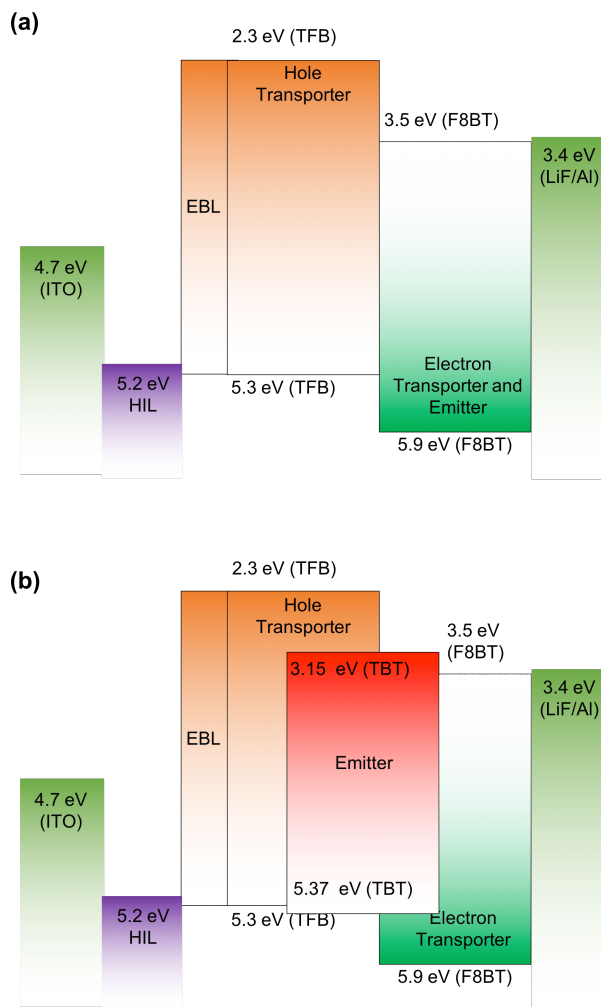
Figure 4.6: **Flatband polyfluorene OLED energy structures.** **(a)** TFB (hole trans-porter):F8BT (electron transporter and emitter) blend OLED for green emission. **(b)** TFB (hole transporter):F8BT (electron transporter):TBT (emitter) blend OLED for red emission. Both devices have an ITO anode, PEDOT:PSS PVP AI4083 hole injection (HIL)/planarization layer, TFB electron blocking layer (EBL), and LiF/Al cathode.
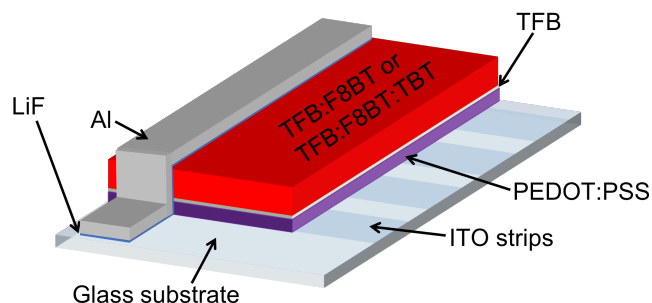
Figure 4.7: **Physical structure of a polyfluorene OLED.** The red and green polyfluorene OLEDs in this chapter were spin-coated on a glass substrate patterned with four strips of ITO (2 mm wide). Blanket coats of PEDOT:PSS, TFB, and the emissive layer were applied. Active pixel areas were defined by the overlap between the cathode and ITO strips, with four pixels per substrate. The cathode was evaporated LiF and Al.
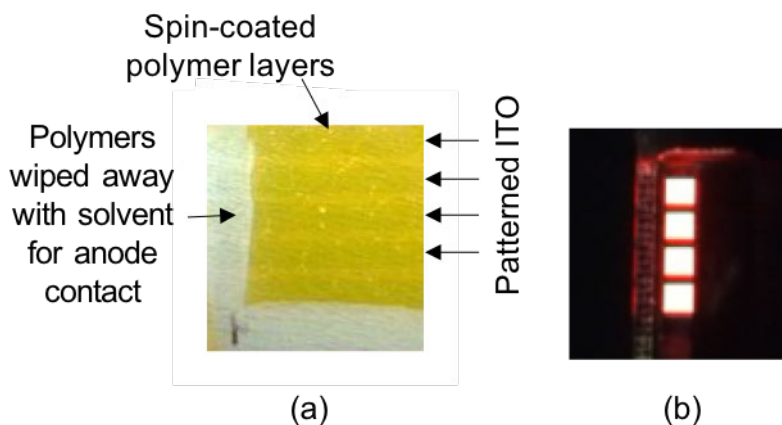
Figure 4.8: **Photographs of a spin-coated TFB:F8BT:TBT OLED. (a)** This is a photograph of a fully spin-coated TFB:F8BT:TBT stack (with PEDOT:PSS and TFB). Before cathode deposition, the polymer was wiped away from a portion of the subsrate so contact could be made with the patterned ITO. **(b)** After cathode evaporation, each substrate had four pixels. This is a photograph of four TFB:F8BT:TBT pixels in operation.
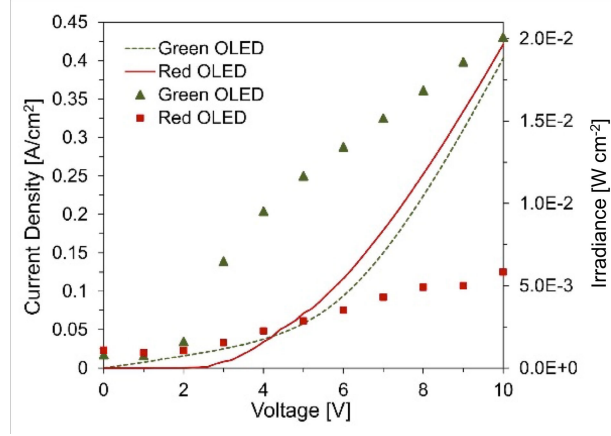
Figure 4.9: **TFB:F8BT and TFB:F8BT:TBT OLED performance**. Current density and irradiance of spin-coated TFB:F8BT and TFB:F8BT:TBT OLEDs as a function of applied voltage.

four times that of the red OLED: at 9 V, the green OLED irradiates 20.1 $mW\,cm^{-2}$ and the red OLED irradiates 5.83 $mW\,cm^{-2}$. However, the scattering of light in human tissue also decreases as wavelength increases [56], so a lower irradiance at a longer wavelength can provide at least the same signal magnitude as a shorter wavelength OLED with a higher irradiance in a biomedical measurement like pulse oximetry, the application for which these OLEDs were used.

4.3 Pulse oximetry with red and green polyfluorene OLEDs

As discussed in Chapter 2, a pulse oximeter measures a person's heart rate and oxygen saturation. Arterial oxygen saturation (SaO_2), or oxygenation, is the concentration of oxy-hemoglobin (hemoglobin bound to oxygen) in arterial blood (blood being pumped from the heart to the body (see Figure 4.10) divided by the sum of the concentration of oxy- and deoxyhemoglobin (hemoglobin not bound to oxygen) in the blood. SpO_2 is the oxygen saturation value measured by a pulse oximeter (along with heart rate) and has been shown to be representative of SaO_2 and thus a reliable indicator of acute respiratory and cardiovascular health [19]. A healthy adult's SpO_2 should be at least 95%. Once SpO_2 falls below 88%, organ function is hindered and permanent organ damage can occur [19].

In order to measure SpO_2, two light emitting diodes (LEDs) operating at different wavelengths and a photodetector (PD) sensitive to those wavelengths are required [149, 19]. The two LEDs shine light through or on the sensing location, most commonly the finger, earlobe, forehead, or wrist, and the photodetector (on the opposite side of the sensing location for transmission mode, or next to the LEDs for reflection mode) senses the amount of light that
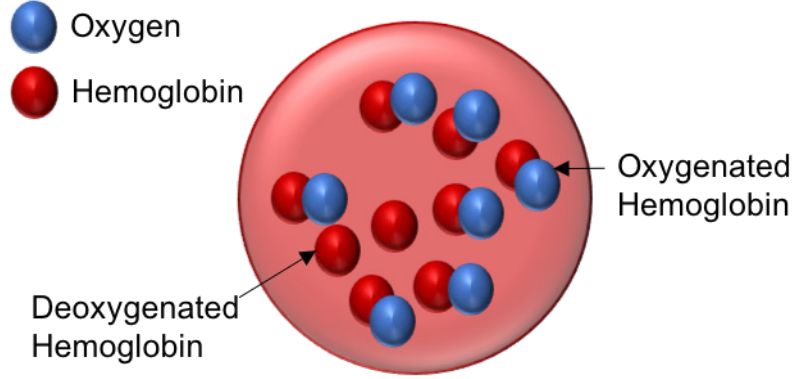
Figure 4.10: **An arterial red blood cell** contains hemoglobin (red) and oxygen (blue) molecules. Hemoglobin is oxygenated when it is bound to an oxygen molecule, and doxygenated when it is not bound to oxygen. Arterial blood cells are pumped into the body by the heart after receiving oxygen from the lungs, and so most hemoglobin species in an arterial red blood cell should be oxygenated.

passes through the tissue, as shown in Figure 4.11(a)). The highest attenuator of that light is blood, and the absorptivity of blood is dependent on both wavelength and the presence of oxygen. Figure 4.12(a) plots the absorptivity of oxygenated and deoxygenated hemoglobin as a function of wavelength. Both blood volume and the concentration of oxyhemoglobin in the blood determines the intensity of light read by a pulse oximeter's photodetector. During the heart beat's systole phase, the transmitted light decreases because there is a high volume of arterial blood flowing through the tissue. During the heart's diastole phase, there is less arterial blood flowing and the amount of transmitted light increases. This fluctuation in arterial blood volume translates to a pulsatile, AC signal. The photodetector signal in a pulse oximeter is called a photoplethysmogram, or PPG. (A schematic of this process is reproduced here in Figure 4.11 from Figure 2.3(a) for the reader's benefit.) There is also a DC portion of the signal resulting from the non-pulsating venous blood and other tissue, which is subtracted from the pulsating signal in the PPG. SpO_2 is derived from the ratio of the photodetector signal upon excitation by each LED and the known absorptivity of oxy- and deoxyhemoglobin at each peak wavelength [22, 150, 19]. Pulse, or heart rate, is derived from the time between peaks in the PPG (Figure 4.11(c)).

Blood oxygen saturation (SO_2) is quantified according to Eq. 4.1. Here, C_{HbO_2} and C_{Hb} are the concentration of oxy-hemoglobin and deoxy-hemoglobin, respectively.

$$SO_2 = \frac{C_{HbO_2}}{C_{HbO_2} + C_{Hb}} \times 100\% \tag{4.1}$$

R_{os}, the ratio of absorbed light from the first light source (A_{λ_1}) and the second light source (A_{λ_2}), depends on the normalized transmitted light intensities at the first wavelength λ_1
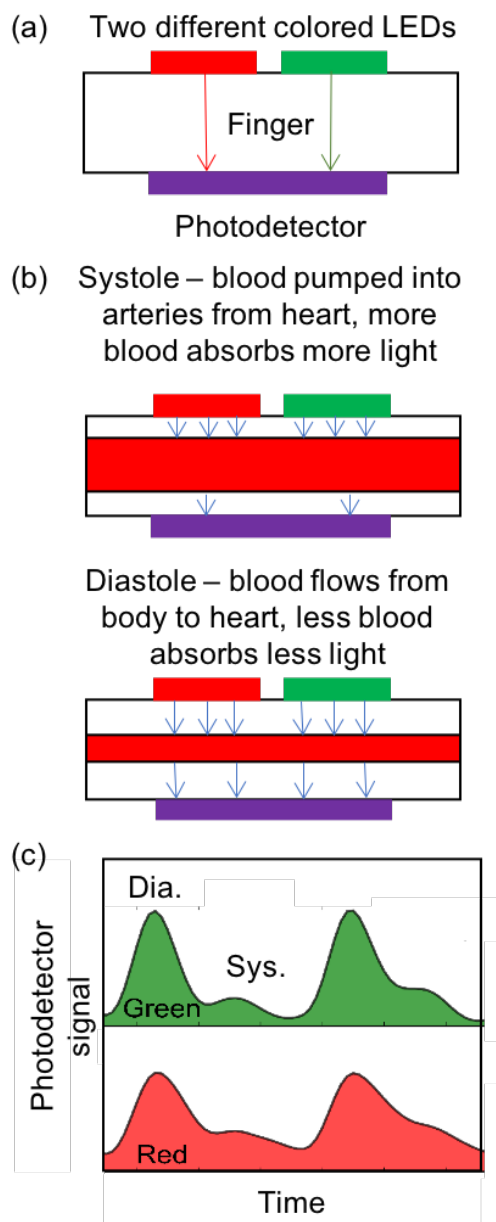
Figure 4.11: **Schematic of photoplethysmogram (PPG) acquisition with a transmission mode pulse oximeter finger probe. (a)** Two different colored LEDs irradiate the finger with a photodetector on the other side. **(b)** During the systole phase of the heart beat, the volume of blood in the arteries is at a maximum, more light is absorbed in the blood, and less light reaches the photodetector. During the diastole phase of the heart beat, the volume of blood in the arteries is at a minimum, less light is absorbed in the blood, and more light reaches the photodetector. **(c)** The photoplethysmogram (PPG) is read from the photodetector signal, with a peak during the heart's diastole phase and a trough during its systole phase.

(T_{n,λ_1}) and the second wavelength λ_2 (T_{n,λ_2}) according to Beer-Lambert's law (shown in Eq. 4.2) [19].

$$R_{os} = \frac{A_{\lambda_1}}{A_{\lambda_2}} = \frac{-ln(T_{n,\lambda_1})}{-ln(T_{n,\lambda_2})} \tag{4.2}$$

Oxygen saturation (SO_2) is calculated from R_{os} calculated using Eq. 4.3. Here, $\varepsilon_{\lambda_1,Hb}$ and $\varepsilon_{\lambda_2,Hb}$ are the absorptivities of deoxyhemoglobin at λ_1 and λ_2, respectively. $\varepsilon_{\lambda_1,HbO_2}$ and $\varepsilon_{\lambda_2,HbO_2}$ are the absorptivity of oxyhemoglobin at λ_1 and λ_2 wavelengths, respectively.

$$SO_2(R_{os}) = \frac{\varepsilon_{\lambda_1,Hb} - \varepsilon_{\lambda_2,Hb}R_{os}}{(\varepsilon_{\lambda_1,Hb} - \varepsilon_{\lambda_1,HbO_2}) + (\varepsilon_{\lambda_2,HbO_2} - \varepsilon_{\lambda_2,Hb})R_{os}} \tag{4.3}$$

Beer Lambert's law does not take scattering into account, but light is scattered in human tissue. Thus the oxygenation value derived from the above equations must be weighted by a calibration curve specific to the pulse oximeter in use in order to give a valid SpO_2 value. The calibration used for the organic optoelectronic oximeter implementing the OLEDs in this chapter is discussed in the supplementary information of the work by Lochner et al. [22].

Traditional transmission mode pulse oximeters use red and near-infrared (NIR) LEDs. At the time that this work was ongoing, however, solution-processable near-infrared OLED materials were not stable in air, very difficult to synthesize, and/or had high turn-on voltages (while one of the goals of this work was to demonstrate a pulse oximeter could be battery-powered) [151, 152]. Thus we elected to use red and green OLEDs instead of red and NIR. The green OLED had a 532 nm peak wavelength and the red OLED had a 626 nm peak. The full emission spectra of each OLED is plotted in Figure 4.12(b). The difference in the absorptivity of oxygenated and deoxygenated hemoglobin at 532 nm is comparable to the difference at the near-infrared wavelengths (800-1000 nm) used in conventional pulse oximeters, as shown in see Figure 4.12(a), so it is an acceptable substitution.

The first test for the OLEDs was to see if they could transmit a signal through a finger. Green and red OLEDs were independently placed on one side of a subject's finger while an inorganic silicon photodiode was place on the other to generate a PPG from each OLED. To ensure the silicon photodiode's functionality, PPGs were also acquired from inorganic infrared (IR) and red LEDs. The smoothed PPGs acquired from the silicon photodiode and each OLED and LED are shown in Figure 4.13. A clear PPG signal was acquired with both sets of LEDs; the green and red OLEDs were able to generate a PPG in the silicon photodetector. (Yasser Khan was responsible for the control electronics and software used for PPG and oxygenation measurements. For a full description, see "System design for organic pulse oximeter" by Khan et al. [150]).

For a closer look at the OLED signal quality, the pulse waveforms (two cardiac cycles worth) generated with a combination of organic and inorganic devices are shown in Figure 4.14. The PPG obtained when a human finger is illuminated by inorganic LEDs and the
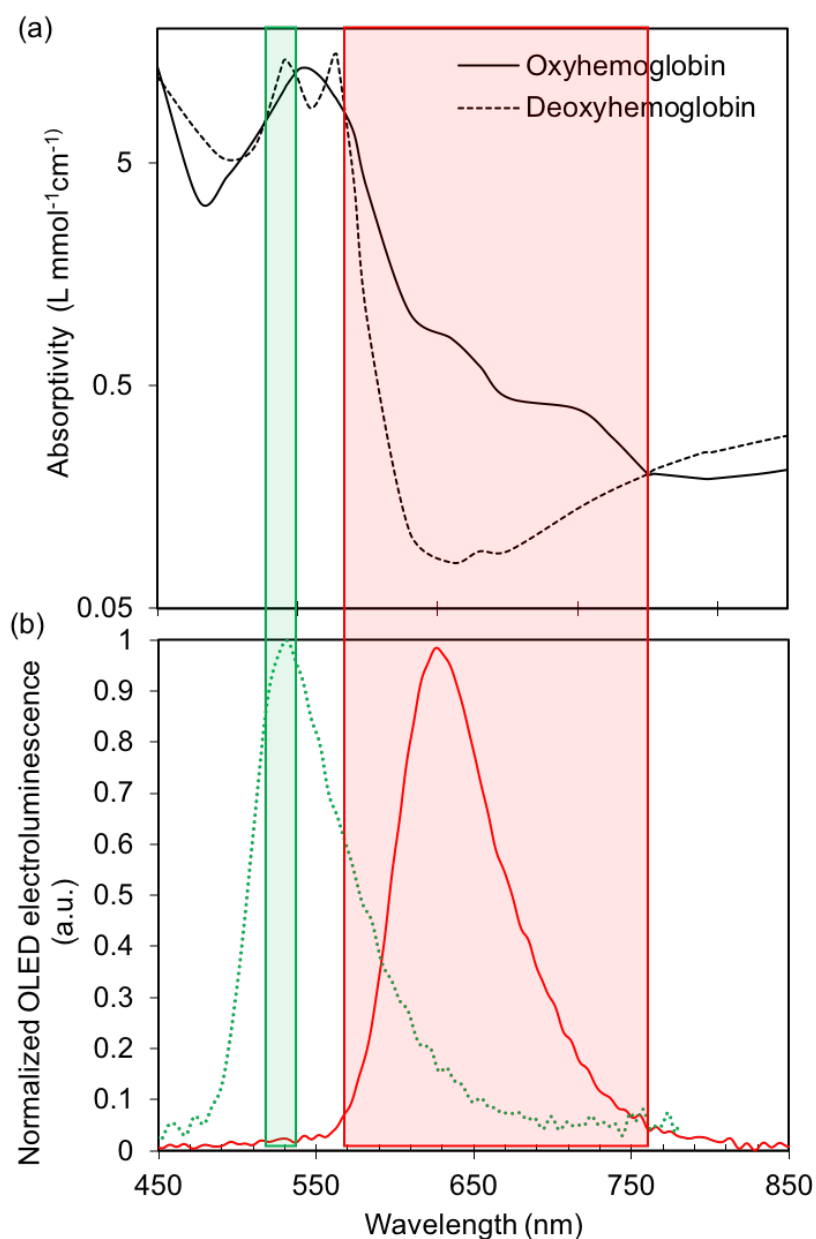
Figure 4.12: **(a) Absorptivity of oxygenated (orange solid line) and deoxygenated (blue dashed line) hemoglobin in arterial blood as a function of wavelength.** The wavelengths corresponding to the peak OLED electroluminesnce (EL) spectra are highlighted to show that there is a difference in deoxy- and oxyhemoglobin absorptivity at the wavelengths of interest. **(b) Electroluminescence spectra of red (red solid line) and green (green dashed line) polyfluorene OLEDs.**
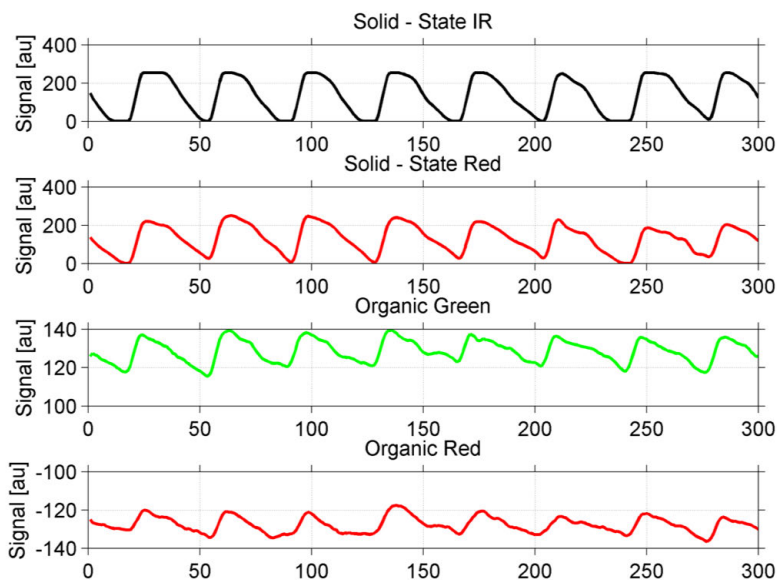
Figure 4.13: **Smoothed PPG** acquired with a silicon photodiode and **(top)** inorganic NIR
LED, **(second from top)** inorganic red LED, **(second from bottom)** green OLED, and
(bottom) red OLED. (Yasser Khan was responsible for the control electronics and software
used for PPG and oxygenation measurements. For a full description, see "System design for
organic pulse oximeter" by Khan et al. [150]).

transmitted light is measured with an OPD is shown in Figure 4.14a. When the same
measurement is performed using OLEDs and a Si photodiode (Figure 4.14b), the magnitude
of the PPG signal is reduced from 26 mV_{p-p} to 16 mV_{p-p} the green and 16 mV_{p-p} to 6
mV_{p-p} for the red due to the lower irradiance of the OLEDs compared to their inorganic
counterparts. Finally both OLEDs and an OPD are used to obtain a PPG (Figure 4.14c),
yielding signal magnitudes of 3 mV_{p-p} for the green and 2.5 mV_{p-p} for the red. A schematic of
the OLED and OPD configuration on the subject's finger for this test is shown in figure 4.15.
In Figure 4.14, it is clear that the magnitude of the signal is reduced with the introduction of
organic-based devices. However, the PPG singals for each device combination has a similar
shape, which will result in similar pulse values. Furthermore, oxygenation is not derived
from PPG signal magnitude, but from the ratio of the PPG signals at each wavelength. As
long as the magnitude is high enough for a pulsating PPG to be resolved, it is enough for a
pulse and oxygenation measurement.

   Two of the benefits of using organic optoelectronics in a pulse oximeter lie in scaling and
flexibility. The active area of both the OLED and OPD can be scaled with relative ease and
low cost compared to solid state devices. As the active area of either device increases, the
magnitude of the photodetector current (I_{OPD}) increases, as shown in Figure 4.16(a). Thus
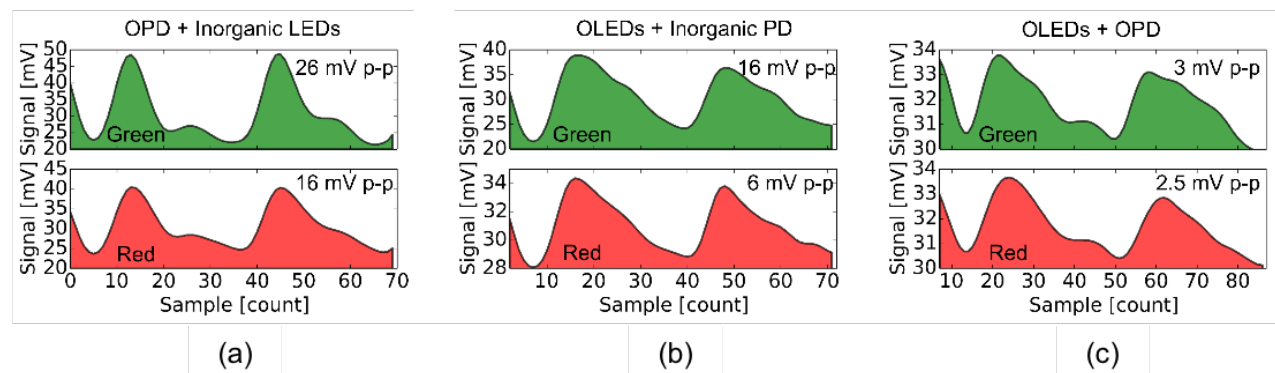
art

Figure 4.14: **Photoplethysmograms (PPGs) acquired using combinations of inorganic and organic LEDs and photodiodes (PDs).** **(a)** PPG signal acquired using inorganic red and green LEDs and an OPD. Green and red PPG signal amplitudes of 26 mV_{p-p} and 16 mV_{p-p} were obtained, respectively. **(b)** PPG Signal acquired using OLEDs and silicon PD - reduced irradiance of the OLEDs bring down signal magnitude to 16 mV_{p-p} and 6 mV_{p-p} upon green and red excitation. **(c)** PPG signal acquired using OLEDs and OPD; although signal magnitudes are reduced to 3 mV_{p-p} and 2.5 mV_{p-p}, the signal is sufficient for resolving the PPG waveform and provide the light absorption ratio (R_{os}) information for blood oxygenation calculation.
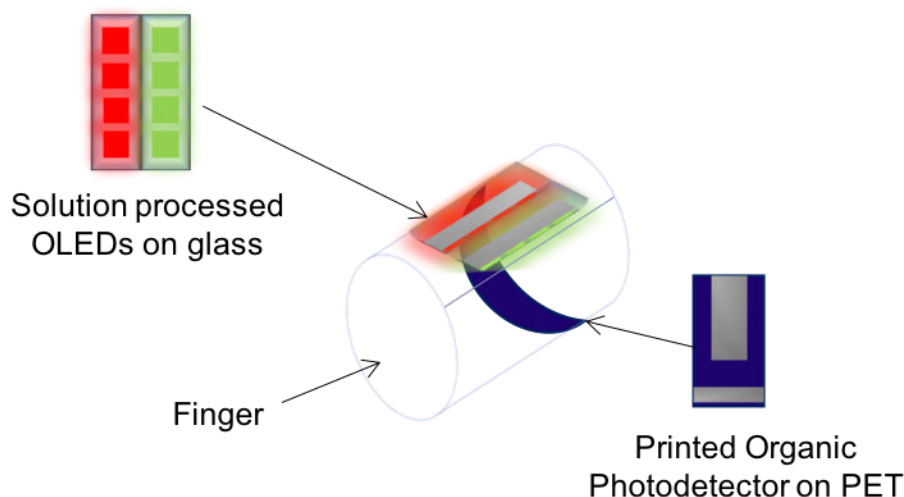
Figure 4.15: **Schematic of an all-organic optoelectronic transmission mode pulse oximeter.** Green and red OLEDs spin-cast on a glass substrate were placed on the top, finger-nail side of the user's finger. One to four pixels of each OLED could be used. An organic photodetector printed on PEN (designed and fabricated by Dr. Adrien Pierre), was placed on the bottom side of the finger.
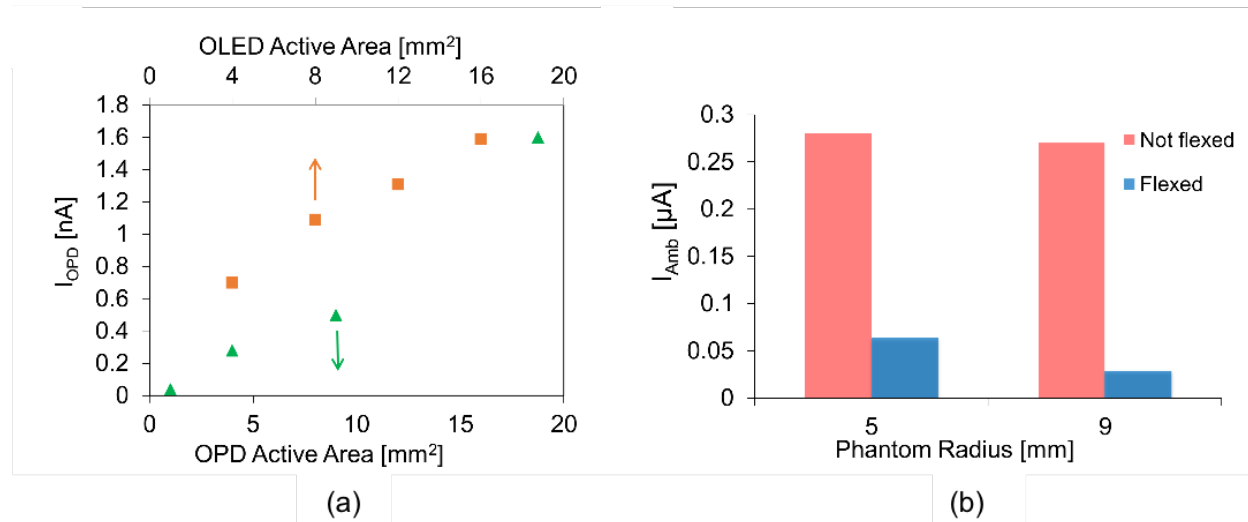
Figure 4.16: **Area scaling effects of OLEDs and OPDs in a pulse oximeter, and reducing ambient noise by flexing the OPD around a finger phantom.** **(a)** OPD current (I_{OPD}) was observed for different OLED and OPD active areas. As expected, higher photo-current resulted with area scaling of the OLEDs and OPDs. **(b)** OPDs were flexed around 5 mm and 9 mm radius phantoms representative of small and large human fingers. 79% and 93% reduction in ambient noise were observed for the OPDs flexed around the phantoms, respectively.

scaling the OLED and OPD acvite areas can make the acquisition of the PPG signal easier. While the OLEDs used in this work were not flexible (flexible OLEDs will be presented in the next chapter of this thesis), the benefit of flexibility was demonstrated with the printed OPD. Ambient noise measurements were performed using the OPD and optical phantoms representing a small and large sized human adult finger (5mm radius and 9 mm radius, respectively), where ambient noise is the photocurrent in the OPD generated by ambient room lighting, a source of noise and inaccuracy in pulse oximeters. OPD photocurrent measurements were taken when the OPD was flexed around each finger phantoms, and when it was not flexed but just held against the phantom. The ambient photocurrent was at least 5 times greater for the unflexed OPD than the flexed, as shown in Figure 4.16(b). This demonstrates that the flexible OPD would have a higher SNR in a pulse oximeter worn on a finger than an inflexible PD.

The final test for the all-organic optoelectronic pulse oximeter using red and green OLEDs was to compare it to a commercially available pulse oximeter meant for clinical use on a human test subject. The commercial pulse oximeter was worn on the index finger of the subject's left hand and the all-organic optoelectronic sensor was worn on the subject's right hand, shown in 4.17. PPGs were recorded simultaneously from each sensor. The measured PPG, heart rate, ratio of absorbed red and NIR or red and green light (R_{os}), and derived
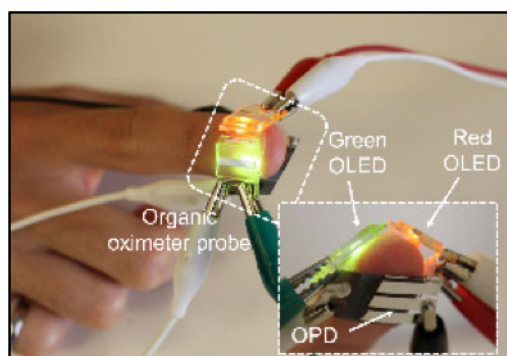
Figure 4.17: **Photograph of an all-organic optoelectronic pulse oximeter finger
probe.**
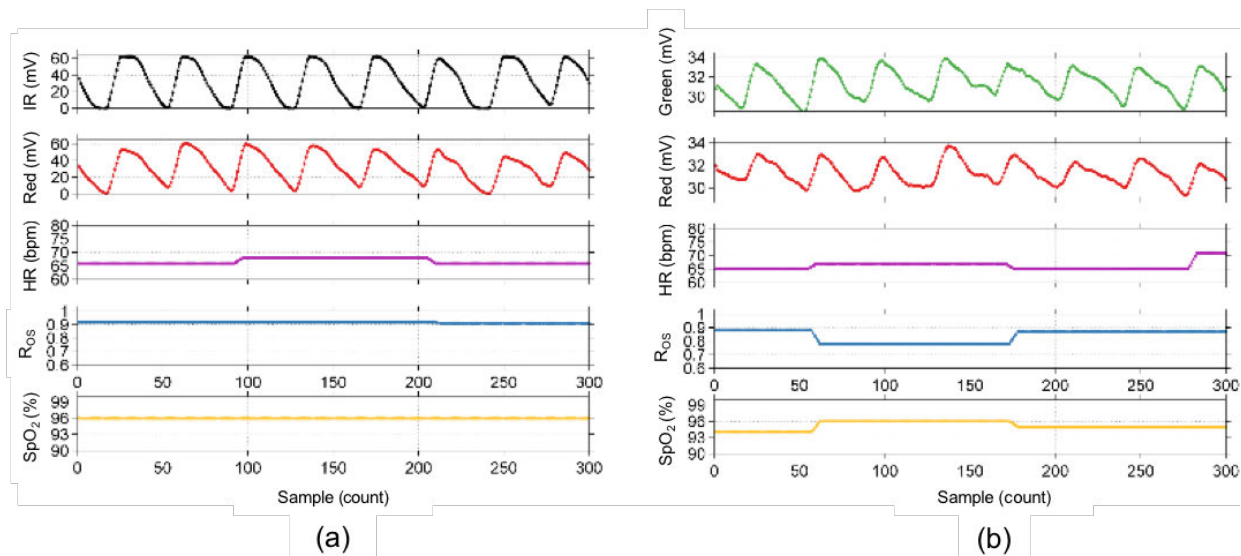
Figure 4.18: **Simultaneously acquired PPG, heart rate, R_{os}, and SpO_2 from (a) an
inorganic commerical pulse oximeter and (b) an all-organic optoelectronic pulse
oximeter.**

SpO_2 are shown for both sensors in Figure 4.18. As expected, the PPG magnitudes were
higher for the commercial oximeter. However, the heart rate and oxygenation values acquired
by each oximeter were in agreement with less than 2% error, proving that the red and green
OLEDs implemented in an organic optoelectronic sensor can accurately measure heart rate
and oxygen saturation.

This organic optoelectronic pulse oximeter demonstrated the potential for OLEDs in
biomedical applications. Looking at Figure 4.17, this pulse oximeter was not imperceptibly
wearable - the OLEDs, while solution processed, were spin-cast on inflexible glass substrates

with ITO anodes. Now that a proof-of-concept optical biomedical device using solution processable OLED materials has been presented, the coming chapters will delve into the design and development of printed and flexible OLEDs for wearable biomedical devices.

Chapter 5

ITO-free polymer NIR OLED printed on a PEN with a thermally evaporated WO$_3$/Ag/WO$_3$ anode

To make OLEDs truly wearable, they must be fabricated on flexible substrates. To achieve high volume low-cost devices, OLEDs should be printed. Most OLEDs fabricated on flexible substrates use ITO as an anode. ITO is commonly used as an anode because it has both high transparency and conductivity [153, 154, 155, 156]. However, ITO is intrinsically brittle, making it a non-ideal electrode for a flexible device [157, 158, 159]. Furthermore, one of the motivations for printed electronics is minimally wasteful additive processing, but patterned ITO electrodes require an etch step - a subtractive process that reduces material use efficiency and produces toxic waste. Many ITO alternatives have been investigated, including carbon nanotubes, metallic nanowires, and conductive and transparent oxides [159, 160, 161]. This chapter presents a NIR polymer OLED printed on a WO$_3$/Ag/WO$_3$ dielectric-metal-dielectric (DMD) anode with 100% additive processing.

5.1   Thermally evaporated WO$_3$/Ag/WO$_3$ electrode

DMD structures have been shown to be a compromise between transparency, conductivity, flexibility, ease of fabrication, and cost [162, 163, 164, 165, 166]. While conductive, a thin metal film on its own suffers from low transmittance because of its high level of surface reflection. Surface reflection is suppressed and overall transmittance is enhanced by sandwiching the thin metal film between two layers of a dielectric with a high refractive index [167, 168].

The DMD structure used in this work is WO$_3$/Ag/WO$_3$, which has previously been demonstrated to be semi-transparent, conductive, and flexible [163, 165, 169, 170, 171]. Between 550 and 900 nm, the refractive index of WO$_3$ ranges from 1.90 to 1.97 [172] and the refractive index of Ag ranges from .124 to .18 [173], satisfying the condition of a low index
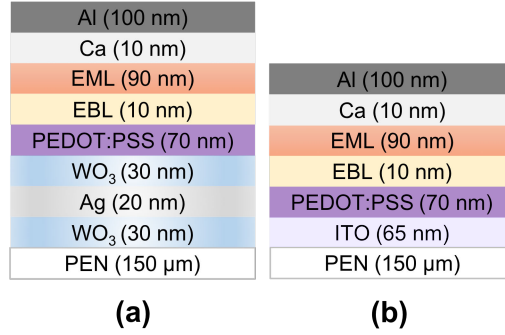
Figure 5.1: **The physical structure of printed polymer NIR OLEDs on PEN with (a)** a WO$_3$/Ag/WO$_3$ anode and textbf(b) an ITO anode.

material sandwiched between a high index material for suppressed reflection.

J. H. Han et al. demonstrated flexible and conductive color filters made from thermally evaporated alternating WO$_3$ and Ag films on a polyethylene terephthalate (PET) substrate [165]. The electrode maintained is conductivity and optical characteristics after a 10,000 cycle bending test around a 10 mm radius. K. Hong et al. demonstrated a fully operational top-emitting OLED with a transparent WO$_3$/Ag/WO$_3$ cathode, all layers of which were thermally evaporated on a glass substrate [171]. Because WO$_3$ has a relatively high work function (4.90 eV), thin LiF/Al layers (conventional OLED cathode materials) were still employed in order to decrease the energy barrier between the cathode and the emissive layer for improved electron injection. The high work function of the WO$_3$/Ag/WO$_3$ makes it more suitable as an anode than a cathode. J. H. Han et al. demonstrated a thermally evaporated red top-emitting OLED with a transparent WO$_3$/Ag/WO$_3$/Ag/WO$_3$ anode on glass and polyethylene terephthalate (PET) substrates [169]. The devices fabricated on PET remained operational while bent, demonstrating the flexibility of a WO$_3$ and Ag electrode in an OLED.

Here, we demonstrate the first NIR polymer OLED printed on a plastic polyethylene napthalate (PEN) substrate with a WO$_3$/Ag/WO$_3$ bottom anode. OLEDs were also printed on a PEN/ITO substrate for direct comparison. The physical structures for each OLED are shown in Figure 5.1. The PEN substrate was purchased with a planarization layer from Dupont Teijin Films (PQA1). The first printed layer on top of the anode was PEDOT:PSS, a smoothing hole injection layer [174]. The next layer was a polymer electron blocking layer (EBL) that prevents non-radiative exciton quenching at the anode [121]. The polymer NIR emissive layer (EML) was then printed and a Ca/Al cathode was thermally evaporated through a shadow mask, defining the active OLED area where cathode and anode layers overlap. The thickness of each polymer layer shown in Figure 1(a) was measured by a Dektak Profilometer.

For the WO$_3$/Ag/WO$_3$ anode OLEDs, each WO$_3$ layer was 30 nm thick and the Ag layer was 20 nm thick, resulting in a semitransparent film with a sheet resistance of 2.06$\pm$.14
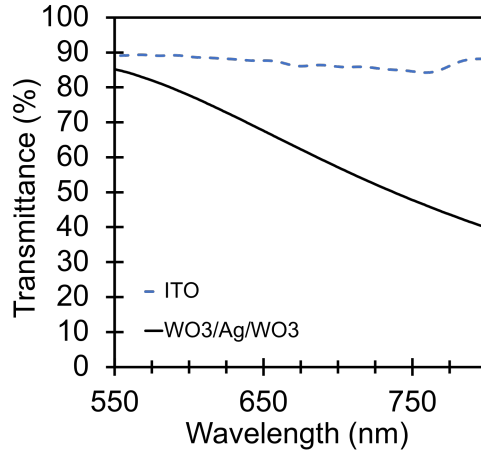
Figure 5.2: **ITO and $WO_3/Ag/WO_3$ transmission spectra.** ITO transmittance (dashed blue line) remains relatively constant at 87% from 550 - 800 nm. The transmittance of the $WO_3/Ag/WO_3$ anode (solid black line) decreases from 85% at 550 nm to 39.8% at 800 nm.

Ω/sq. (as measured by a four-point probe). The transmittance of the $WO_3/Ag/WO_3$ film is shown as a function of wavelength in the inset of Figure 5.2, measured with a Shimadzu UV-Vis-NIR spectrometer. While the transmittance of the ITO anode was relatively constant at 87%, the transmittance of the thermally evaporated $WO_3/Ag/WO_3$ decreased from a maximum of 85% at 550 nm to a minimum of 39.8% at 800 nm, as shown in Figure 5.2.

5.2 Blade coated OLED fabrication

Aside from their anodes, the ITO and $WO_3/Ag/WO_3$ OLEDs had an identical fabrication procedure. For the $WO_3/Ag/WO_3$ anode devices, a PEN substrate (PQA1 from Dupont Teijin Films) was adhered to a glass carrier with Gel Pak DGL X4 6.5 mil (thermally stable up to 225°C) in order to prevent substrate deformation during the multiple heating stages in the fabrication process. The substrate came covered by a protective liner that was removed from the PEN before dehydrating the sample in a vacuum oven at 180° for 3 hours. The substrate was then treated with an oxygen plasma (50 W for 15 seconds) before thermally evaporating a strip of $WO_3/Ag/WO_3$ defined by a shadow mask. First, 30 nm of WO_3 was thermally evaporated at a rate of 2 Å/s. The 20 nm Ag layer was evaporated at a rate of 9 Å/s, followed by the final 30 nm of WO_3, which was evaporated at 2 Å/s. A fifteen-minute interval took place between each evaporation step to let the system cool, and each evaporation took place under 4×10^{-6} Torr vacuum. For ITO anode devices, planarized PEN substrates with patterned ITO were supplied by Cambridge Display Technology and were also dehydrated in a vacuum oven at 180^{circ}C for 3 hours and treated with oxygen plasma (50 W for 15 seconds) before printing subsequent layers.

The printed polymer layers (PEDOT:PSS, EBL, and EML) were blade coated using a
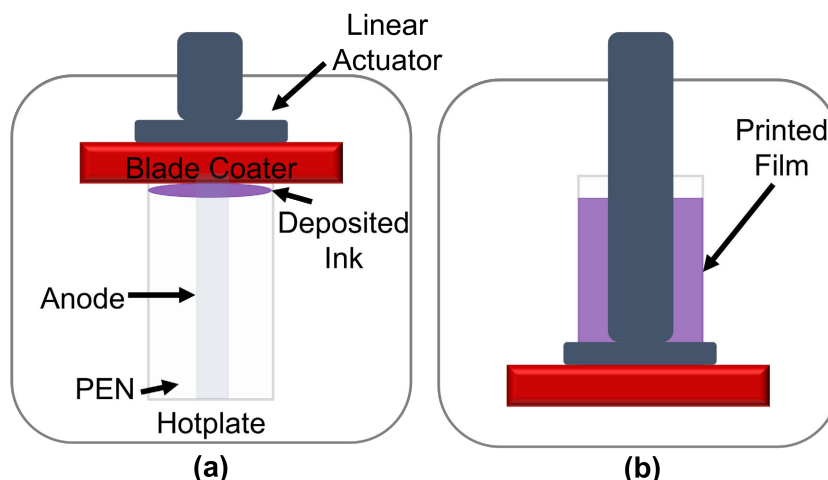
Figure 5.3: **Schematic of the blade coating process.(a)** The substrate is secured to a
hotplate (with Kapton tape). The blade coater (Zehntner ZUA 2000.80 universal applicator),
is positioned at the top of the substrate with a set blade height. Ink is deposited onto the
substrate immediately in front of the blade coater's blade edge. **(b)** A linear actuator moves
the blade coater forward at a set uniform speed. A meniscus forms between the blade and
the deposited ink. The blade coater pushes the meniscus across the substrate, depositing a
film of the ink material.

using a Zehntner ZUA 2000.80 blade coater, as shown in Figure 5.3. The substrates were
secured to a hot plate with Kapton tape in order to adjust the substrate temperature during
printing. A pipette was used to deposit polymer solution inks onto the substrate directly
in front of the blade coater (see Figure 5.3(a)), which was moved over the substrate at a
constant speed by a linear actuator. As the blade coater moved forward, the polymer inks
were spread out over the substrate, as shown in Figure 5.3(b). The hot plate temperature
was adjusted to hasten the ink's drying in order to prevent mottling, but not too hot so as
to dry the majority of the ink at the top of the substrate. The ink volume, distance between
the blade and the substrate (blade height), and print speed were experimentally determined
to achieve desired printed layer thicknesses.

   The thickness of a blade coated film can be altered by changing the ink volume, print
speed, blade height between the blade and the substrate, and/or ink concentration [175].
For example, when the EML polymer ink was printed with a 200 μm blade height, 60 μL ink
volume, 65^{circ}C substrate temperature, and 3 cm/s print speed, the printed film thickness
ranged from 50 nm at 3 cm down from the start of the print, to 20 nm at 5 cm from the
start of the print, to running out of ink before reaching the bottom of the print (7 cm from
the start). A schematic of the printed film distance measured from the start of the print
is shown in Figure 5.4. When the ink volume was increased to 120 μL, the EML thickness
ranged from 130 $\pm$ 5 nm at 3.5 cm from where the ink was deposited, to 104 $\pm$ 4 nm at 5

Anode   Printed
         Film

0 cm
1 cm
2 cm
3 cm
4 cm
5 cm
6 cm
7 cm
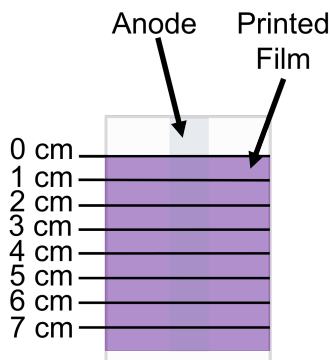
Figure 5.4: **Printed film thickness measurement scheme.** Printed polymer films were measured with a DekTak Profilometer in the center of the printed film, over the anode, at regular distances from the start of the print.

cm down the substrate, to 90 ± 6 nm at 6 cm down, to 70 ± 8 nm at 7 cm from where the ink was deposited.

The PEDOT:PSS used was Clevios P VP AI 4083 (Haerus). In order to improve print yield, Zonyl FSO fluorosurfactant (Sigma Aldrich) was mixed into the PEDOT:PSS solution at a .05 wt% concentration to improve its wetting properties on the $WO_3/Ag/WO_3$ anode. The PEDOT:PSS:surfactant solution had a 48 degree contact angle on $WO_3/Ag/WO_3$, as shown in Figure 5.5(a). 80 μL of the PEDOT:PSS and surfactant solution was blade coated in air while the substrate was heated to 90^{circ}C. The height between the blade and the substrate was 75 μm and the print speed was 3 cm/s. The sample was then annealed in a vacuum oven at 120^{circ}C for one hour in order to evaporate remaining solvent from the printed film.

The PEDOT:PSS .05 wt% Zonyl fluorosurfactant films showed greater film uniformity with distance from the start of the print. At 3.5 cm from the start of the print, the PEDOT:PSS film was 90 nm thick, 80 nm thick at 4 cm, and 70 nm thick from 4.5 cm to 7 cm. The OLED data within this work was measured from OLEDs fabricated the same distance from the start of the print on both the ITO and $WO_3/Ag/WO_3$ anodes to ensure that the polymer layer thicknesses were the same.

After annealing the PEDOT:PSS film, its surface was treated with oxygen plasma at 50 W for 7 seconds in order to increase its hydrophilicity. Without this plasma treatment, the EBL did not wet the surface of the PEDOT:PSS. After the plasma treatment, the EBL had a 27^{circ} contact angle with the PEDOT:PSS film, as shown in Figure 5.5(b). The EBL material itself, known as IL-2, was a proprietary material supplied by Cambridge Display Technology and dissolved in o-xylene at a 6 mg/mL concentration. It was printed in a controlled nitrogen environment with a 50 μm blade height, 80 μL ink volume, 90^{circ}C substrate temperature, and 1.4 cm/s print speed. The sample was then annealed at 180^{circ}C in vacuum for one hour, heating the EBL above its glass transition temperature in order to avoid dissolution

.05 wt% zonyl surfactant
PEDOT:PSS PVP AI4083
on WO₃

IL-2 on .05 wt% zonyl
surfactant PEDOT:PSS PVP
AI4083

(a) (b)
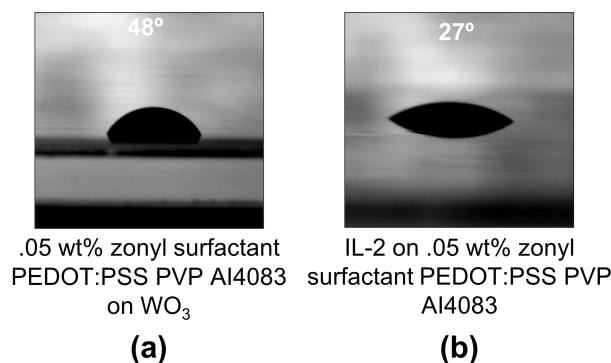
Figure 5.5: **Goniometric image of (a) PEDOT:PSS PVP AI4083 .05 wt% Zonyl surfactant on WO₃ and (b) IL-2 on a plasma treated PEDOT:PSS film** The contact angle is of the PEDOT:PSS .05 wt% zonyl surfactant is 48 degrees and the contact angle of IL-2 on the plasma treated PEDOT:PSS is 24 degrees, indicating preferential wetting properties for each ink on its printing surface.

upon printing the emissive layer (EML) with a non-orthogonal solvent. The sample was cooled to room temperature before printing the EML. The EML polymer was dissolved at 15 mg/mL in toluene. It was printed in nitrogen with a 200 μm blade height, 120 μL ink volume, 65^{circ}C substrate temperature, and 3.0 cm/s print speed. The sample was annealed at 150^{circ}C for 30 minutes under vacuum in order to evaporate any toluene remaining in the printed film.

After all of the polymer layers had been printed, the cathode was thermally evaporated. 10 nm of Ca was evaporated at a rate of 2 Å/s, and 100 nm of Al was evaporated at a rate of 3 Å/s over the course of two evaporation stages (50 nm per stage) under 4×10^{-6} Torr. The system was allowed to cool for 15 minutes between each evaporation stage. Once the cathode evaporation was complete, the system was allowed to cool for 30 minutes before removing the sample. The finished devices were encapsulated in a nitrogen environment with Delo Photobond LP424, an ultra-violet (UV) curable epoxy (the thermal evaporator was in the same nitrogen glovebox where the devices were encapsulated so that calcium degradation would not occur in between the two processes). Epoxy was deposited over the active pixel area (defined by the overlap between anode and cathode layers) and covered with a PEN cover-slip. The epoxy was then cured with a 30 W UV lamp for ten minutes before exposing the OLEDs to ambient air for testing.

It is worth noting that while the blade coating method described here is sufficient for a small-scale research laboratory operation, a uniform printed film thickness over the entire length of substrate is desired for large scale manufacturing. By adding a constant supply of ink throughout a print as opposed to a single reservoir at the top of the substrate, the amount of ink between the blade and the substrate can remain constant and thus film thickness uniformity would be improved, as is the case with slot die coating [176].
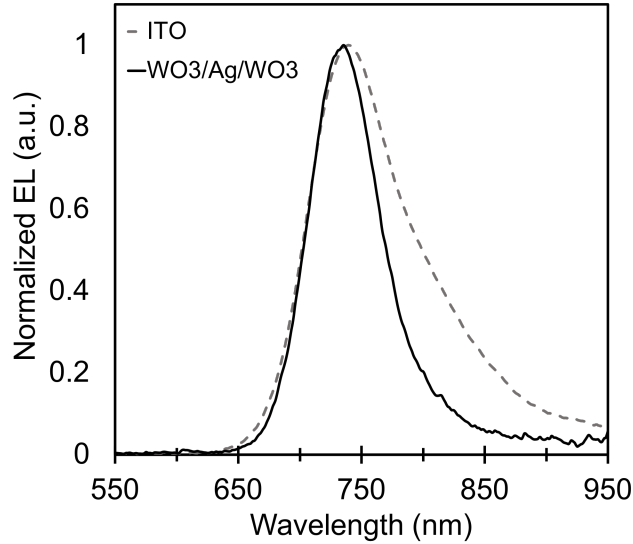
Figure 5.6: **Emission spectra of NIR OLEDs printed on ITO and WO$_3$/Ag/WO$_3$.** The WO$_3$/Ag/WO$_3$ anode OLED's emission spectrum (solid black line) peaks at 735 nm with a 67 nm FWHM. The ITO OLED's emission spectrum (dashed blue line) peaks at 739 nm with a 98 nm FWHM.

5.3 OLED optical characteristics

As shown in Figure 5.6, the WO$_3$/Ag/WO$_3$ OLED's normalized emission spectrum (measured with an Orb Optronix SP-75 spectrometer) has a narrower full-width at half-maximum (FWHM) and lower electroluminescence intensity at longer wavelengths compared to the normalized emission spectrum of the ITO OLED. The WO$_3$/Ag/WO$_3$ anode device had an emission peak at 735 nm with a 67 nm FWHM while the ITO anode device had an emission peak at 739 nm with a 98 nm FWHM. The decreased FWHM and electroluminescent intensity at longer wavelengths can be attributed to the WO$_3$/Ag/WO$_3$ anode's decreased transmittance. However, the expected EL spectrum calculated by multiplying the ITO device's emission spectrum by the normalized transmission spectrum of the WO$_3$/Ag/WO$_3$ yields an 87 nm FWHM (shown as the dotted black line in Figure 5.7(b)), indicating that the decreased transmittance alone does not account for the observed 67 nm FWHM. It is possible that a weak microcavity effect is at play in the OLED, which has previously been observed in OLEDs with DMD electrodes [164, 166].

In order to investigate the possibility of internal interference from an optical microcavity, the spectrum of the ITO anode device was remeasured after thermally evaporating a WO$_3$/Ag/WO$_3$ film on the underside of the substrate as shown in Figure 5.7(a)). With this structure, the optical effect of the WO$_3$/Ag/WO$_3$ film was decoupled from internal interference within the OLED. The resulting FWHM of this OLED configuration was 84 nm, 17 nm

wider than the OLED with the $WO_3/Ag/WO_3$ anode, (as shown in Figure 5.7(b)), and in closer agreement with the FWHM calculated from the $WO_3/Ag/WO_3$ layer's transmittance, suggesting that internal interference from a microcavity effect due to the $WO_3/Ag/WO_3$ anode is at play in addition to its transmission spectrum.

5.4 OLED performance

The OLEDs were electrically and optically characterized with an Orb Optronix LED measurement system equipped with a Keithley 2601, SP-75 spectrometer, and integrating sphere. Figure 3 plots the current density as a function of voltage (Figure 5.8(a)), flux per pixel area (Figure 5.8(b)), and external quantum efficiency (Figure 5.8(c)) of the OLEDs with the $WO_3/Ag/WO_3$ anode and ITO anode. In terms of current density, the OLED with the $WO_3/Ag/WO_3$ anode showed inferior diode characteristics with a higher leakage current (.113 $mAcm^{-2}$ at 1 V as opposed to 0 $mAcm^{-2}$ in the ITO anode device) and lower current density after turn-on. The $WO_3/Ag/WO_3$ anode OLED reached .367 $mWcm^{-2}$ flux per pixel area and 2.17% external quantum efficiency at 10 $mAcm^{-2}$ and the ITO anode OLED exhibited .802 $mWcm^{-2}$ flux per pixel area and 4.49% external quantum efficiency at the same current density.

To examine potential causes of the leakage current in the $WO_3/Ag/WO_3$, the surface morphology of ITO and evaporated $WO_3/Ag/WO_3$ films were measured by atomic force microscopy (AFM) on a Park Systems Atomic Force Microscope. Height images were captured in non-contact mode over a 5×5 μm area, as shown in Figure 5.9. The $WO_3/Ag/WO_3$ film presented a 1.5 nm RMS surface roughness with a 25.4 nm peak roughness. The ITO film had a .5 nm RMS surface roughness with 1.4 nm peak roughness. Any surface roughness on an OLED's bottom electrode, like the 25.4 nm peak in the $WO_3/Ag/WO_3$ film, can lead to shorts through the device that draw leakage current and hamper the OLED's performance. Thus the lower efficiency and flux in the $WO_3/Ag/WO_3$ anode OLED is attributed to the combination of short-induced leakage current and the anodes lower transmittance. For future work, we suggest that efforts are made to planarize the evaporated $WO_3/Ag/WO_3$ surface to prevent shorting. Additionally, the transmittance of the $WO_3/Ag/WO_3$ electrode might be improved without compromising conductivity by using a DMDMD structure with thinner Ag layers [162, 177].

5.5 Conclusion

In conclusion, a 100% additively processed and ITO-free NIR polymer OLED printed via blade coating on a thermally evaporated $WO_3/Ag/WO_3$ anode and plastic substrate has been demonstrated. For the NIR OLEDs herein, the efficiency of the $WO_3/Ag/WO_3$ anode was less than that of an ITO anode, and so it cannot replace ITO in all OLED applications without reproducibly smoother $WO_3/Ag/WO_3$ films. However, here it is shown that polymer

(a)

| Al (100 nm) |
| Ca (10 nm) |
| EML (90 nm) |
| EBL (10 nm) |
| PEDOT:PSS (70 nm) |
| WO$_3$ (30 nm) |
| Ag (20 nm) |
| WO$_3$ (30 nm) |
| PEN (150 µm) |

| Al (100 nm) |
| Ca (10 nm) |
| EML (90 nm) |
| EBL (10 nm) |
| PEDOT:PSS (70 nm) |
| ITO (65 nm) |
| PEN (150 µm) |

| Al (100 nm) |
| Ca (10 nm) |
| EML (90 nm) |
| EBL (10 nm) |
| PEDOT:PSS (70 nm) |
| ITO (65 nm) |
| PEN (150 µm) |
| WO$_3$ (30 nm) |
| Ag (20 nm) |
| WO$_3$ (30 nm) |

(b)
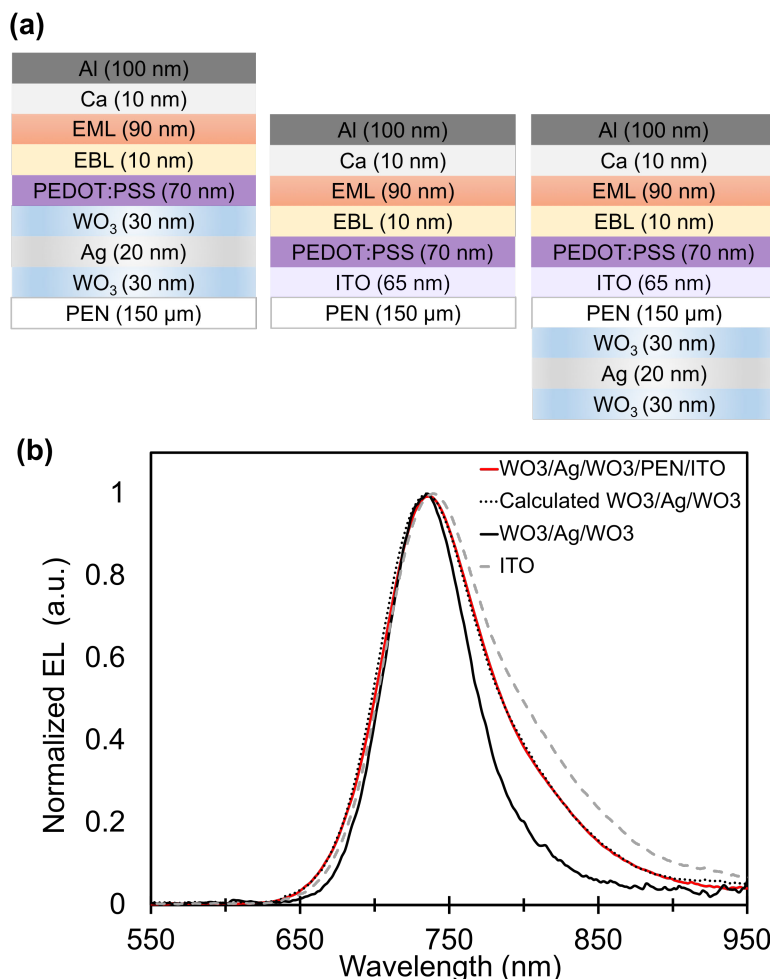
Figure 5.7: **Physical structure and emission spectra of NIR OLEDs printed on PEN/WO$_3$/Ag/WO$_3$, PEN/ITO, and WO$_3$/Ag/WO$_3$/PEN/ITO.** **(a)** NIR OLED spectra were measured for three bottom electrode configurations: PEN/WO3/Ag/WO3 (left), PEN/ITO (center), and WO3/Ag/WO3/PEN/ITO (right). **(b)** The normalized electroluminescence intensity of each OLED configuration. The emission spectrum of the PEN/ITO anode OLED is the dashed grey line. After measuring the emission spectrum of the PEN/ITO device, WO$_3$(30 nm)/Ag (20 nm)/WO$_3$(30 nm) was thermally evaporated on the underside of the OLED's substrate and its emission spectrum was remeasured (solid red line). The calculated WO$_3$/Ag/WO$_3$ spectrum (dotted black line) was determined by weighting the ITO OLED emission spectrum by the transmittance of the WO$_3$/Ag/WO$_3$ anode. The calculated WO$_3$/Ag/WO$_3$ emission spectrum closely overlaps the WO$_3$/Ag/WO$_3$/PEN/ITO OLED's spectrum, both of which have a larger FWHM than the experimentally obtained emission spectrum of the PEN/WO$_3$/Ag/WO$_3$ OLED (solid black line).
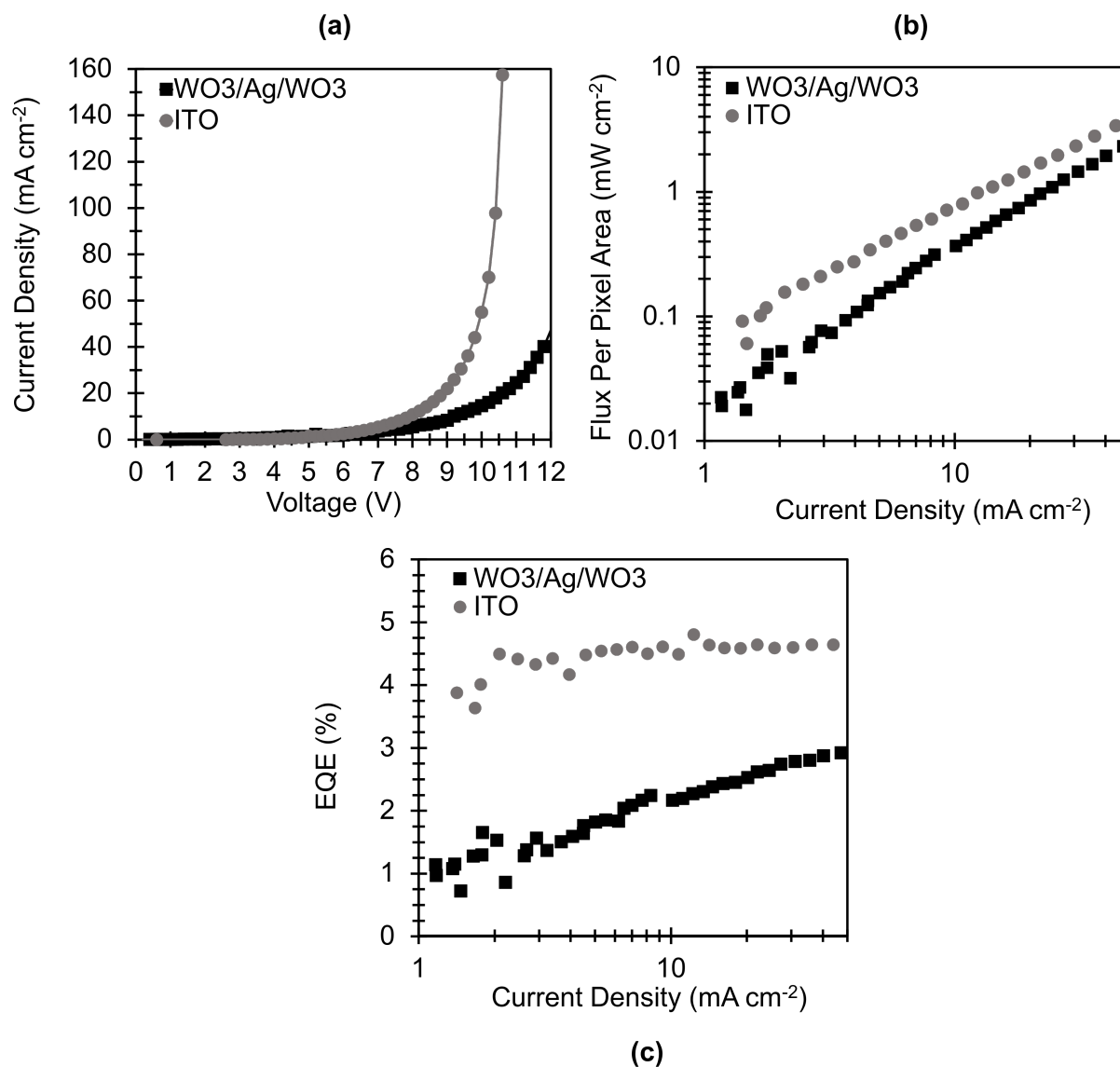
Figure 5.8: **Performance of NIR polymer OLEDs printed on ITO (grey circles) and WO₃/Ag/WO₃ (black squares) anodes.** **(a)** Current density as a function of applied voltage. **(b)** Flux per pixel area as a function of current density. **(c)** External quantum efficiency (EQE) as a function of current density.
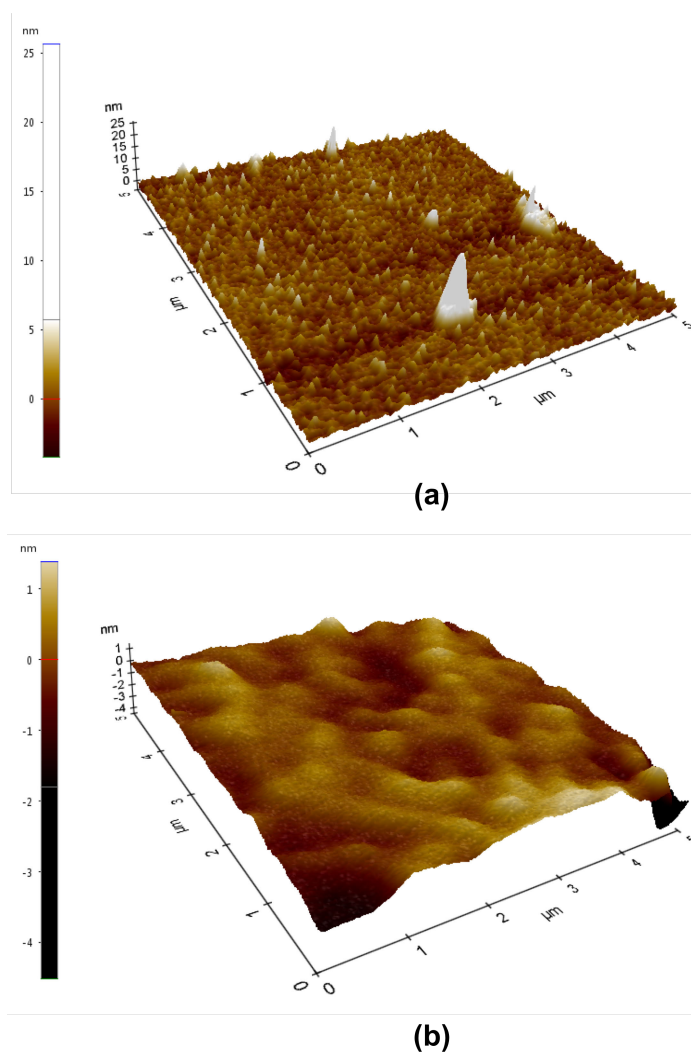
Figure 5.9: **urface roughness of WO$_3$/Ag/WO$_3$ and ITO anodes**. 3D AFM height images of **(a)** WO$_3$/Ag/WO$_3$ and **(b)** ITO on PEN acquired by non-contact mode Park Systems Atomic Force Microscope. The WO$_3$/Ag/WO$_3$ film has a 1.5 nm RMS surface roughness and 25.4 nm peak roughness. The ITO film has a .5 nm RMS surface roughness and 1.4 nm peak roughness.

OLEDs printed on a WO$_3$/Ag/WO$_3$ anode are functional and thus have the potential for implementation in novel flexible applications. For example, flexible NIR OLEDs could be implemented in wearable biomedical applications such as pulse oximetry, photodynamic therapy, and functional near infrared spectroscopy (fNIRS)[8, 178, 37]. The WO$_3$/Ag/WO$_3$ OLED's narrower emission spectrum may be of particular interest for fNIRS, which requires multiple wavelength NIR sources with minimal spectral overlap [179, 180].

The WO$_3$/Ag/WO$_3$ OLEDs presented in this chapter were made with 100% additive processing and printed polymer layers. To maximize processing efficiency and reduce the cost of the finished product, and thus a potential biomedical device, the next phase in the path of OLED development is to implement printed electrodes. The next chapter in this thesis presents work towards achieving OLEDs with a printed anode.

Chapter 6

Printed red OLEDs with partially and fully printed WO$_3$/Ag/WO$_3$ anodes

A common goal for printed electronics engineers is to achieve fully printed devices to maximize roll-to-roll processing throughput and efficiency. So far this has been achieved with passive components [181], OTFTs [135], super capacitors [182], photodiodes [183], phototransistors [184] and solar cells [185]. Fully printed OLEDs on the other hand have been difficult to manufacture because they require high conductivity electrodes (OLEDs use mAs of current) and a low work function cathode (less than 3 eV).

The first, and unsuccessful, attempt at a printed anode in this work used a high conductivity formulation of ink jet grade PEDOT:PSS from Sigma Aldrich. This material is meant to be used for electrodes, and has been used to print electrodes for photodetectors and OTFTs that carry μAs of current by Pierre et al. [183, 135]. Patterned PEDOT:PSS electrodes (shown in Figure 6.1(a)) in this work were doctor blade coated on PQA1 substrate using a surface energy patterning method developed by Pierre et al. [135]. This patterning technique uses (heptadecafl uoro1,1,2,2-tetrahydrodecyl)trichlorosilane (FDTS, from Gelest) (FDTS) to make the substrate surface hydrophobic. A FDTS self-assembled monolayer is applied by vapor deposition for 15 minutes in a glovebox antechamber under vacuum (at -30 Torr). After deposition, the FDTS is selectively etched under a mask in oxygen plasma, leaving some hydrophillic patterns in the hydrophobic film. When the PEDOT:PSS is doctor blade coated over the substrate, it wets the hydrophillic patterns while leaving the hydrophobic areas clear, as shown in Figure 6.1(a). After PEDOT:PSS deposition, the sample was treated with O_2 plasma again, this time without a mask, to render the entire surface hydrophilic. Nafion was printed next in order to increase the PEDOT:PSS layer's work function [186] for improved hole in injection into the TFB:F8BT emissive layer (higher conductivity PEDOT:PSS inks have lower work functions than standard PEDOT:PSS PVP AI4083). TFB:F8BT (1:9) was printed from a 20 mg/mL o-xylene solution and a LiF (1 nm)/Al (100 nm) cathode was thermally evaporated. This structure is shown in Figure 6.1(b). The resulting OLEDs suffered from uneven turn-on, shown in Figure 6.1(c), at high voltages with low current densities (the OLED carried only only .175 $mAcm^{-2}$ current at 10 V), attributed
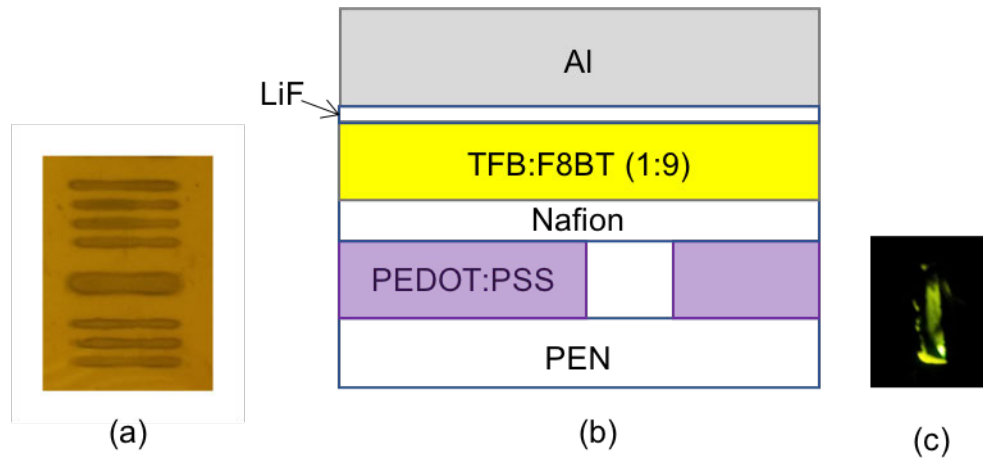
Figure 6.1: **PEDOT:PSS anode OLED. (a)** Surface energy patterned conductive PE-DOT:PSS blade coated on PEN. **(b)** Structure of a TFB:F8BT OLED blade coated on the printed PEDOT:PSS anode. Nafion was blade coated on top of the PEDOT:PSS to increase its work function for improved hole injection into the emissive layer[186]. A 100 nm layer of TFB:F8BT (1:9 ratio) was printed from a 20 mg/mL o-xylene solution. A LiF (1 nm)/Al (100 nm) cathode was thermally evaporated. **(c)** The OLED did turn on, but at 10 V with only .175 $mAcm^-2$ and a flux was too low to be detected by the sensor in the integrating sphere. As a result, the PEDOT:PSS anode was deemed not conductive enough for OLEDs.

to the PEDOT:PSS anode not being conductive enough for the mA's of current required by an OLED.

In the literature, high conductivity PEDOT:PSS electrodes have been used in OLEDs, but they have been supplemented with Ag in order to boost their conductivity. Ag nanowires have been incorporated into PEDOT:PSS inks [187], and PEDOT:PSS has been deposited on top of Ag nanowire films [188] or ink jet printed Ag mesh [189]. For the nanowire films especially, these anodes require a planarization layer on top before depositing the rest of the OLED to prevent shorting.

In addition to low conductivity, another drawback to using the PEDOT:PSS anode in this structure is that uses FDTS for electrode patterning. FDTS is a very harmful chemical if contacted or inhaled, and biomedical devices that are meant to be mass manufactured and worn on the body should not contain highly toxic materials.

Thus PEDOT:PSS anodes were set aside for fully printed $WO_3/Ag/WO_3$ anodes, in an attempt to reproduce the results of Chapter 5 with the anode being printed instead of thermally evaporated. In fact, one of the reasons that WO_3 and Ag were chosen for the structure described in Chapter 5 was that both materials are commercially available as inks. The rest of this chapter will detail the work towards developing an OLED with a printed $WO_3/Ag/WO_3$ anode.

6.1 Thin Ag films printed via blade coating

The Ag layer of the WO$_3$/Ag/WO$_3$ anode presented in Chapter 5 was 20 nm thick. Printing a smooth and conductive 20 nm film of Ag is challenging. The first step was to choose an appropriate ink. There are many Ag inks on the market, ranging from thick pastes for screen printing to less viscous inks for ink jet printing or rotary gravure printing, however many Ag inks produce printed films with surface roughness too high for a bottom electrode in a printed OLED. The ink selected for this work was TEC-PR-010 from InkTec, an an organo-metallic Ag ink designed for gravure and flexography printing. TEC-PR-010 ink contains 10 wt% Ag in isopropyl alcohol and. Organometallic inks have been shown to have low cure temperatures ($< 200°$C) and produce reflective printed films with low surface roughness [190]. For a 1 μm thick film, TEC-PR-010's recommended cure temperature is 120-170°C for 2-5 minutes for a 1 μm thick printed film.

Doctor blade coating was chosen to print the Ag ink because it is capable of printing large area, thin, smooth films with high-throughput. As discussed in Chapter 3, the thickness of a doctor blade coated film is dependent on the ink concentration, the blade height, the ink volume, and the print speed. The target Ag layer thickness was 20 nm. The first strategy to obtain such a thin printed layer was diluting the TEC-PR-010 ink with isopropyl alocohol, but the films printed from the diluted ink did not become uniformly reflective films after curing. The strategy that was successful for a 20 nm Ag film was to use a very low blade height, low ink volume, and a slow print speed. The blade height was set to 15 μm, its minimum without making contact with the substrate during printing. The printing speed was 3 cm/s or slower, and the ink volume used in a single print was 5 μL. Ethylene glycol, a common additive for printed inks [191], can be added to at a .1 wt% concentration to improve printed film uniformity and repeatability. Before printing, the Ag ink was mixed for 30 s on a vortex mixer. The Ag films were printed at room temperature and cured at 170°C for 3 minutes. With these conditions, the dimensions of the printed Ag film were 5 cm long and 2 cm wide.

While conducting this work, it was found that the atmospheric conditions in which the Ag film is cured impact film quality. TEC-PR-010 prints clear, and should change from brown to a mirror-like silver as it is cured. Figure 6.2(a) shows a > 100 nm doctor blade coated Ag film cured un-covered in a ventilated area (fume hood). The cured film is very reflective and silver in color (the reflection of the pink cellphone used to capture the photo appears in the film). Figure 6.2(b) shows a Ag film printed at the same time but cured while covered by a glass petri dish, keeping more evaporated solvent in contact with the film while it was curing. Instead of becoming reflective, this film turned an opaque milky white. The same behavior was seen for Ag films annealed inside an organic solvent-rich nitrogen atmosphere (in a glovebox). Thus, it is important that the Ag film be annealed in a low-humidity area.

As can be expected, the printed Ag films' sheet resistance varied with the printed film thickness/print speed. Film thicknesses were measured with a Dektak profilometer, on which film thicknesses below 15 nm could not be accurately measured. However, it can be assumed that slower print speeds resulted in thinner films. For 20 nm thick Ag, printed at 2.4
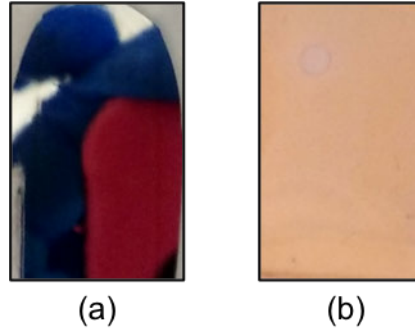
Figure 6.2: **Printed TEC-PR-010 Ag ink sensitivity to environmental conditions while curing. (a)** A printed Ag film cured in a low-humidity environment was silver in color and highly reflective. **(b)** An identically printed Ag film enclosed in a glass petri dish while curing has an opaque, milky-white appearance. This shows that it is important for printed TEC-PR-010 to be cured in a low humidity environment.

cms^{-2}, the sheet restiance was 9.02±1.36 Ω/sq. 15 nm thick Ag printed at 2.0 cm/s had a 34.49p/m9.65 Ω/sq sheet resistance. The Ag printed at 1.4 cm/s had a 42.06±9.93 Ω/sq sheet resistance and films printed a 1.1 cm/s were not conductive. These values are summarized in Table 6.1.

Transmittance also varied with print speed/film thickness, as shown in Figure 6.4. The maximum transmittance was 54% for the thinnest film printed at 1.1 cms^{-1}, followed by 34% for the film printed at 1.4 cm/s, 31% for the film printed at 2.0 cm/s, and 19% for the 20 nm film printed at 2.4 cm/s. The slowest print speed resulted in the film with highest transmittance, but it was not conductive. The most conductive film on the other hand had the lowest transmittance. The 20 nm, 2.4 cm/s printed film is deemed best because it has the most reproducible low sheet resistance.

In order for the film to be conductive, the Ag needs to meld into connected conductive pathways as it is cured, as seen in Figure 6.3, a surface height image of a 20 nm Ag film printed on glass, acquired by non-contact mode AFM. At the same time, the higher the density of conjoined Ag pathways, the lower the film's transmittance. Hence there is a trade-off between transparency and conductivity. Also from this image, the Ag film's RMS surface roughness was measured to be 12.9 nm.

This concludes the section on printing thin and conductive Ag films with blade coating. Device performance of OLEDs printed on a printed Ag film (sandwiched in between printed WO$_3$/Ag/WO$_3$) will be presented later in this chapter. The next section presents printed WO$_3$, the next component in a fully printed WO$_3$/Ag/WO$_3$ anode.
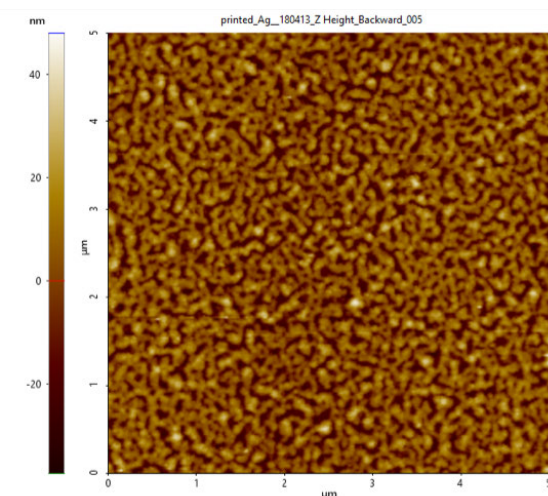
Figure 6.3: **AFM height image of printed Ag on glass.** If thick enough, curing the TEC-PR-010 film causes its Ag content to forms a conductive conjoined network. The RMS surface roughness measured from this AFM image was 12.9 nm.

Print Speed (cm s^{-1})	Thickness (nm)	Sheet Resistance (Ω/Square)
1.1	<15	∞
1.4	<15	42.06 ± 9.93
2.0	15	34.49 ± 9.65
2.4	20	9.02 ± 1.36

Table 6.1: [**Printed Ag sheet resistance as a function of print speed and thickness.** As print speed for Ag deposition decreased, so too did the film thickness and conductivity.

6.2 Blade coated WO$_3$

WO$_3$ films were much simpler to print than the Ag. A WO$_3$ nanoparticle ink was used, Avantama P-10, purchased from Avantama (formerly Nanograde). Avanatama P-10 contains 16 nm WO$_3$ nanoparticles in a 2.5 wt% isopropyl alcohol solution. Before printing, the WO$_3$ ink was mixed for 30 s at maximum speed on a vortex mixer, as recommended. For a 30 nm printed WO$_3$ film, 80 μL of ink was dispensed blade coated with a 150 μm blade height and 1.4 cm/s print speed at room temperature. The printed film covered the substrate in a blanket coat. In order to cure the nanoparticles, the printed film was annealed at 90° for ten minutes. After annealing, the printed WO$_3$'s RMS surface roughness (on glass) was 13.2 nm, as measured by non-contact mode AFM. The AFM height image of the printed WO$_3$ film is shown in Figure 6.5. The transmittance of the film was measured to be 100% from 500 - 1200 nm.
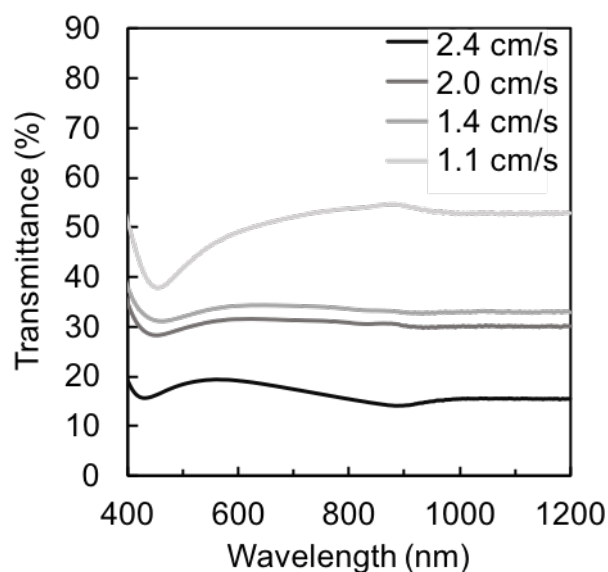
Figure 6.4: **Transmission spectra of Ag films as a function of print speed.** Ag films were printed at 2.4 cm/s (black line), 2.0 cm/s (dark grey line), 1.4 cm/s (medium grey line), and 1.1 cm/s (lightest grey line). As the printing speed decreases, so does the thickness of the printed Ag film, and thus the transmittance increases.
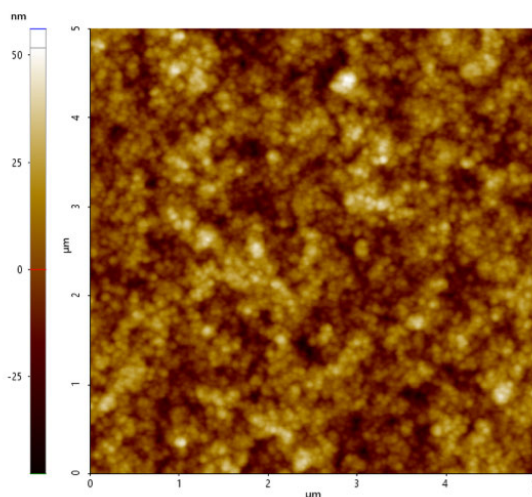
Figure 6.5: **AFM height image of a printed WO₃ film on glass.** The RMS surface roughness was 13.2 nm. The constituent WO₃ nanoparticles are visible in the film, even after annealing for at 90°C for 10 minutes.
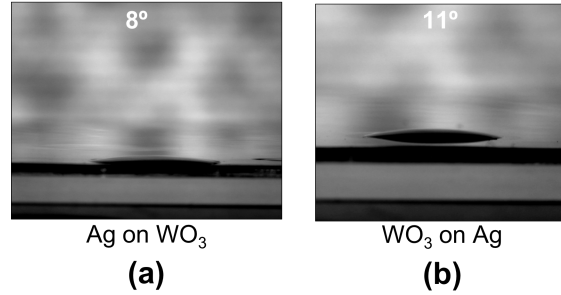
Figure 6.6: **Goniometric images and contact angles of (a) printed Ag on WO$_3$ and (b) WO$_3$ on Ag.** The contact angle of the Ag ink on WO$_3$ is 8° and the contact angle of the WO$_3$ nanoparticle ink on the Ag film is 11°.

6.3 Printed red OLEDs on partially and fully printed WO$_3$/Ag/WO$_3$ anodes

Once printing techniques for both 20 nm Ag and 30 nm WO$_3$ were developed, the WO$_3$/Ag/WO$_3$ anode of Chapter 5 could be printed. For the fully printed anode, the contact angle of each layer on the one before was measured to determine their compatibility for being printed on one another. As shown in Figure 6.6, the Ag ink has a 8° contact angle on a printed WO$_3$ film and the WO$_3$ ink had a 11° contact angle on printed Ag, indicating very good wetting properties.

Red OLEDs with a TFB:F8BT:TBT (25:70:5) emissive layer were fabricated on both partially and fully printed anodes. For the partially printed anode, the WO$_3$ layers were printed and the Ag layer was thermally evaporated. On top of the WO$_3$/Ag/WO$_3$ each anode, PEDOT:PSS .01 wt% zonyl surfactant, an IL-2 EBL (from 6 mg/mL o-xylene solution), and the emissive layer (from 20 mg/mL solution) were printed. A Ca (10 nm)/Al (100 nm) cathode was thermally evaporated. A schematic of the device structure is shown in Figure 6.7(d).

The emission spectra, flux per pixel area, current density, and physical structure schematic of the OLEDs printed on the fully and partially printed anodes are compared in Figure 6.7. As can be seen immediately from the spectral flux of each OLED in Figure 6.7(a) and (b), the OLED with the partially printed anode out-performed the OLED with the fully printed anode. The OLED with the partially printed anode had a $4.38 \times 10^{-6} Wnm^{-1}$ emission peak at 617 nm and a 73 nm FWHM. The OLED with the fully printed anode had a $6.9 \times 10^{-7} Wnm^{-1}$ peak at 675 nm and a 172 nm FWHM. The partially printed anode OLED reached 8.17 $mWcm^{-2}$ flux per pixel area. The fully printed anode OLED on the other hand burnt out before a full measurement sweep could be completed. In Figure 6.7(c), it can be seen that upon first measurement the current density vs. voltage characteristics of both OLEDs were almost identical. It was during the fully printed anode OLED's second voltage sweep that it began to decay until it was completely shorted.
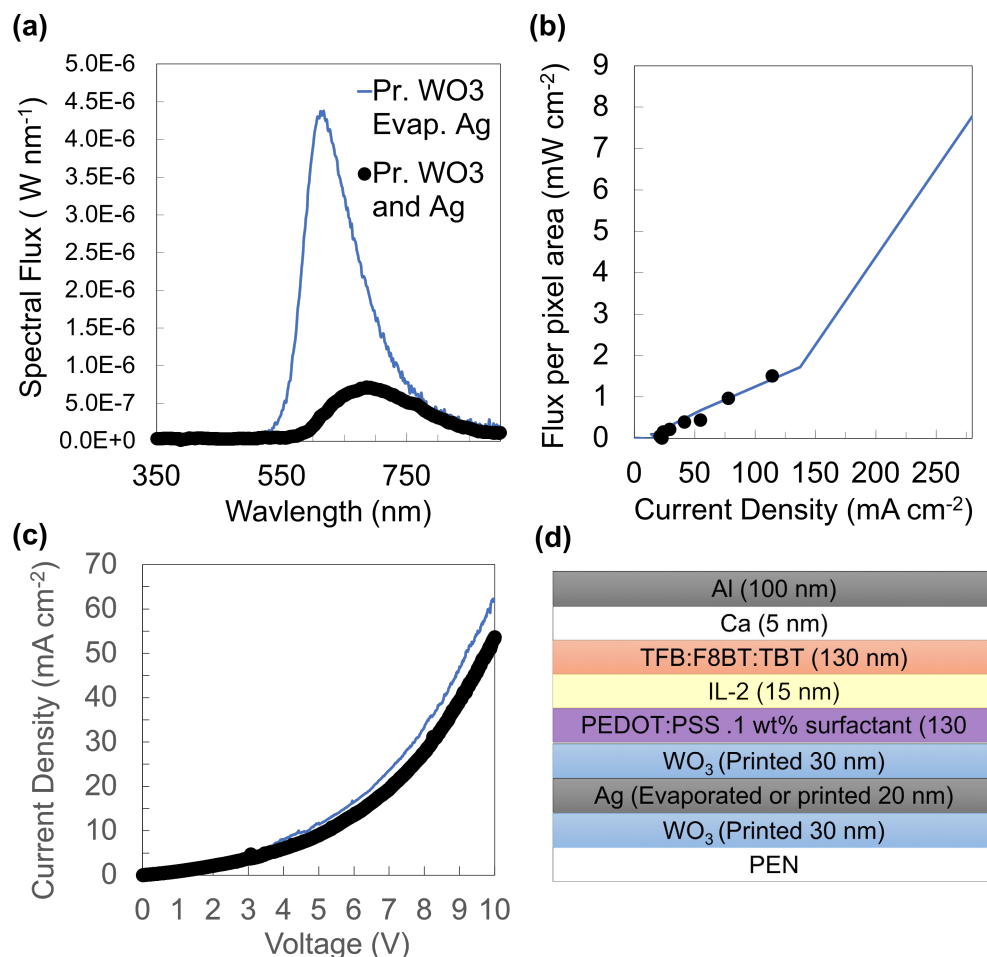
Figure 6.7: **Performance of red polyfluorene OLEDs blade coated on fully and
partially printed WO$_3$/Ag/WO$_3$ anodes (a) The measured spectral flux of each
OLED.** The OLED with the partially printed anode had a $4.38 \times 10^{-6} W nm^{-1}$ emission peak
at 617 nm and a 73 nm FWHM (blue line). The OLED with the fully printed anode had a
$6.9 \times 10^{-7} W nm^{-1}$ peak at 675 nm and a 172 nm FWHM (black line). During measurement,
the OLED with the fully printed anode quickly degraded and no longer functioned within
the time it took for testing. **(b) Flux per pixel area as a function of current density.**
The partially printed anode OLED (blue line) reached 8.17 $mW cm^{-2}$ of flux output, while
the fully printed anode OLED (black circles) burnt out before a full measurement sweep
could be completed. **(c)** The fully (black line) and partially printed anode devices' (orange
line) current densities were almost identical as a function of voltage. **(d)** Physical structure
schematic of the OLEDs with partially and fully printed anodes.
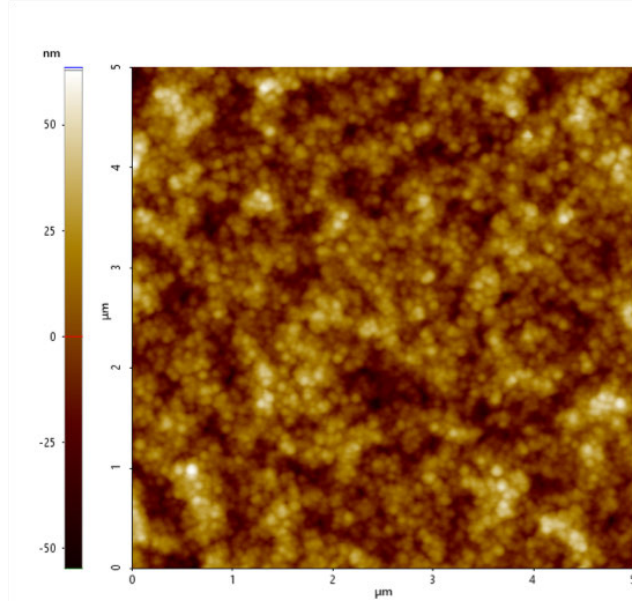
Figure 6.8: **AFM height image of a fully printed WO$_3$/Ag/WO$_3$ film on glass.** The RMS surface roughness was 16 nm.

One common cause for leakage current and shorting in OLEDs is anode surface roughness. The AFM height image of the fully printed WO$_3$/Ag/WO$_3$ electrode is shown in Figure 6.8. The anode's RMS surface roughness was only 16 nm. However, the fact that the OLED printed on the partially printed WO$_3$/Ag/WO$_3$ anode, with a surface roughness dominated by the WO$_3$ nanopartical films, did not suffer from fatal shorting indicates that surface roughness was not its cause. Instead, the rapid degradation and shorting of the fully printed WO$_3$/Ag/WO$_3$ anode OLED is attributed to non-uniformity in the printed Ag's conductivity. As reported in Table 6.1, a difference of 5 nm in Ag thickness can result in a 4x difference in sheet resistance. The 20 nm doctor blade coated Ag films are not perfectly uniform, so differences in film thickness and conductivity within will cause uneven current distribution in the OLED. 'Hot spots' where the Ag film is most conductive draws the bulk of the current, causing localized heating in the polymer layers that creates shorts and destroys the device. A similar effect has been observed in OLEDs built on Ag nanowire electrodes, where the random distribution of Ag nanowires in the electrode causes uneven conductivity and mAs of current are preferentially injected into the polymer layers over the highest conductivity areas and burns the device [192].

6.4 Conclusion

In future work, the flux of OLEDs fabricated with this structure may be improved by using a thinner PEDOT:PSS layer (to increase its transmittance), and their turn on voltage

could be decreased by using a lower concentration of Zonyl surfactant in the PEDOT:PSS ink (for lower series resistance). Furthermore, while the fully printed WO_3/Ag/WO_3 anode is not practical to fabricate via blade coating at this time, the continuing development of conductive low-temperature processed Ag inks may enable this structure at a later time.

In this work, the red OLED fabricated with a partially printed WO_3/Ag/WO_3 anode exhibited flux per unit area on the order of 1-10 $mW\,cm^{-2}$, values that fulfill the irradiance requirement for a number of the biomedical devices reviewed in Chapter 2. Thus this partially printed anode is another step towards a fully printed OLED that could be applied to biomedical applications.

Chapter 7

Interfacing OLEDs with the human body

7.1 Printed NIR OLEDs with NIR-shifted electroluminescence applied to photoplethysmography

As presented in Chapter 3, the OLEDs in the first solution-processed organic optoelectronic pulse oximeter had different peak wavelengths than most of their inorganic counterparts - red and green instead of red and NIR [22]. The primary reason for using a green OLED instead of a NIR OLED was that solution processable NIR emitting materials have been more challenging to produce than visible spectrum emitters. Still today, efficient solution processable NIR emitters with emission peaks beyond 800 nm are few and far between [193, 194]. However, NIR light has better penetration depth in human tissue compared to visible wavelengths [56], so biomedical devices would benefit from OLEDs with deeper NIR emission. In this section a printed NIR OLED with a NIR-shifted emission spectrum and the spectral shift's effect on PPG acquisition is presented.

OLEDs' emission spectra have been observed to a have a dependence on the thickness of their emissive layer [195, 196, 197, 198], a dependence that has been partially attributed to weak microcavity effects within the devices [199]. Here too, an altered emissive layer thickness produced an altered emission spectrum. One NIR OLED was printed with a 150 nm thick emissive layer and the other with a 250 nm thick emissive layer. The anode for each OLED was thermally evaporated WO_3 (20 nm)/Ag (30 nm)/WO_3 (20 nm) on a PEN substrate. Every polymer layer was printed with the same doctor blade coating procedure presented in Chapter 5.

The emission spectrum of both OLEDs is shown in Figure 7.1. The 150 nm emissive layer OLED had a single emission spectrum peak at 745 nm and a half-maximum point at 807 nm. The OLED with the 250 nm emissive layer had an emission spectrum with a primary peak
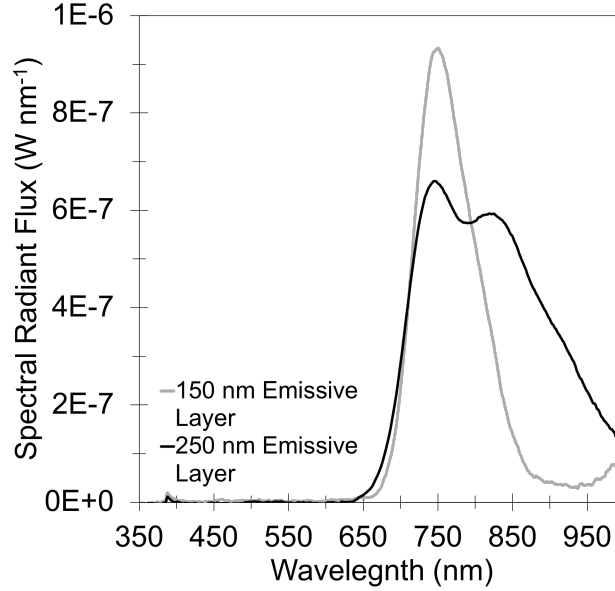
Figure 7.1: **Red-shifted NIR OLED emission spectrum.** The emission spectrum of the NIR OLED printed with a 150 nm emissive layer has a 745 nm peak and it's higher half-maximum point at 807 nm (grey line). The emission spectrum of the NIR+ OLED printed with a 250 nm emissive layer has a primary peak at 745 nm, a secondary peak at 815 nm, and it's higher half-maximum point at 916 nm (black line). The emission is plotted as spectral radiant flux (Wnm^{-1}) to illustrate the difference in light intensity.

at 745 nm, a secondary emission peak at 815 nm, and a half-maximum point at 916 nm. The presence of two emission peaks has previously been reported in OLEDs with similarly thick emissive layers and has been attributed to the optical interference of waveguided light reflected between the devices anode and cathode layers[195, 196, 197, 198].

To illustrate the benefits of deeper NIR emission, PPG signals were acquired by both the NIR (150 nm emissive layer) and NIR+ (250 nm emissive layer) OLEDs paired with a silicon photodiode on either side of a subject's finger, as shown in Figure 7.2. The resulting PPG signal from each OLED is shown in Figure 7.3. The higher the peak-to-peak magnitude of a PPG signal, the better, because the signal is cleaner for heart rate and oxygenation derivation. The magnitude of the calibrated PPG signal obtained here was on average 32.87% higher using the NIR+ OLED than the calibrated PPG obtained with the NIR OLED (comparing 4 measurements taken with each OLED). To ensure a comparison of spectral effects alone, the PPG signals were calibrated to each OLED spectrum's overlap with the photodiode's responsivity spectrum, as well as the maximum current generated in the photodiode when it was directly illuminated by each OLED (with no finger in between). This signal improvement is attributed to the fact that light scattering in human tissue decreases exponentially with increasing wavelength 7.4.

In terms of device performance as an OLED, there is a trade-off between the device struc-

Figure 7.2: **Photograph of a NIR OLED above a subject's finger used in conjunction with a Si photodiode for PPG acquisition.** The OLED was placed flush with the finger while recording the PPG. The finger was placed flush on top of the Si photodiode.
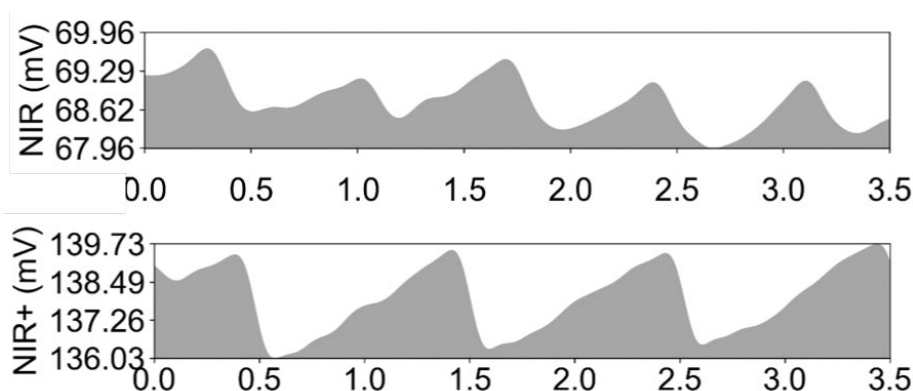
Figure 7.3: **PPG signals acquired by printed NIR and NIR+ OLEDs.** The NIR PPG (top frame) magnitude was approximately 1.3 mV$_{p-p}$ and the NIR+ PPG (bottom frame) magnitude was approximately 3.7 mV$_{p-p}$. PPG data was acquired with a system built by and the assistance of Yasser Khan, Jonathan Ting, and Dr. Donggeon Han.
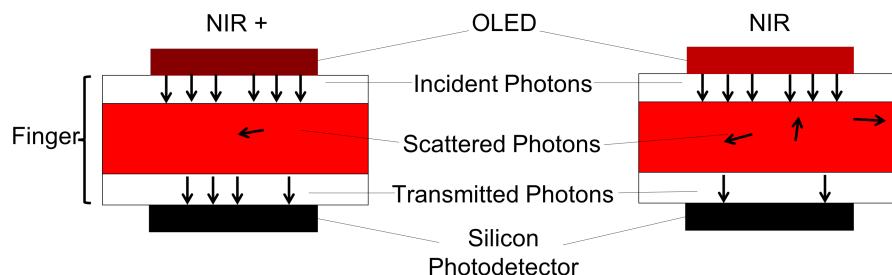
Figure 7.4: **Schematic of NIR+ and NIR light scattering in a human finger between the light source and photodiode.** Each arrow represents a photon. Fewer NIR+ photons than NIR photons are scattered within the finger, and so more NIR+ photons reach the photodetector.
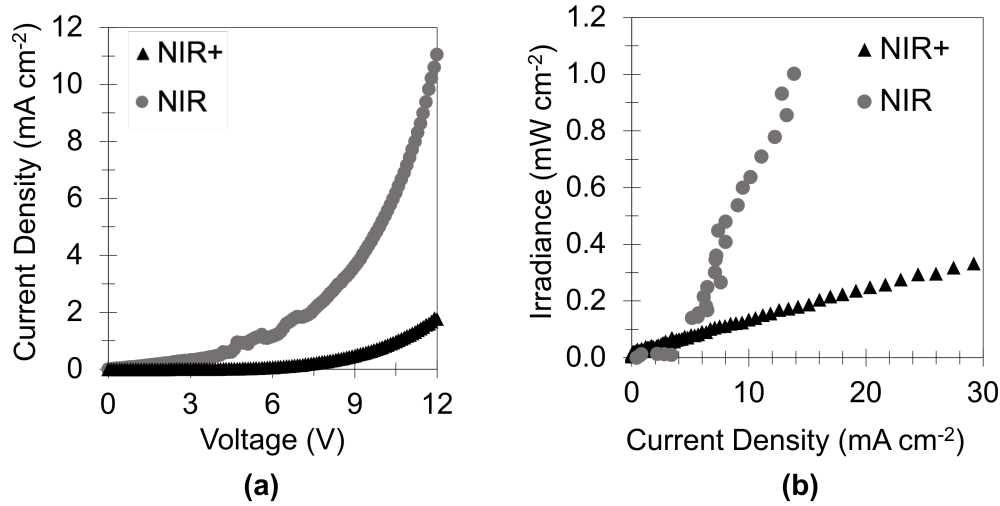
Figure 7.5: **NIR and NIR+ OLED device performance.** Looking at the NIR and NIR+ OLED's stand-alone device performance characteristics, the NIR+ OLED has inferior diode characteristics with (a) lower current densities as a function of voltage and (b) irradiance as a function of current density. While the NIR OLED's maximum irradiance was 1 $mW\,cm^{-2}$, the NIR+ OLED's irradiance only reached .33 $mW\,cm^{-2}$. This underscores the importance and impact of wavelength in an optical biomedical device: despite poor device characteristics, the NIR+ OLED produced a better PPG signal (as shown in Figure 7.3).

ture used to obtain NIR+ emission and efficiency. Compared to the 150 nm emissive layer, the thicker 250 nm emissive layer device had a higher turn-on voltage, lower current density (without poor behavior), and lower irradiance, as shown in Figure 7.5(a) and (b), respectively. While the NIR OLED's maximum irradiance was 1 $mW\,cm^{-2}$, the NIR+ OLED's irradiance only reached .33 $mW\,cm^{-2}$. Despite having a lower irradiance and poor diode current characteristics, the NIR+ OLED produced a better PPG signal. This demonstrates the importance and impact of wavelength in an optical biomedical device.

In the next section, specific clinical applications for organic-optoelectronic pulse oximters with flexible OLEDs are explored.

7.2 Clinical applications for organic-optoelectronic pulse oxiemters

Two types of flexible reflection mode pulse oximeter prototypes were shown to physicians for feedback on design and potential for application in their practice. The first type is a single pixel reflection mode pulse oximeter, shown in Figure 7.6(a), designed and fabricated by Cambridge Display Technology with input from the Arias group at UC Berkeley. In the
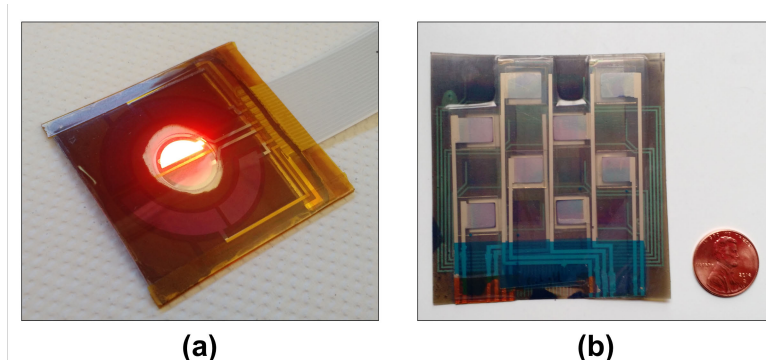
Figure 7.6: **Flexible organic optoelectronic reflection mode pulse oximeters.** **(a)** A single pixel pulse oximeter with red and NIR OLEDs surrounded by a photodetector ring. This pulse oximeter was designed and fabricated by Cambridge Display Technology. **(b)** A flexible pulse oximetry array composed of red and NIR OLED and OPD pixels. This array was designed by Yasser Khan, Dr. Adrien Pierre, Jonathan Ting, Dr. Donggeon Han, and Claire M. Lochner. The OLEDs were fabricated by Dr. Donggeon Han and the OPDs were fabricated by Dr. Adrien Pierre and Jonathan Ting.

single pixel oximeter, two half-hemisphere OLEDs (one red and one NIR) are surrounded by four OPDs. The PPG signal can be acquired from an individual OPD, or an average of a combination of the four.The second type is a reflection mode pulse oximetry array, as shown in Figure 7.6(b), designed by Yasser Khan, Dr. Adrien Pierre, Claire M. Lochner, Dr. Donggeon Han and Jonathan Ting. The OLED array was fabricated by Dr. Donggeon Han and OPD arrays were fabricated by Dr. Adrien Pierre and Jonathan Ting. The array contains four pairs of red and NIR OLEDs and four pairs of OPDs. The OLEDs appear as silver squares and the OPDs are the dark squares interspersed between. Each pair of OPDs and OLEDs make up one oximetry "pixel." A raster-scan through each pixel can create a 2-D map of tissue oxygenation.

Interviews were conducted with physicians to assess current pulse oximetry usage and the potential utility of flexible organic optoelectronic reflection mode pulse oximeters. The full interview transcripts are contained in the appendix of this thesis, and the most compelling applications for organic optoelectronic oximetry resulting from these interviews will be discussed here. The largest interest for an oximetry patch came from physicians with patients that conventional finger probe pulse oximeters dont work well on - a U.S. Air Force trauma surgeon, pediatricians, pulmonologists specializing in chronic respiratory disease management, and a vascular/endovascular surgeon.

Trauma medicine

Trauma surgeons working in mass casualty zones typically have only one pulse oximeter in their supply kit, measuring each patient's heart rate and oxygen saturation in the short amount of time they have to assess his or her condition before moving on to the next patient. Coupled with motion artifacts disrupting the oximetry measurement while carrying patients in a helicopter or transport convoy, better pulse oximeters are needed in the field. An ideal oximeter for this application would be lightweight, packable in a supply kit, easily adhered to a patient who may be covered in dirt and blood (the redundancy of a pulse oximeter array would be useful here), and would have an integrated pulse and oxygenation read-out screen built onto the backside of the device, all of which are possible with OLEDs [200].

Pediatrics

Pediatricians emphasized that respiratory distress is one of the leading causes of hospitalization for children. While oximetry measurements are the main indicator of respiratory distress severity, pulse oximeters are impractical to use with children most at risk: infants and children with impaired motor function and/or peripheral circulation. A single pixel reflection mode pulse oximeter placed on a child's back, chest, or abdomen would improve the reliability and accuracy of oximetry in these patients.

Autonomic disorders

The autonomic nervous system regulates a person's involuntary bodily functions that are essential for survival: blood pressure, heart rate, respiration, digestion, and body temperature. A person can be born with an autonomic disorder or develop one through a disease or injury to the nervous system. Symptoms include excess sweating, involuntary movement, depressed respiration, depressed cardiovascular function, and seizures.

One autonomic disorder is Rett Syndrome. Those with Rett Syndrome are born with it (typically females) and there is no cure. Rett syndrome patients suffer from cardiac arrhythmia, seizures, and breath holding. Parents and caregivers of these children would like to continuously monitor the child's heart rate and oxygen saturation, to be able to predict an imminent seizure or be alerted if the child stops breathing. Conventional wrist-worn heart rate monitoring devices do not suffice because people with Rett syndrome often wring their hands ("hand washing"), and the sensor does not stay in place. Our single pixel reflection mode pulse oximeter on the other hand could be used to continuously monitor a child's heart rate and oxygen saturation if it is worn on her core or back, where it won't be disturbed by erratic movements.

Chronic respiratory disease

Another case for a single pixel reflection mode oximetry patch is continuous vital sign monitoring for chronically ill patients. Chronically ill patient groups include those with chronic obstructive pulmonary disease (COPD) or interstitial lung disease (ILD). The number of people affected by chronic respiratory disease is expected to increase in the coming years, and their care already costs \$72 billion a year in the United States alone [201]. As of now, there is no clinically accurate oxygenation sensor that can be worn continuously, wirelessly, and unobtrusively throughout a patient's daily routines. The continuous monitoring enabled by a single pixel reflection mode oximeter could not only help patients monitor their own health and guide supplemental oxygen use, but also help physicians study the effectiveness of new medications and prescribed therapies.

Tissue oxygenation mapping

The motivation for the development of the 2-D oximetry array has been its potential to map tissue oxygenation. Because 2-D tissue oxygenation measurements are mostly untested, the lowest barrier to entry for an oximeter array would be in an application where no alternative exists. A prime example of this is to monitor spinal oxygenation, which can be compromised during vascular and endovascular surgery. Five to twenty percent of patients become paralyzed during multibranched thoracoabdominal stent-graft aneurysm repairs because of compromised spinal perfusion, and doctors have no way to monitor and prevent this before it is irreversible. An oximetry array positioned near the spine, over the psoas muscle, may be able to alert surgeons to changes in tissue oxygenation in time to restore blood flow and prevent paralysis.

The array oximeter could be tested on multibranched thoracoabdominal stent-graft aneurysm repair patients in a wired or wireless form. The patient would be on his or her back during the procedure and one or two sensors would be attached to each psoas muscle, a long ribbon cable connecting them to a control/read-out computer during and in the 2-3 days following the procedure. The tissue oxygenation values sensed by the arrays would be compared to the standard pulse oximeter measurements already being taken and surgical outcomes. To test if oximetry on the back is viable, we measured PPG with the single pixel oximeter secured on the users back, next to the spine and over the psoas muscle. A clear PPG signal was acquired from both the NIR and Red OLEDs at this location (shown Figure 7.7). If an oximetry array provides useful measurements in this application, its design and system integration should be further developed for implementation in internal organ perfusion monitoring during any surgery.
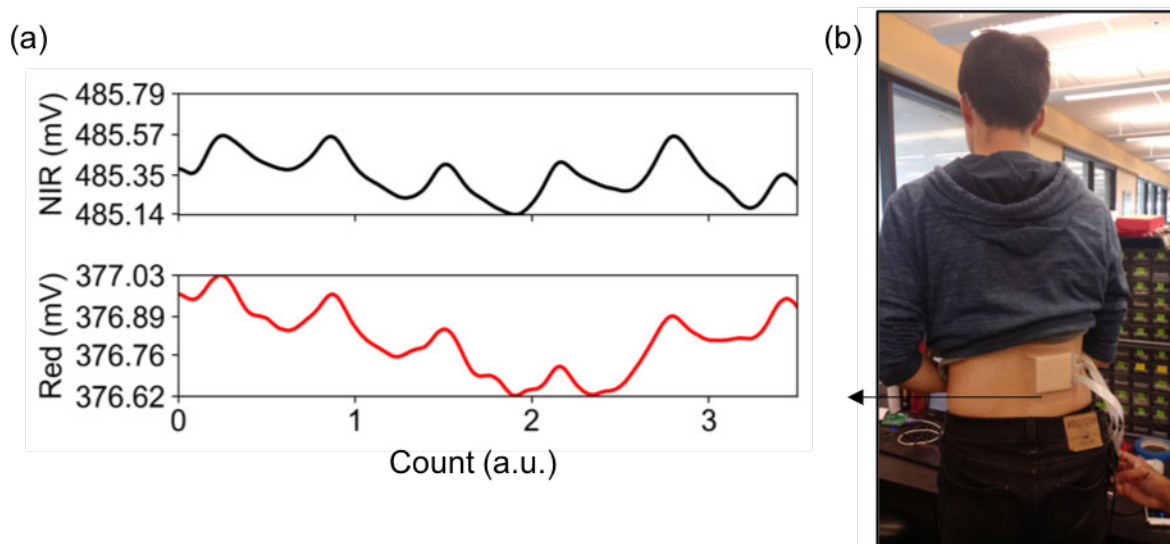
Figure 7.7: **PPG acquired from a single pixel reflection mode organic-optoelectronic pulse oximeter worn on the lower back.** (a) PPG signal acquired by the single pixel oximeter patch worn on the lower back by red and NIR OLEDs. Signal peaks are detectable and could be used to generate oxygention values. (b) The single pixel oximetry patch was worn over the psoas muscle.

7.3   The flexible organic optoelectronic oximeter/human interface

It is important that organic-optoelectronic oximeters can be worn with maximum comfort and no harm to the wearer. This can be done by packaging the flexible sensors within bandages and adhesives designed for sensitive skin and pressure-ulcer prevention. Commercially available wound dressings have been developed for application on open wounds and bedsores. Mepilex and Mepitel One from Molnlycke were used to interface a flexible all-organic optotlectronic pulse oximeter with the human body. The adhesive used in both of these dressings is Safetac, a material engineered to provide maximum adhesion with minimum tissue trauma. Both dressings are advertised to be wearable for 14 consecutive days.

The Mepilex line of products are similar to a conventional bandage: there is a padded central area that contacts the wound and an adhesive border. The main difference between Mepilex and an ordinary bandage is that the entire underside of the bandage is coated in Safetac adhesive, including the central padded area. Mepitel One is a perforated, transparent flexible sheet that has Safetac adhesive on one side.

To create a pulse oximeter 'patch,' the oximeter was attached directly to the adhesive on the center padded square of a 10 cm x 10 cm Mepilex Border bandage, as shown in Figure 7.8. A square of Mepitel One was cut from a larger sheet to cover the face of the oximeter, with
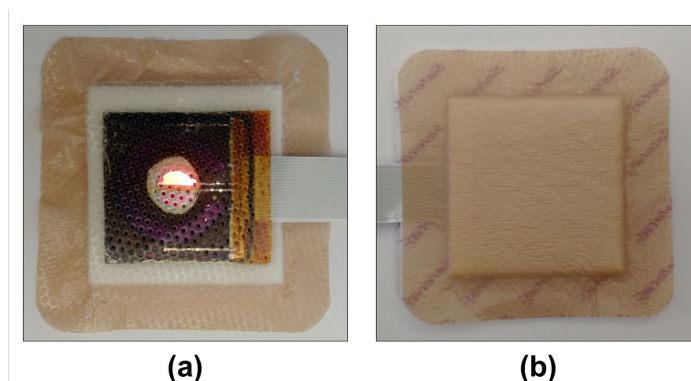
Figure 7.8: **Reflection mode flexible organic-optoelectronic pulse oximeter integrated with a wound dressing bandage and adhesive interlayer.** (a) Front view. The adhesive interlayer is secured over the pulse oximeter where its border overlaps the exposed adhesive on the bandage. The interlayer's adhesive side is facing upwards. An FCC connects the oximeter probe to control electronics and data processing computer. (b) Back view.

some overlap onto the exposed adhesive of the Mepilex Border. The Mepitel One serves as an interlayer between the sensor and the skin to prevent irritation in patients with sensitive skin. The bandage/oximeter assembly can then applied to the desired location on the body, as shown in Figures 7.7(b).

The wound dressing adhesives not only protects the wearer's tissue from possible discomfort, they also improve signal quality by securing the oximeter in place, decreasing sensor motion in reference to tissue and associated signal artifacts. In Figure 7.9, pulse oximetry measurements were acquired from a user's abdominal upper left quadrant with the single pixel oximeter. The PPG signals acquired from the red and NIR OLEDs are shown for a patch with and without a Mepitel One interlayer between the sensor and the skin. The PPG signals acquired with the additional adhesion from the Mepitel One interlayer are cleaner (Figure 7.9(b)), with less drift and more consistent signal magnitudes than the PPG signals acquired without the interlayer (Figure 7.9(a)).

To test whether or not the signal improvement from the interlayer was mechanical or optical, PPGs were also acquired with the adhesive side of the Mepitl One interlayer facing away from the body. These PPG signals were not as clean as the signals where the interlayer adhesive was attached to the body, indicating that the signal improvement is due to a decrease in relative motion between the sensor and the tissue under test, rather than an improved optical coupling from the Mepitel One layer. This underscores the importance of a close fit for on-body optical sensors. Because the OLEDs in the pulse oximeter are on a flat and flexible substrate, they are easily integrated with the adhesive wound dressing materials that improve patient comfort and signal clarity.
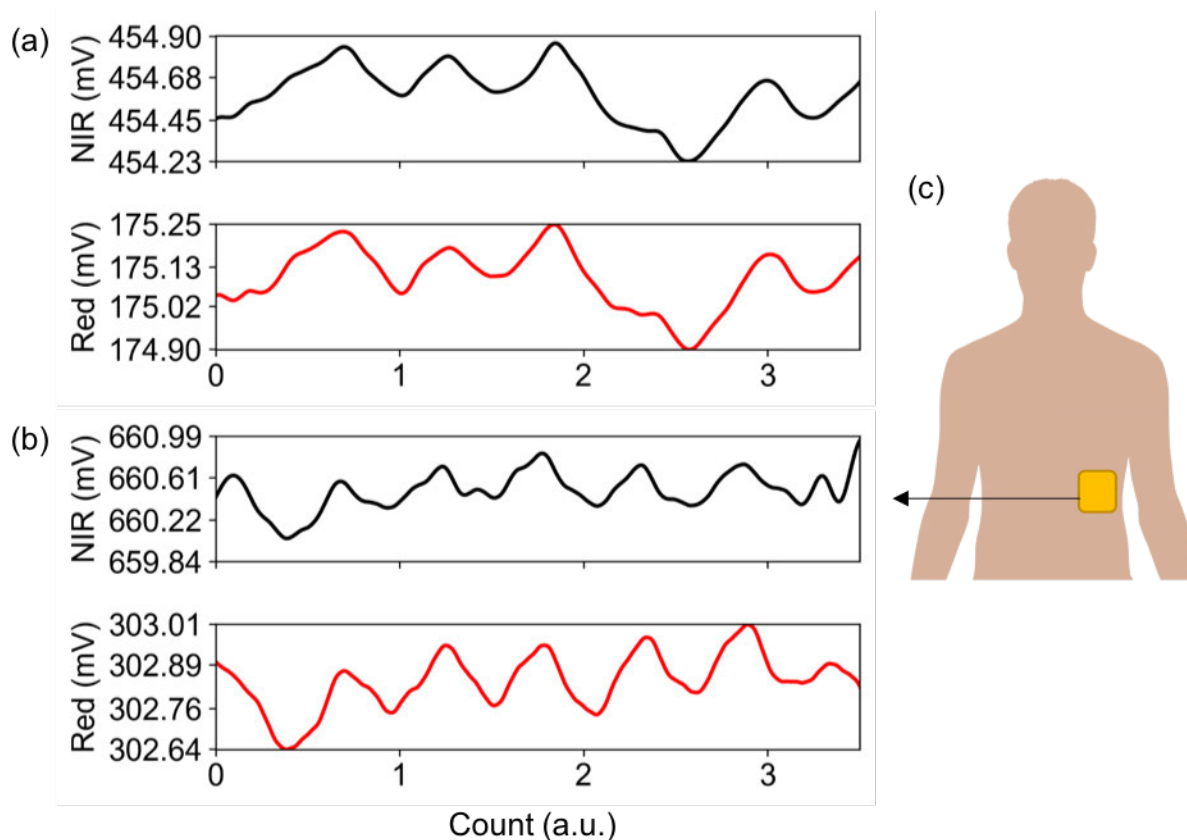
Figure 7.9: **PPG acquired from an organic-optoelectronic pulse oximetry patch worn on the abdominal upper left quadrant. (a)** The magnitude of the peaks in the PPG signal from the red and NIR OLEDs on the patch drift over time. **(b)** The magnitude of the PPG signal's peaks from the patch with an adhesive interlayer remain relatively constant over time. **(c)** The reflectance oximetry patch was worn on the abdominal upper left quadrant during PPG acquisition.

7.4   Conclusion

This chapter demonstrates improved PPG signal acquisition with deeper NIR OLED emission and exemplifies how flexible OLEDs can enable new and improved pulse oximetry applications. A pulse oximeter is only one example of flexible OLEDs enhancing a biomedical device. The other biomedical devices reviewed in Chapter 2 may also be improved using the same or similar methods.

Chapter 8

Conclusions and suggestions for future work

This dissertation has focused on the development of OLEDs specifically for biomedical applications. Whether it is for pulse oximetry, near-infrared spectrscopy, or phototherapy, the ideal OLED for a biomedical device should be flexible, so that it can fit the contours of the human body. It should be printed, to enable large area coverage at a low cost. And it should also have the optimal peak wavelength for its application.

Solution processed red and green polyfluorene OLEDs were used to accurately measure a person's heart rate and oxygenation in a pulse oximeter, proving that polymer OLEDs can be used in that biomedical application. These OLEDs were spin-coated, a fabrication process that has a high level of material waste and limited device area scalability. They were also made on glass with a patterned ITO anode, a material that is not flexible and requires subtractive processing, again decreasing material consumption efficiency.

In order to ameliorate these sticking points, a process was developed to print polymer OLEDs on a plastic PEN substrate with a thermally evaporated $WO_3/Ag/WO_3$ anode. Blade coated NIR OLEDs were demonstrated with over 2% EQE. They also had a narrowed emission spectrum compared to the same OLED printed on an ITO anode, a property that may be of interest for fNIRS and other biomedical applications that require multi-wavelength emitters with minimal spectral overlap. This presents an opportunity for future exploration of the effect of narrowed OLED emission in biomedical signal acquisition (for fNIRS) or triggering (for optogenetics) and targeted photodynamic therapies.

In an attempt to further improve process scalability, OLEDs with printed $WO_3/Ag/WO_3$ anodes were fabricated. The devices with a fully printed anode had limited lifetimes before shorting, due to the uncontrolled thickness dependence of the printed Ag film's conductivity. Red polyfluorene OLEDs printed on a partially printed anode with a thermally evaporated Ag layer were stable, with 1% EQE. In the future, the concentration of Zonyl surfactant in the PEDOT:PSS layer should be decreased in order to improve the bottom electrode's conductivity and thus the device efficiency. Additionally, conductive metallic inks are in development in academia and industry, and an ink than can be printed with uniform conductivity at

sub-50 nm thicknesses may become available. If so, a fully printed $WO_3/Ag/WO_3$ electrode should be re-visited.

Also in future work, a printed cathode should be incorporated into $WO_3/Ag/WO_3$ anode OLEDs. This can be done using a combination of a conjugated polyelectrolyte and a printable metal. Conjugated polyelectrolytes are soluble [202] and have been shown to decrease the work function of metals by creating a dipole moment between the metal and the polymer emissive layer [203, 204]. Preliminary experiments conducted during the course of this work showed that a poly [(9,9-bis(3'-(N,N-dimethylamino)propyl)-2,7-fluorene)-alt-2,7-(9,9dioctylfluorene)] (PFN)/Ag cathode has similar current injection characteristics to a LiF/Al cathode in a polyfluorene OLED. Figure 8.1 shows current as a function of voltage for a green polyfluorene OLED with various concentrations of PFN spin-coated on top of the emissive layer and a thermally evaporated Ag cathode. For comparison, the current of an identically fabricated OLED with a LiF/Al cathode is also plotted. As seen in Figure 8.1, the concentration of the PFN solution (in methanol) affects the electron injection properties from the cathode into the emissive layer. By decreasing the PFN solution concentration, and thus its thickness, current values on par with the LiF/Al anode OLED were achieved. As for printability of the Ag layer, thick Ag films are easier to print with uniform conductivity than sub-20 nm films. The main concern in a printed Ag top electrode would be to not create shorts through the emissive layer. It will be more challenging to print the PFN layer, as the electron injection properties of the PFN/Ag cathode appear to rely on PFN layer thickness, as shown in Figure 8.1.

In addition to printed OLEDs with an additively processed anode more compatible with large area flexible biomedical devices, this dissertation also demonstrated a NIR OLED with a secondary 815 nm emission peak, a wavelength longer than what most solution-processed NIR OLEDs are capable of emitting. The benefit of emission beyond 800 nm was demonstrated with the acquisition of a stronger PPG signal from a subject's forefinger using the NIR-shifted 745/815 nm OLED compared to the original 745 nm NIR OLED, despite the fact that the NIR-shifted OLED had a lower light output.

From a system level perspective, new pulse oximetry applications enabled by flexible organic optoelectronics were proposed with input from physicians. Flexible OLEDs enable oximeters that can be worn on different body parts other than the finger or wrist, a feature that pediatricians, pulmonologists, cardiologists, and trauma surgeons interviewed believe could improve their patients' care. However, the oximeter prototypes shown to physicians are not yet standalone; they still require a wired connection to a power supply, external control board, and PC for data processing.

In order to create fully functioning OLED-containing biomedical devices, system integration is the next challenge to solve. OLEDs will need to be integrated with flexible batteries and single chip control electronics. They could also be combined with printed photodetectors, electrodes that sense electrical biosignals (eg. ECG, impedance), and thermistors to create a multi-functional device. Figures 8.2, 8.3, and 8.4 show three examples of wearable biomedical devices that could be created by integrating OLEDs with other flexible electronic components.
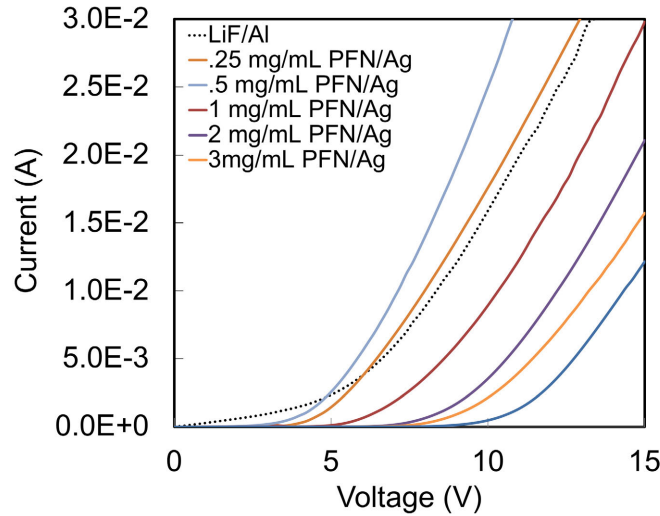
Figure 8.1: **Current vs. voltage characteristic of OLEDs with PFN/Ag and LiF/Al anodes.** The PFN films were spin-coated from methanol and .2% acetic acid solutions with concentrations ranging between .25 mg/mL and 3 mg/mL (solid lines). The higher the concentration, the thicker the PFN layer. OLEDs made with the the .5 and .25 mg/mL solution showed similar and even improved I/V characteristics than an identical OLED with a LiF/Al cathode (dotted line).

In the system proposed in Figure 8.2, ECG electrodes are printed onto the same substrate as a printed reflection mode pulse oximeter. A flexible thin-film battery is used to power the sensor and a single chip mote [103] is used for sensor control and signal acquisition. The single chip mote transmits the sensors' data via low energy bluetooth to the user's mobile devices. Using an app, the user can monitor his or her heart rate and oxygen saturation in real time. The ECG signal can be interpreted to detect heart beat abnormalities and alert the user if an arrhythmia occurs. The user could even choose to send a report to his or her physician, providing data that can help doctors better diagnose and monitor their patients' health.

Figure 8.3 shows a proposed patch containing a pulse oximeter, thermistor, flexible battery, and a single chip mote. If made small enough, this patch could be worn on an infant's underarm to measure heart rate, oxygenation, and body temperature. These three vital signs are important indicators of neonatal health. If they could all be gathered from a single device that can be gently attached to a neonate, the ease of monitoring neonatal health would be significantly improved. Using low cost roll-to-roll manufacturing methods to make the device would enable its use in low-resource communities where infant mortality rates are highest.

Figure 8.4 shows a proposed pajama shirt embedded with red and blue OLEDs to treat acne on the back and chest with phototherapy. The power supply for the OLEDs can be
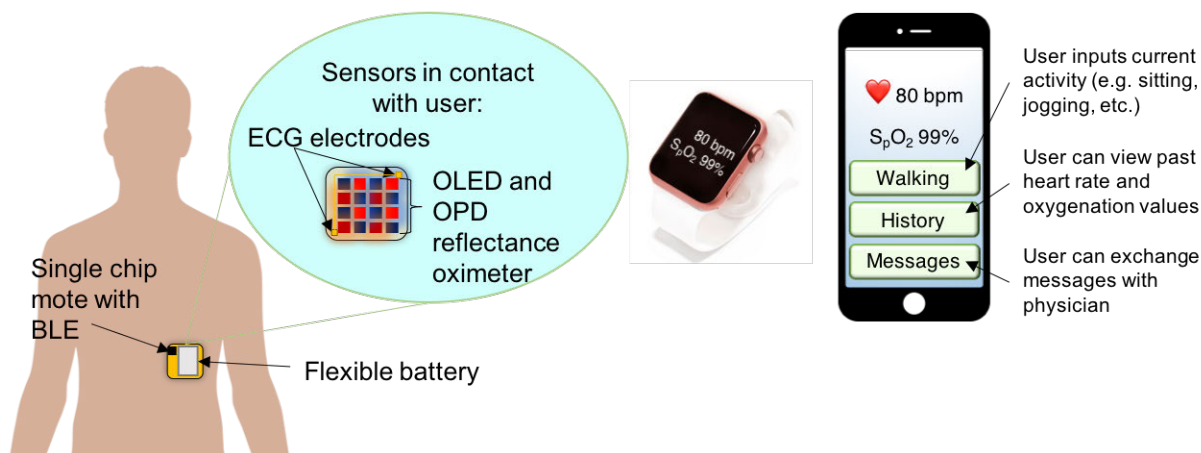
Figure 8.2: **Proposed integrated vital sign monitoring patch** Heart rate and oxygen saturation are measured with a printed ECG and organic optoelectronic reflection mode oximeter. A single chip mote controls signal acquisition and transfer to the user's cellphone and/or smart watch for data processing and display. The patch is powered by a flexible battery.
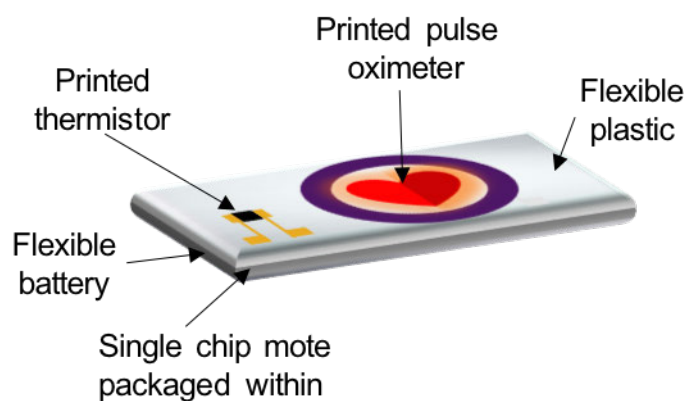
Figure 8.3: **Proposed integrated vital sign monitoring patch for infants** Heart rate and oxygen saturation are measured an organic optoelectronic reflection mode oximeter, which can be manufactured in a child-friendly design. If worn in the underarm, a printed thermistor can measure body temperature. An integrated single chip mote and flexible battery controls and powers the sensors.
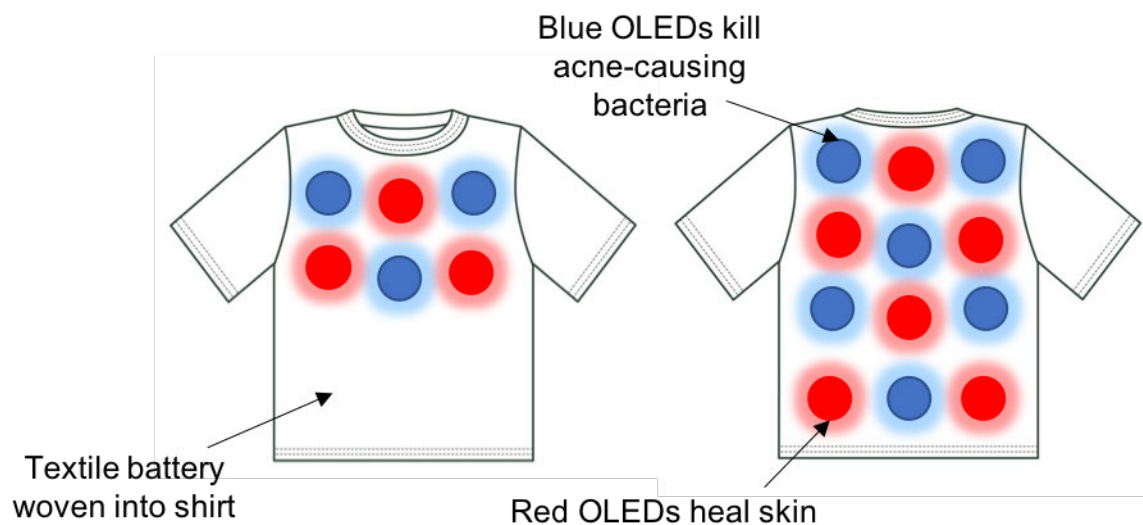
Figure 8.4: **Proposed acne-treating pajamas.** Sewn into a shirt, blue OLEDs kill acne-causing bacteria and red OLEDs heal skin. The OLEDs are powered by a textile battery contained within the shirt fabric.

woven into the fabric of the shirt with a textile battery [205, 206]. Users could wear this acne-fighting top while they sleep, undergoing phototherapy treatments as often as needed to heal their skin with minimal side-effects.

These are just a few examples of what could be done with the printed polymer OLEDs developed in this dissertation. It is hoped that this work will inspire others and be used as a resource for the continued development of biomedical wearables that can improve peoples' quality of life.

Bibliography

[1] Chihaya Adachi et al. "Electroluminescence in organic films with three-layer structure". In: *Japanese Journal of Applied Physics* 27.2A (1988), p. L269.

[2] JH Burroughes et al. "Light-emitting diodes based on conjugated polymers". In: *nature* 347.6293 (1990), p. 539.

[3] Roar R Sondergaard, Markus Hosel, and Frederik C Krebs. "Roll-to-Roll fabrication of large area functional organic materials". In: *Journal of Polymer Science Part B: Polymer Physics* 51.1 (2013), pp. 16–34.

[4] Takatoshi Tsujimura et al. "Development of flexible organic light-emitting diode on barrier film and roll-to-roll manufacturing". In: *Journal of the Society for Information Display* 22.8 (2014), pp. 412–418.

[5] Nick Holonyak Jr and SF Bevacqua. "Coherent (visible) light emission from Ga (As1-x P x) junctions". In: *Applied Physics Letters* 1.4 (1962), pp. 82–83.

[6] Shuji Nakamura, Takashi Mukai, and Masayuki Senoh. "High-power GaN pn junction blue-light-emitting diodes". In: *Japanese Journal of Applied Physics* 30.12A (1991), p. L1998.

[7] Ching W Tang and Steven A VanSlyke. "Organic electroluminescent diodes". In: *Applied physics letters* 51.12 (1987), pp. 913–915.

[8] Donggeon Han et al. "Flexible Blade-Coated Multicolor Polymer Light-Emitting Diodes for Optoelectronic Sensors". In: *Advanced Materials* 29.22 (2017).

[9] ShunChi Chang et al. "Multicolor organic lightemitting diodes processed by hybrid inkjet printing". In: *Advanced Materials* 11.9 (1999), pp. 734–737.

[10] P. Kopola et al. "Gravure printed organic light emitting diodes for lighting applications". In: *Thin Solid Films* 517.19 (2009), pp. 5757–5762. ISSN: 0040-6090. DOI: https://doi.org/10.1016/j.tsf.2009.03.209. URL: http://www.sciencedirect.com/science/article/pii/S0040609009007202.

[11] Tomoyuki Yokota et al. "Ultraflexible organic photonic skin". In: *Sci Adv* 2.4 (2016), e1501856. ISSN: 2375-2548. DOI: 10.1126/sciadv.1501856.

[12]   Taehwan Kim et al. "Kirigami-based three-dimensional OLED concepts for architectural lighting". In: *Organic Light Emitting Materials and Devices XXI*. Vol. 10362. International Society for Optics and Photonics. 2017, p. 1036220.

[13]   Ana Claudia Arias et al. "Materials and applications for large area electronics: solution-based approaches". In: *Chemical reviews* 110.1 (2010), pp. 3–24.

[14]   Saleem Khan, Leandro Lorenzelli, and Ravinder S Dahiya. "Technologies for printing sensors and electronics over large flexible substrates: a review". In: *IEEE Sensors Journal* 15.6 (2015), pp. 3164–3185.

[15]   Nonin Medical Inc. *The WristOx2, Model 3150 Wrist-worn Pulse Oximeter*. 2016. URL: `http://www.nonin.com/OEMSolutions/WristOx23150-OEM` (visited on 03/31/2018).

[16]   Polina Anikeeva et al. "Optetrode: a multichannel readout for optogenetic control in freely moving mice". In: *Nature neuroscience* 15.1 (2012), p. 163.

[17]   Ambicare Health. *Ambulight PDT Overview*. 2018. URL: `http://www.ambicarehealth.com/ambulight-pdt/` (visited on 03/15/2018).

[18]   Sarah D Power, Azadeh Kushki, and Tom Chau. "Towards a system-paced near-infrared spectroscopy brain-computer interface: differentiating prefrontal activity due to mental arithmetic and mental singing from the no-control state". In: *J Neural Eng* 8.6 (2011), p. 066004. DOI: `10.1088/1741-2560/8/6/066004`.

[19]   John G Webster. *Design of pulse oximeters*. CRC Press, 1997.

[20]   JP De Kock and L Tarassenko. "Pulse oximetry: Theoretical and experimental models". In: *Medical and Biological Engineering and Computing* 31.3 (1993), pp. 291–300.

[21]   Takuo Aoyagi. "Pulse oximetry: its invention, theory, and future". In: *Journal of anesthesia* 17.4 (2003), pp. 259–266.

[22]   Claire M Lochner et al. "All-organic optoelectronic sensor for pulse oximetry". In: *Nature communications* 5 (2014), p. 5745.

[23]   Keisuke Matsushita et al. "Fundamental study of reflection pulse oximetry". In: *Optical review* 10.5 (2003), pp. 482–487.

[24]   James L Reuss and Daniel Siker. "The pulse in reflectance pulse oximetry: modeling and experimental studies". In: *Journal of clinical monitoring and computing* 18.4 (2004), pp. 289–299.

[25]   James L Reuss. "Multilayer modeling of reflectance pulse oximetry". In: *IEEE transactions on biomedical engineering* 52.2 (2005), pp. 153–159.

[26]   Yitzhak Mendelson and Burt D Ochs. "Noninvasive pulse oximetry utilizing skin reflectance photoplethysmography". In: *IEEE Transactions on Biomedical Engineering* 35.10 (1988), pp. 798–805.

[27] Tina Zaman, Panayiotis A Kyriacou, and SK Pal. "Free flap pulse oximetry utilizing reflectance photoplethysmography". In: *Engineering in Medicine and Biology Society (EMBC), 2013 35th Annual International Conference of the IEEE*. IEEE. 2013, pp. 4046–4049.

[28] Branko G Celler, Nigel H Lovell, Jim Basilakis, et al. "Using information technology to improve the management of chronic disease". In: *Medical Journal of Australia* 179.5 (2003), pp. 242–246.

[29] Benjamin Noah et al. "Impact of remote patient monitoring on clinical outcomes: an updated meta-analysis of randomized controlled trials". In: *NPJ Digital Medicine* 1.1 (2018), p. 2.

[30] Robert Wang et al. "Accuracy of wrist-worn heart rate monitors". In: *Jama cardiology* 2.1 (2017), pp. 104–106.

[31] Nasirul J Ekbal et al. "Monitoring tissue perfusion, oxygenation, and metabolism in critically ill patients". In: *Chest* 143.6 (2013), pp. 1799–1808.

[32] Jenifer M Schnettler and James A Wallace. "Pulse oximetry as a diagnostic tool of pulpal vitality". In: *Journal of endodontics* 17.10 (1991), pp. 488–490.

[33] Velayutham Gopikrishna, Kush Tinagupta, and Deivanayagam Kandaswamy. "Comparison of electrical, thermal, and pulse oximetry methods for assessing pulp vitality in recently traumatized teeth". In: *Journal of endodontics* 33.5 (2007), pp. 531–535.

[34] Simony Hidee Hamoy Kataoka et al. "Late effects of head and neck radiotherapy on pulp vitality assessed by pulse oximetry". In: *Journal of endodontics* 42.6 (2016), pp. 886–889.

[35] Paolo Giacometti and Solomon G Diamond. "Diffuse optical tomography for brain imaging: continuous wave instrumentation and linear analysis methods". In: *Optical Methods and Instrumentation in Brain Imaging and Therapy*. Springer, 2013, pp. 57–85.

[36] Martin Wolf, Marco Ferrari, and Valentina Quaresima. "Progress of near-infrared spectroscopy and topography for brain and muscle clinical applications". In: *Journal of biomedical optics* 12.6 (2007), p. 062104.

[37] Felix Scholkmann et al. "A review on continuous wave functional near-infrared spectroscopy and imaging instrumentation and methodology". In: *Neuroimage* 85 (2014), pp. 6–27.

[38] Frans F Jobsis. "Noninvasive, infrared monitoring of cerebral and myocardial oxygen sufficiency and circulatory parameters". In: *Science* 198.4323 (1977), pp. 1264–1267.

[39] P-E Seguela et al. "Ductal closure and near-infrared spectroscopy for regional oxygenation monitoring in ductus-dependent congenital heart disease". In: *Archives De Pediatrie* 22.8 (2015), pp. 857–860.

[40] Marco Ferrari and Valentina Quaresima. "A brief review on the history of human functional near-infrared spectroscopy (fNIRS) development and fields of application". In: *Neuroimage* 63.2 (2012), pp. 921–935.

[41] Arno Villringer et al. "Near infrared spectroscopy (NIRS): a new tool to study hemodynamic changes during activation of brain function in human adults". In: *Neuroscience letters* 154.1-2 (1993), pp. 101–104.

[42] Gorm Greisen, Terence Leung, and Martin Wolf. "Has the time come to use near-infrared spectroscopy as a routine clinical tool in preterm infants undergoing intensive care?" In: *Phil. Trans. R. Soc. A* 369.1955 (2011), pp. 4440–4451.

[43] S Chakravarti and S Srivastava. "Near infrared spectroscopy (NIRS) in children". In: *Seminars in Cardiothoracic and Vascular Anesthesia* (2008). ISSN: 1089-2532. DOI: `10.1177/1089253208316444`.

[44] Dandan Zhang et al. "Discrimination of emotional prosodies in human neonates: A pilot fNIRS study". In: *Neuroscience letters* 658 (2017), pp. 62–66.

[45] T Fekete et al. "Small-world network properties in prefrontal cortex correlate with predictors of psychopathology risk in young children: A NIRS study". In: *NeuroImage* (2014).

[46] CK Kim et al. "Development of wireless NIRS system with dynamic removal of motion artifacts". In: *Biomedical Engineering Letters* (2011).

[47] Thomas Muehlemann, Daniel Haensse, and Martin Wolf. "Wireless miniaturized in-vivo near infrared imaging". In: *Opt. Express* 16.14 (July 2008), pp. 10323–10330. DOI: `10.1364/OE.16.010323`. URL: `http://www.opticsexpress.org/abstract.cfm?URI=oe-16-14-10323`.

[48] Fenghua Tian, George Alexandrakis, and Hanli Liu. "Optimization of probe geometry for diffuse optical brain imaging based on measurement density and distribution". In: *Appl. Opt.* 48.13 (May 2009), pp. 2496–2504. DOI: `10.1364/AO.48.002496`. URL: `http://ao.osa.org/abstract.cfm?URI=ao-48-13-2496`.

[49] Hamid Dehghani et al. "Depth sensitivity and image reconstruction analysis of dense imaging arrays for mapping brain function with diffuse optical tomography". In: *Appl. Opt.* 48.10 (Apr. 2009), pp. D137–D143. DOI: `10.1364/AO.48.00D137`. URL: `http://ao.osa.org/abstract.cfm?URI=ao-48-10-D137`.

[50] Shankar P Gopinath et al. "Early detection of delayed traumatic intracranial hematomas using near-infrared spectroscopy". In: *Journal of neurosurgery* 83.3 (1995), pp. 438–444.

[51] Serdar Kahraman et al. "The Accuracy of Near-Infrared Spectroscopy in Detection of Subdural and Epidural Hematomas". In: *Journal of Trauma and Acute Care Surgery* 61.6 (June 2006), p. 1480. ISSN: 2163-0755. DOI: `10.1097/01.ta.0000197616.10279.48`. URL: `http://dx.doi.org/10.1097/01.ta.0000197616.10279.48`.

[52] Jason D Riley et al. "A hematoma detector-a practical application of instrumental motion as signal in near infra-red imaging". In: *Biomedical optics express* 3.1 (2012), pp. 192–205.

[53] Ashu K Bansal et al. "Wearable organic optoelectronic sensors for medicine". In: *Advanced Materials* 27.46 (2015), pp. 7638–7644.

[54] Kiet Tuong Ly et al. "Near-infrared organic light-emitting diodes with very high external quantum efficiency and radiance". In: *Nature Photonics* 11.1 (2017), p. 63.

[55] Takahiko Yamanaka et al. "Near-infrared organic light-emitting diodes for biosensing with high operating stability". In: *Applied Physics Express* 10.7 (2017), p. 074101.

[56] AN Bashkatov et al. "Optical properties of human skin, subcutaneous and mucous tissues in the wavelength range from 400 to 2000 nm". In: *Journal of Physics D: Applied Physics* 38.15 (2005), p. 2543.

[57] Lief Fenno, Ofer Yizhar, and Karl Deisseroth. "The development and application of optogenetics". In: *Annual review of neuroscience* 34 (2011).

[58] Joanna Mattis et al. "Principles for applying optogenetic tools derived from direct comparative analysis of microbial opsins". In: *Nature methods* 9.2 (2012), p. 159.

[59] Feng Zhang et al. "Optogenetic interrogation of neural circuits: technology for probing mammalian brain structures". In: *Nature protocols* 5.3 (2010), p. 439.

[60] Andrew Morton et al. "High-brightness organic light-emitting diodes for optogenetic control of Drosophila locomotor behaviour". In: *Scientific reports* 6 (2016), p. 31117.

[61] Anja Steude et al. "Controlling the behavior of single live cells with high density arrays of microscopic OLEDs". In: *Advanced Materials* 27.46 (2015), pp. 7657–7661.

[62] Anja Steude et al. "Arrays of microscopic organic LEDs for high-resolution optogenetics". In: *Science advances* 2.5 (2016), e1600061.

[63] Erika Pastrana. "Optogenetics: controlling cell function with light". In: *Nature Methods* 8.1 (2010), p. 24.

[64] Joseph T Smith et al. "Application of flexible OLED display technology for electro-optical stimulation and/or silencing of neural activity". In: *Journal of Display Technology* 10.6 (2014), pp. 514–520.

[65] J Smith et al. "Optogenetic neurostimulation of auricular vagus using flexible OLED display technology to treat chronic inflammatory disease and mental health disorders". In: *Electronics Letters* 52.11 (2016), pp. 900–902.

[66] Adrian Handforth et al. "Vagus nerve stimulation therapy for partial-onset seizures A randomized active-control trial". In: *Neurology* 51.1 (1998), pp. 48–55.

[67] A John Rush et al. "Vagus nerve stimulation (VNS) for treatment-resistant depressions: a multicenter study". In: *Biological psychiatry* 47.4 (2000), pp. 276–286.

[68] MD Daniell and JS Hill. "A HISTORY OF PHOTODYNAMIC THERAPY". In: *Aust Nz J Surg* 61.5 (1991), pp. 340–348. ISSN: 1445-2197. DOI: 10.1111/j.1445-2197.1991.tb00230.x.

[69] KM Beauchemin and P Hays. "Phototherapy is a useful adjunct in the treatment of depressed in-patients". In: *Acta Psychiatrica Scandinavica* 95.5 (1997), pp. 424–427.

[70] Christopher D Fahey and Phyllis C Zee. "Circadian rhythm sleep disorders and phototherapy". In: *Psychiatric Clinics* 29.4 (2006), pp. 989–1007.

[71] M Jeffrey Maisels and Antony F McDonagh. "Phototherapy for neonatal jaundice". In: *New England Journal of Medicine* 358.9 (2008), pp. 920–928.

[72] P Papageorgiou, A Katsambas, and A Chu. "Phototherapy with blue (415 nm) and red (660 nm) light in the treatment of acne vulgaris". In: *British journal of Dermatology* 142.5 (2000), pp. 973–978.

[73] Akira Kawada et al. "Acne phototherapy with a high-intensity, enhanced, narrow-band, blue light source: an open study and in vitro investigation". In: *Journal of dermatological science* 30.2 (2002), pp. 129–135.

[74] Seung Yoon Lee, Chung Eui You, and Mi Youn Park. "Blue and red light combination LED phototherapy for acne vulgaris in patients with skin phototype IV". In: *Lasers in surgery and medicine* 39.2 (2007), pp. 180–188.

[75] WJ Cunliffe and V Goulden. "Phototherapy and acne vulgaris". In: *British journal of Dermatology* 142.5 (2000), pp. 855–856.

[76] Philipp Babilas et al. "Photodynamic therapy in dermatology: state-of-the-art". In: *Photodermatol Photoimmunol Photomed* 26.3 (2010), pp. 118–132. ISSN: 1600-0781. DOI: 10.1111/j.1600-0781.2010.00507.x.

[77] Demian van Straten et al. "Oncologic Photodynamic Therapy: Basic Principles, Current Clinical Status and Future Directions". In: *Cancers* 9.2 (2017), p. 19. DOI: 10.3390/cancers9020019.

[78] Harry Whelan et al. "Effect of NASA Light-Emitting Diode Irradiation on Wound Healing". In: *J Clin Laser Medicine Html_ent Glyph Amp Ascii Amp Surg* 19.6 (2001), pp. 305–314. ISSN: 1061-6128. DOI: 10.1089/104454701753342758.

[79] Sungkyoo Lim. "Phototherapy and the benefits of LEDs". In: *J Soc Inf Display* 19.12 (2011), pp. 882–887. ISSN: 1938-3657. DOI: 10.1889/JSID19.12.882.

[80] Daniel Barolet. "Light-emitting diodes (LEDs) in dermatology". In: *Seminars in cutaneous medicine and surgery*. Vol. 27. 4. Frontline Medical Communications. 2008, pp. 227–238.

[81] Ying-Ying Huang et al. "Biphasic dose response in low level light therapy–an update". In: *Dose-Response* 9.4 (2011), dose–response.

[82] Reza Fekrazad and Nasim Chiniforush. "Oral mucositis prevention and management by therapeutic laser in head and neck cancers." In: *J Lasers Medical Sci* 5.1 (2014), pp. 1–7. ISSN: 2008-9783.

[83] Luigi Corti et al. "Treatment of chemotherapy-induced oral mucositis with light-emitting diode." In: *Photomed Laser Surg* 24.2 (2006), pp. 207–13. ISSN: 1549-5418.

[84] Brian D Hodgson et al. "Amelioration of oral mucositis pain by NASA near- infrared light-emitting diodes in bone marrow transplant patients". In: *Support Care Cancer* 20.7 (2012), pp. 1405–1415. ISSN: 0941-4355. DOI: `10.1007/s00520-011-1223-8`.

[85] Xingjia Wu et al. "Organic light emitting diode improves diabetic cutaneous wound healing in rats". In: *Wound Repair Regen* 23.1 (2015), pp. 104–114. ISSN: 1524-475X. DOI: `10.1111/wrr.12258`.

[86] Malgorzata Wachowska et al. "Aminolevulinic Acid (ALA) as a Prodrug in Photodynamic Therapy of Cancer". In: *Molecules* 16.5 (2011), pp. 4140–4164. ISSN: 1420-3049. DOI: `10.3390/molecules16054140`.

[87] SR Wiegell et al. "Daylight photodynamic therapy for actinic keratosis: an international consensus". In: *Journal of the European Academy of Dermatology and Venereology* 26.6 (2012), pp. 673–679.

[88] Cintia Teles de Andrade et al. "Photodynamic therapy for non-melanoma skin cancer". In: *Highlights in Skin Cancer*. InTech, 2013.

[89] Alexey N Bashkatov, Elina A Genina, and Valery V Tuchin. "Optical properties of skin, subcutaneous, and muscle tissues: a review". In: *Journal of Innovative Optical Health Sciences* 4.01 (2011), pp. 9–38.

[90] Kenneth A. Krohn, Jeanne M. Link, and Ralph P. Mason. "Molecular Imaging of Hypoxia". In: *Journal of Nuclear Medicine* 49.Suppl 2 (Aug. 2008), 129S–148S. ISSN: 0161-5505. DOI: `10.2967/jnumed.107.045914`. URL: `http://dx.doi.org/10.2967/jnumed.107.045914`.

[91] Barbara W. Henderson, Theresa M. Busch, and John W. Snyder. "Fluence rate as a modulator of PDT mechanisms". In: *Lasers in Surgery and Medicine* 38.5 (June 2006), pp. 489–493. ISSN: 1096-9101. DOI: `10.1002/lsm.20327`. URL: `http://dx.doi.org/10.1002/lsm.20327`.

[92] Han-Wen Guo et al. "Low-fluence rate, long duration photodynamic therapy in glioma mouse model using organic light emitting diode (OLED)". In: *Photodiagn Photodyn* 12.3 (2015), pp. 504–510. ISSN: 1572-1000. DOI: `10.1016/j.pdpdt.2015.04.007`.

[93] S.K. Attili et al. "An open pilot study of ambulatory photodynamic therapy using a wearable low-irradiance organic light-emitting diode light source in the treatment of non-melanoma skin cancer". In: *Brit J Dermatol* 161.1 (2009), pp. 170–173. ISSN: 1365-2133. DOI: `10.1111/j.1365-2133.2009.09096.x`.

[94]   Anick Berard et al. "Isotretinoin, pregnancies, abortions and birth defects: a population-based perspective". In: *British journal of clinical pharmacology* 63.2 (2007), pp. 196–205.

[95]   Robert S Stern, Franz Rosa, and Carlene Baum. "Isotretinoin and pregnancy". In: *Journal of the American Academy of Dermatology* 10.5 (1984), pp. 851–854.

[96]   HH Kwon et al. "The clinical and histological effect of home-use, combination blue–red LED phototherapy for mild-to-moderate acne vulgaris in Korean patients: a double-blind, randomized controlled trial". In: *British Journal of Dermatology* 168.5 (2013), pp. 1088–1094.

[97]   Johnson and Johnson Consumer Inc. *Light Therapy Acne Mask.* 2018. URL: `https://www.neutrogena.com/skin/skin-acne/light-therapy-acne-mask/6810124.html` (visited on 04/07/2018).

[98]   Johnson and Johnson Consumer Inc. *Light Therapy Acne Spot Treatment.* 2018. URL: `https://www.neutrogena.com/skin/skin-acne/light-therapy-acne-spot-treatment/6810131.html` (visited on 04/07/2018).

[99]   Qing Qing Dou et al. "Effective near-infrared photodynamic therapy assisted by up-conversion nanoparticles conjugated with photosensitizers". In: *International journal of nanomedicine* 10 (2015), p. 419.

[100] Titao Jing et al. "A reduction-responsive polypeptide nanogel encapsulating NIR photosensitizer for imaging guided photodynamic therapy". In: *Polymer Chemistry* 7.4 (2016), pp. 951–957.

[101] Liqiang Luan et al. "A naphthalocyanine based near-infrared photosensitizer: Synthesis and in vitro photodynamic activities". In: *Bioorganic & medicinal chemistry letters* 23.13 (2013), pp. 3775–3779.

[102] Shizuo Tokito, Tetsuo Tsutsui, and Yasunori Taga. "Microcavity organic light-emitting diodes for strongly directed pure red, green, and blue emissions". In: *Journal of applied physics* 86.5 (1999), pp. 2407–2411.

[103] Brett Warneke et al. "Smart dust: Communicating with a cubic-millimeter computer". In: *Computer* 34.1 (2001), pp. 44–51.

[104] Abhinav M Gaikwad et al. "A high areal capacity flexible lithium-ion battery with a strain-compliant design". In: *Advanced Energy Materials* 5.3 (2015).

[105] Abhinav M Gaikwad, Ana Claudia Arias, and Daniel A Steingart. "Recent progress on printed flexible batteries: mechanical challenges, printing technologies, and future prospects". In: *Energy Technology* 3.4 (2015), pp. 305–328.

[106] Yasser Khan et al. "Flexible Hybrid electronics: direct interfacing of soft and hard electronics for wearable health monitoring". In: *Advanced Functional Materials* 26.47 (2016), pp. 8764–8775.

[107] Yasser Khan et al. "Monitoring of vital signs with flexible and wearable medical devices". In: *Advanced Materials* 28.22 (2016), pp. 4373–4395.

[108] Jeong-Hwan Lee et al. "An exciplex forming host for highly efficient blue organic light emitting diodes with low driving voltage". In: *Advanced Functional Materials* 25.3 (2015), pp. 361–366.

[109] Ryutaro Komatsu et al. "Light-blue thermally activated delayed fluorescent emitters realizing a high external quantum efficiency of 25% and unprecedented low drive voltages in OLEDs". In: *Journal of Materials Chemistry C* 4.12 (2016), pp. 2274–2278.

[110] Dongcheng Chen et al. "Fluorescent Organic Planar pn Heterojunction Light-Emitting Diodes with Simplified Structure, Extremely Low Driving Voltage, and High Efficiency". In: *Advanced Materials* 28.2 (2016), pp. 239–244.

[111] P Rolfe. "In vivo near-infrared spectroscopy." In: *Annu Rev Biomed Eng* 2 (2000), pp. 715–54. ISSN: 1523-9829. DOI: 10.1146/annurev.bioeng.2.1.715.

[112] Magnus Berggren, David Nilsson, and Nathaniel D Robinson. "Organic materials for printed electronics". In: *Nature materials* 6.1 (2007), p. 3.

[113] Chizu Sekine et al. "Recent progress of high performance polymer OLED and OPV materials for organic printed electronics". In: *Sci Technol Adv Mat* 15.3 (2016), p. 034203. ISSN: 1468-6996. DOI: 10.1088/1468-6996/15/3/034203.

[114] Chizu Sekine et al. "Recent progress of high performance polymer OLED and OPV materials for organic printed electronics". In: *Science and technology of advanced materials* 15.3 (2014), p. 034203.

[115] M Baldo et al. "Very high-efficiency green organic light-emitting devices based on electrophosphorescence". In: *Appl Phys Lett* 75.1 (1999), pp. 4–6. ISSN: 0003-6951. DOI: 10.1063/1.124258.

[116] Vicki Cleave et al. "Harvesting Singlet and Triplet Energy in Polymer LEDs". In: *Adv Mater* 11.4 (1999), pp. 285–288. ISSN: 1521-4095. DOI: 10.1002/(SICI)1521-4095(199903)11:4<285::AID-ADMA285>3.0.CO;2-N.

[117] G Vaubel, H Baessler, and D Mobius. "Reaction of singlet excitons at an anthracene/metal interface: energy transfer". In: *Chemical Physics Letters* 10.3 (1971), pp. 334–336.

[118] M Kuik et al. "Non-radiative recombination losses in polymer light-emitting diodes". In: *Organic Electronics* 13.6 (2012), pp. 969–974.

[119] DE Markov and PWM Blom. "Migration-assisted energy transfer at conjugated polymer/metal interfaces". In: *Physical Review B* 72.16 (2005), p. 161401.

[120] Abhinav M Gaikwad et al. "Identifying orthogonal solvents for solution processed organic transistors". In: *Organic Electronics* 30 (2016), pp. 18–29.

[121] Ji-Seon Kim et al. "Spin-cast thin semiconducting polymer interlayer for improving device efficiency of polymer light-emitting diodes". In: 87.2 (2005), p. 023506. ISSN: 0003-6951. DOI: `10.1063/1.1992658`.

[122] He Yan et al. "Enhanced Polymer Light-Emitting Diode Performance Using a Crosslinked-Network Electron-Blocking Interlayer". In: *Advanced materials* 16.21 (2004), pp. 1948–1953.

[123] Biwu Ma et al. "Multifunctional crosslinkable iridium complexes as hole transporting/electron blocking and emitting materials for solution-processed multilayer organic light-emitting diodes". In: *Advanced Functional Materials* 19.7 (2009), pp. 1024–1031.

[124] Y-H Niu et al. "Crosslinkable Hole-Transport Layer on Conducting Polymer for High-Efficiency White Polymer Light-Emitting Diodes". In: *Advanced Materials* 19.2 (2007), pp. 300–304.

[125] JS Kim and C Murphy. "Organic-Organic Semiconductor Interfaces for Molecular Electronic Devices". In: (2011).

[126] E Moons. "Conjugated polymer blends: linking film morphology to performance of light emitting diodes and photodiodes". In: *Journal of Physics: Condensed Matter* (2002).

[127] Lian Duan, Kai Xie, and Yong Qiu. "Progress on efficient cathodes for organic light-emitting diodes". In: *J Soc Inf Display* 19.6 (2011), pp. 453–461. ISSN: 1938-3657. DOI: `10.1889/JSID19.6.453`.

[128] J Lee et al. "High efficiency organic light-emitting devices with Al/NaF cathode". In: *Applied Physics Letters* 82.2 (2003), pp. 173–175.

[129] Paul E Burrows et al. "Ultra barrier flexible substrates for flat panel displays". In: *Displays* 22.2 (2001), pp. 65–69.

[130] Jay S Lewis and Michael S Weaver. "Thin-film permeation-barrier technology for flexible organic light-emitting devices". In: *IEEE Journal of selected topics in quantum electronics* 10.1 (2004), pp. 45–57.

[131] Jin-Seong Park et al. "Thin film encapsulation for flexible AM-OLED: a review". In: *Semiconductor science and technology* 26.3 (2011), p. 034001.

[132] Fred B McCormick, Paul F Baude, and Michael A Haase. *Encapsulation of organic electronic devices using adsorbent loaded adhesives*. US Patent 6,936,131. Aug. 2005.

[133] Tesa SE. *Barrier tape solutions for lateral OLED encapsuatlion*. 2018. URL: `http://www.tesatape.com/industry/electronics/applications/encapsulation` (visited on 04/12/2018).

[134] David B Hall, Patrick Underhill, and John M Torkelson. "Spin coating of thin and ultrathin polymer films". In: *Polymer Engineering & Science* 38.12 (1998), pp. 2039–2045.

[135] Adrien Pierre et al. "All-printed flexible organic transistors enabled by surface tension-guided blade coating". In: *Advanced Materials* 26.32 (2014), pp. 5722–5727.

[136] Michael Vosgueritchian, Darren J Lipomi, and Zhenan Bao. "Highly Conductive and Transparent PEDOT:PSS Films with a Fluorosurfactant for Stretchable and Flexible Transparent Electrodes". In: *Adv Funct Mater* 22.2 (2012), pp. 421–428. DOI: 10.1002/adfm.201101775.

[137] Kirill Efimenko, William E Wallace, and Jan Genzer. "Surface modification of Sylgard-184 poly (dimethyl siloxane) networks by ultraviolet and ultraviolet/ozone treatment". In: *Journal of colloid and interface science* 254.2 (2002), pp. 306–315.

[138] AC Arias et al. "Vertically segregated polymer-blend photovoltaic thin-film structures through surface-mediated solution processing". In: *Applied Physics Letters* 80.10 (2002), pp. 1695–1697.

[139] AC Arias et al. "Photovoltaic performance and morphology of polyfluorene blends: a combined microscopic and photovoltaic investigation". In: *Macromolecules* 34.17 (2001), pp. 6005–6013.

[140] Henry J Snaith et al. "Charge generation kinetics and transport mechanisms in blended polyfluorene photovoltaic devices". In: *Nano Letters* 2.12 (2002), pp. 1353–1357.

[141] Arne C Morteani et al. "Barrier-Free Electron–Hole Capture in Polymer Blend Heterojunction Light-Emitting Diodes". In: *Advanced Materials* 15.20 (2003), pp. 1708–1712.

[142] K Murata, S Cina, and NC Greenham. "Barriers to electron extraction in polymer light-emitting diodes". In: *Applied Physics Letters* 79.8 (2001), pp. 1193–1195.

[143] Michael C Gwinner et al. "Solution-Processed Zinc Oxide as High-Performance Air-Stable Electron Injector in Organic Ambipolar Light-Emitting Field-Effect Transistors". In: *Advanced Functional Materials* 20.20 (2010), pp. 3457–3465.

[144] Th. Forster. "10th Spiers Memorial Lecture. Transfer mechanisms of electronic excitation". In: *Discuss Faraday Soc* 27.0 (1959), pp. 7–17. ISSN: 0366-9033. DOI: 10.1039/DF9592700007.

[145] Keng-Hoong Yim et al. "Surface-Directed Phase Separation of Conjugated Polymer Blends for Efficient Light-Emitting Diodes". In: *Advanced Functional Materials* 18.19 (2008), pp. 2897–2904.

[146] Monika Voigt et al. "The interplay between the optical and electronic properties of light-emitting-diode applicable conjugated polymer blends and their phase-separated morphology". In: *Organic electronics* 6.1 (2005), pp. 35–45.

[147] N Corcoran et al. "Increased efficiency in vertically segregated thin-film conjugated polymer blends for light-emitting diodes". In: *Applied physics letters* 82.2 (2003), pp. 299–301.

[148] Keng-Hoong Yim et al. "Phase-separated thin film structures for efficient polymer blend light-emitting diodes". In: *Nano letters* 10.2 (2010), pp. 385–392.

[149] Mark Yelderman and William New. "Evaluation of pulse oximetry". In: *Anesthesiology: The Journal of the American Society of Anesthesiologists* 59.4 (1983), pp. 349–351.

[150] Yasser Khan et al. "System design for organic pulse oximeter". In: *Advances in Sensors and Interfaces (IWASI), 2015 6th IEEE International Workshop on.* IEEE. 2015, pp. 83–86.

[151] Jonathan V Caspar et al. "Application of the energy gap law to the decay of charge-transfer excited states". In: *Journal of the American Chemical Society* 104.2 (1982), pp. 630–632.

[152] Jonathan R Sommer et al. "Efficient near-infrared polymer and organic light-emitting diodes based on electrophosphorescence from (tetraphenyltetranaphtho [2, 3] porphyrin) platinum (II)". In: *ACS applied materials & interfaces* 1.2 (2009), pp. 274–278.

[153] T Osada et al. "Polymer-based light-emitting devices: investigations on the role of the indium-tin oxide (ITO) electrode". In: *Synthetic metals* 96.1 (1998), pp. 77–80.

[154] Yoon-Heung Tak et al. "Criteria for ITO (indium–tin-oxide) thin film as the bottom electrode of an organic light emitting diode". In: *Thin Solid Films* 411.1 (2002), pp. 12–16.

[155] JS Kim et al. "Indium-tin oxide treatments for single-and double-layer polymeric light-emitting diodes: The relation between the anode physical, chemical, and morphological properties and the device performance". In: *Journal of Applied Physics* 84.12 (1998), pp. 6859–6870.

[156] Sung Kyu Park et al. "Deposition of indium–tin-oxide films on polymer substrates for application in plastic-based flat panel displays". In: *Thin Solid Films* 397.1-2 (2001), pp. 49–55.

[157] Sung Kyu Park et al. "Mechanical stability of externally deformed indium–tin–oxide films on polymer substrates". In: *Japanese journal of applied physics* 42.2R (2003), p. 623.

[158] Darran R Cairns et al. "Strain-dependent electrical resistance of tin-doped indium oxide on polymer substrates". In: *Applied Physics Letters* 76.11 (2000), pp. 1425–1427.

[159] Weiran Cao et al. "Transparent electrodes for organic optoelectronic devices: a review". In: *Journal of Photonics for Energy* 4.1 (2014), p. 040990.

[160] Liangbing Hu et al. "Scalable coating and properties of transparent, flexible, silver nanowire electrodes". In: *ACS nano* 4.5 (2010), pp. 2955–2963.

[161] Liangbing Hu et al. "Flexible organic light-emitting diodes with transparent carbon nanotube electrodes: problems and solutions". In: *Nanotechnology* 21.15 (2010), p. 155202.

[162] Sung-Min Lee et al. "A Review of flexible OLEDs toward highly durable unusual displays". In: *IEEE Transactions on Electron Devices* 64.5 (2017), pp. 1922–1931.

[163] Yi Yin et al. "Reactive sputter deposition of WO3/Ag/WO3 film for indium tin oxide (ITO)-free electrochromic devices". In: *ACS applied materials & interfaces* 8.6 (2016), pp. 3861–3867.

[164] Sungjun Kim and Jong-Lam Lee. "Design of dielectric/metal/dielectric transparent electrodes for flexible electronics". In: *Journal of Photonics for Energy* 2.1 (2012), p. 021215.

[165] Jun Hee Han et al. "Highly conductive and flexible color filter electrode using multilayer film structure". In: *Scientific reports* 6 (2016), p. 29341.

[166] Hyunsu Cho, Changhun Yun, and Seunghyup Yoo. "Multilayer transparent electrode for organic light-emitting diodes: tuning its optical characteristics". In: *Optics express* 18.4 (2010), pp. 3404–3414.

[167] Sung-Min Lee et al. "Low resistive transparent and flexible ZnO/Ag/ZnO/Ag/WO3 electrode for organic light-emitting diodes". In: *Organic Electronics* 13.9 (2012), pp. 1654–1659.

[168] Hongyan Liu et al. "Strong interference-based ultrathin conductive anti-reflection coating on metal substrates for optoelectronics". In: *NPG Asia Materials* 10.4 (2018), pp. 309–317. ISSN: 1884-4049. DOI: 10.1038/s41427-018-0011-z. URL: http://dx.doi.org/10.1038/s41427-018-0011-z.

[169] Jun Hee Han et al. "Highly conductive transparent and flexible electrodes including double-stacked thin metal films for transparent flexible electronics". In: *ACS applied materials & interfaces* 9.19 (2017), pp. 16343–16350.

[170] Jens Meyer et al. "Transition metal oxides for organic electronics: energetics, device physics and applications". In: *Advanced Materials* 24.40 (2012), pp. 5408–5427.

[171] Kihyon Hong et al. "Optical properties of WO3/Ag/WO3 multilayer as transparent cathode in top-emitting organic light emitting diodes". In: *The Journal of Physical Chemistry C* 115.8 (2011), pp. 3453–3459.

[172] K. von Rottkay, M. Rubin, and S.-J. Wen. "Optical indices of electrochromic tungsten oxide". In: *Thin Solid Films* 306.1 (1997), pp. 10–16. ISSN: 0040-6090. DOI: https://doi.org/10.1016/S0040-6090(97)00254-X. URL: http://www.sciencedirect.com/science/article/pii/S004060909700254X.

[173] P Winsemius et al. "Temperature dependence of the optical properties of Au, Ag and Cu". In: *Journal of Physics F: Metal Physics* 6.8 (1976), p. 1583. URL: http://stacks.iop.org/0305-4608/6/i=8/a=017.

[174] MM De Kok et al. "Modification of PEDOT: PSS as hole injection layer in polymer LEDs". In: *physica status solidi (a)* 201.6 (2004), pp. 1342–1359.

[175] A. Berni, M. Mennig, and H. Schmidt. *Doctor Blade.* Ed. by M.A. Aegerter and M Mennig. Springer, 2004. ISBN: 9781441954558. DOI: 10.1007/978-0-387-88953-5_10.

[176] Xiaodan Gu et al. "The meniscus-guided deposition of semiconducting polymers". In: *Nat Commun* 9.1 (2018), p. 534. DOI: 10.1038/s41467-018-02833-9.

[177] Shih-Hao Chuang et al. "Transparent conductive oxide films embedded with plasmonic nanostructure for light-emitting diode applications". In: *ACS applied materials & interfaces* 7.4 (2015), pp. 2546–2553.

[178] Wenpei Fan, Peng Huang, and Xiaoyuan Chen. "Overcoming the Achilles' heel of photodynamic therapy". In: *Chemical Society Reviews* 45.23 (2016), pp. 6488–6519.

[179] M Thavasothy et al. "A comparison of cerebral oxygenation as measured by the NIRO 300 and the INVOS 5100 near-infrared spectrophotometers". In: *Anaesthesia* 57.10 (2002), pp. 999–1006.

[180] A von Luhmann. *Design and Evaluation of a System for Mobile Brain Activity Measurements using Functional Near-Infrared Spectroscopy.* 2014.

[181] Aminy E Ostfeld et al. "Single-walled carbon nanotube transparent conductive films fabricated by reductive dissolution and spray coating for organic photovoltaics". In: *Applied Physics Letters* 105.25 (2014), 187_1.

[182] Balthazar P Lechene et al. "Organic solar cells and fully printed super-capacitors optimized for indoor light energy harvesting". In: *Nano Energy* 26 (2016), pp. 631–640.

[183] Adrien Pierre et al. "High Detectivity All-Printed Organic Photodiodes". In: *Advanced Materials* 27.41 (2015), pp. 6411–6417.

[184] Adrien Pierre, Abhinav Gaikwad, and Ana Claudia Arias. "Charge-integrating organic heterojunction phototransistors for wide-dynamic-range image sensors". In: *Nature Photonics* (Feb. 2017). Article. ISSN: 1749-4893.

[185] TM Eggenhuisen et al. "High efficiency, fully inkjet printed organic solar cells with freedom of design". In: *Journal of Materials Chemistry A* 3.14 (2015), pp. 7255–7262.

[186] Stephan van Reenen et al. "Origin of Work Function Modification by Ionic and Amine-Based Interface Layers". In: *Advanced Materials Interfaces* 1.8 (2014).

[187] Yu-shan Liu et al. "Ultrasmooth, highly conductive and transparent PEDOT: PSS/silver nanowire composite electrode for flexible organic light-emitting devices". In: *Organic Electronics* 31 (2016), pp. 247–252.

[188] Xiao-Yan Zeng et al. "A new transparent conductor: silver nanowire film buried at the surface of a transparent polymer". In: *Advanced materials* 22.40 (2010), pp. 4484–4488.

[189] Stephan Harkema et al. "Large area ITO-free flexible white OLEDs with Orgacon PEDOT: PSS and printed metal shunting lines". In: *Organic Light Emitting Materials and Devices XIII*. Vol. 7415. International Society for Optics and Photonics. 2009, 74150T.

[190] Jolke Perelaer et al. "One-step inkjet printing of conductive silver tracks on polymer substrates". In: *Nanotechnology* 20.16 (2009), p. 165303.

[191] Dongjo Kim and Jooho Moon. "Highly conductive ink jet printed films of nanosilver particles for printable electronics". In: *Electrochemical and Solid-State Letters* 8.11 (2005), J30–J33.

[192] George Burkhard. *CTO of Sinovia Technologies*. 2017.

[193] Afshin Shahalizad et al. "Near infrared electroluminescence from Nd (TTA) 3phen in solution-processed small molecule organic light-emitting diodes". In: *Organic Electronics* 44 (2017), pp. 50–58.

[194] Sagar Kesarkar et al. "Near-IR Emitting Iridium (III) Complexes with Heteroaromatic β-Diketonate Ancillary Ligands for Efficient Solution-Processed OLEDs: Structure–Property Correlations". In: *Angewandte Chemie* 128.8 (2016), pp. 2764–2768.

[195] CH Cheung et al. "Change of the emission spectra in organic light-emitting diodes by layer thickness modification". In: *Applied physics letters* 85.14 (2004), pp. 2944–2946.

[196] Jin Xu et al. "Color tuning in inverted blue light-emitting diodes based on a polyfluorene derivative by adjusting the thickness of the light-emitting layer". In: *Journal of Materials Chemistry C* 3.38 (2015), pp. 9819–9826.

[197] CH Cheung et al. "Dependence of the emission from tris (8-hydroxyquinoline) aluminum based microcavity on device thickness and the emission layer position". In: *Thin Solid Films* 489.1-2 (2005), pp. 235–244.

[198] Tal Ellenbogen and Kenneth B Crozier. "Exciton-polariton emission from organic semiconductor optical waveguides". In: *Physical Review B* 84.16 (2011), p. 161304.

[199] V Bulovic et al. "Weak microcavity effects in organic light-emitting devices". In: *Physical Review B* 58.7 (1998), pp. 3730–3740. ISSN: 0163-1829. DOI: 10.1103/physrevb.58.3730. URL: http://dx.doi.org/10.1103/physrevb.58.3730.

[200] Donggeon Han et al. "Emission Area Patterning of Organic Light-Emitting Diodes (OLEDs) via Printed Dielectrics". In: *Advanced Functional Materials* (2018), p. 1802986.

[201] Amir Khakban et al. "The projected epidemic of chronic obstructive pulmonary disease hospitalizations over the next 15 years. A population-based perspective". In: *American journal of respiratory and critical care medicine* 195.3 (2017), pp. 287–291.

[202] Aidee Duarte et al. "Recent advances in conjugated polyelectrolytes for emerging optoelectronic applications". In: *Chemistry of Materials* 23.3 (2010), pp. 501–515.

[203] Fei Huang et al. "A Conjugated, Neutral Surfactant as Electron-Injection Material for High-Efficiency Polymer Light-Emitting Diodes". In: *Advanced Materials* 19.15 (2007), pp. 2010–2014.

[204] Tatsuro Yamamoto, Hirotake Kajii, and Yutaka Ohmori. "Improved electron injection from silver electrode for all solution-processed polymer light-emitting diodes with Cs2CO3: conjugated polyelectrolyte blended interfacial layer". In: *Organic Electronics* 15.6 (2014), pp. 1077–1082.

[205] Abhinav M Gaikwad et al. "Highly stretchable alkaline batteries based on an embedded conductive fabric". In: *Advanced Materials* 24.37 (2012), pp. 5071–5076.

[206] Alla M Zamarayeva et al. "Flexible and stretchable power sources for wearable electronics". In: *Science advances* 3.6 (2017), e1602051.

Appendix A

Physician Interviews

.1 Dr. Rob Brownell, Pulmonologist, UCSF Medical Center, San Francisco, California

Interview Summary:

Our reflectance oximetry patch could be useful during drug trial studies for interstitial lung disease patients. Dr. Brownell and Dr. Collard would be interested in consulting for our development process and letting us test our pulse oximeter patches on their patients in their clinic at UCSF once we have successfully tested them with varying oxygenation levels in-house.

Dr. Rob Brownell is a senior Fellow working with Dr. Collard, who is an interstitial lung disease specialist and director of UCSF Clinical and Translational Science Institute (CTSI). They are currently conducting research on patients with idiopathic pulmonary fibrosis (IPF), a chronic degenerative disease wherein patients lung tissue is irreversibly scarred. Once diagnosed, IPS patients have life expectancy of only 2-5 years. New medicines are being researched to slow the progression of the disease. At this time, pulmonologists are unable to continuously monitor patients oxygenation outside of their clinics.

Dr. Brownell will be conducting a study where patients will wear fitbits to monitor their activity and heart rate and will regularly measure their breathing capacity with a spirometer. He said that our oximeter patch could make a good addition in future studies for measuring oxygenation.

Doctors don't know yet whether long-term continuous patient monitoring is helpful - there would be a lot of data but they dont know what it means yet. But it would be immediately interesting and useful to have continuous oxygenation data points during drug trials. When starting a patient on a new drug, it would be useful to remotely monitor their oxygenation for a few days to see how the drug is affecting their oxygen intake.

Dr. Brownell and Dr. Collard would be willing to let us test our pulse ox patches on patients in their lab (wireless preferred - concerned that changing from wired to wireless

system could affect the measurement - would rather do one round of testing than one with a wired system and then another with a wireless system).

For a disposable sensor, the more frequent the "dosing," the more likely a patient is to remember - i.e. patient should replace sensor every day as opposed to every two days. A water proof sensor would be the ideal, as patients can desaturate while showering.

It would be helpful if a physician could set a threshold, x fall in oxygenation level for x amount of time, before the patient and/or physician is alerted. It would also be useful for the patient to record their activity into a phone app, so the doctor knows how the patients activity level corresponds to their oxygenation.

Currently in their clinic, they use a clip-on oximeter that only reports pulse and oxygenation values without showing a PPG.

.2 Dr. Rachel Hecht Bandi, Anesthesiologist Northwestern University Medical Center, Chicago, Illinois

Interview Summary:

Conventional pulse oximeters are sufficient and reliable for anesthesiologists. An improved pulse oximeter would be easy to place near the head and chest, but the most meaningful improvement would be making the sensor wireless.

1. **How do you currently use pulse oximetry?**

   During surgery to monitor patients under anesthesia.

2. **How do you currently measure tissue oxygenation?**

   For cardiac patients- transcranial oxygenation measurement of the brain while patient is on bypass. Dr. Charles Hogue - NIRS

3. **What (if any) limitations does a conventional pulse oximeter have in your work?**

   Vasculopathic patients have bad arteries, can't get read - put on ear, lip, nose - somewhere more proximal to heart with less signal degradation. Use disposable oximeters.

Rarely use permanent ones. Sticker ones are $40-$50, the permanent ones are $90.

4. **If you could perform pulse oximetry anywhere on the body, where would you perform it?**

   The hand isn't the best place, also use blood pressure every 3-5 minutes, on one hand, pulse ox on the other. Would like to put it on the face or on the neck. Closer to head. Use disposable pulse ox.

5. **If you could perform pulse oximetry during any procedure, when would you perform it?**

   Every surgery, in ICU

6. **How often would you like to perform an oxygenation measurement and over what period of time?**

   Start before anesthesia, ends in recovery room. Surgery can be 10 mins to 12 hrs. Avg is 2-4 hrs.

7. **How reliable do you consider conventional pulse oximeters?**

   Extremely. They work so well, through acrylic nails if theyre the right color, almost all gel nails. Only issues with acrylics if theyre dark colors - black/blue.

8. **If an oximeter consisted of multiple pixels that each gave their own measurement, would you consider the oximeter to be more reliable than a conventional pulse oximeter?**

   Not really.

9. **Would creating a 2D map of relative tissue oxygenation be beneficial to your work?**

   Not really. Could see it being useful in plastics, podiatry. Could be really useful for skin grafts.

10. **Looking at our current reflectance oximeter array prototype, what do you like about it? Do you foresee any limitations of its current design?**

    NEED WIRELESS. anesthesiologist spends minutes organizing cords. At least 5 chords and 6 EKG for one IV. Could be 12 more. Maybe people would be willing to pay a little more for wireless. Really good for patients who need continuous pulse ox in the ICU to have wireless.

11. **How would you like to see the information provided by the pulse oximeter?**

    In ICU, everyone on telemetry, in PACU (post-anesthesia care unit) there is central area where all information goes. See saturation number and alarm if problem, and at bedside. Nursing station has all info, and by patient's bedside. Want to see the waveform, never believe anything without a waveform.

12. **How can patients use pulse oximetry on their own to monitor their health?**

    It may not be as intriguing a use, any patient you're concerned about oxygenation if more sick, so more useful in ICU - very sick patients with fluctuating oxygen levels you want to watch closely, area of perfusion for skin flap would be a very good novel use. People are willing to pay a lot more for things that add value in the ICU than at home. This doctor goes through about through 3-4 disposable $50 pulse ox per day, per patient. Can foresee hospitals willing to pay at least $100s for blood perfusion map devices, probably more.

13. **How would our technology aid you in your day to day working practices, decision making processes, the added level of information that you would gain when liaising with patients?**

    Same as conventional pulse oximeters.

14. **What are the other technology solutions that are being trialled or considered and what is/are the advantage(s) of our technology if our solution was to work?**

    Not really.

15. **What (if any), may be the barriers to adoption of this technology from the doctors' point of view? For example including aspects such as the costs of the technology, what would be the maximum acceptable pricing for such a product?**

    Expense, it has to be proven, disposable, if there is no pre-existing good technology - novel use. Current pulse oximeter works well for 95% of surgeries, but don't see a need for our type of device to be standardly stocked unless they were cheaper, or same price and reliable would adopt something more flexible.

16. **What type of approval process(es) would need to be gained before such a technology could be used (assuming that of all the technical targets/goals would be met).**

    Don't know.

17. **What is the minimum number of patients that would need to be included in a clinical test in order for the results to be sufficient to justify further more extensive trials?**

    Don't know. What range is it accurate in, show correlation of measurement to blood gas volume in a variety of people, not sure how many needed.

18. **In a clinical trial, how frequently would the devices need to be changed and could the devices be re-used? Would they need changing (and why?) What would be the typical operational and storage life-times?**

    It depends, people like disposable, but it depends how easy to clean and how well you can clean. Standard wipes "toxic baby wipes" really caustic, don't touch with bare skin. No idea on storage time.

Other notes: Never heard of the Masimo rainbow set, co-oximeter (it doesn't seem to be FDA approved yet in the US). In surgery, pull directly from placement read on ventilator and from arterial line. Would be handy to measure $SpCO_2$ with pulse ox when you dont have an arterial line.

.3 Dr. Mozziyar Etemadi, Anesthesiologist, Feinberg School of Medicine, Northwestern University, Research Assistant Professor, Biomedical Engineering, McCormick School of Engineering

Interview Summary:

A reflectance oximetry array as a substitute to conventional pulse oximetry for anesthesiologists in surgery isn't very compelling, as what they use right now works well enough. It would be more useful if it could perform co-oximetry, measuring CO concentration in the blood as well as oxygen. It could also be useful for near-infrared-spectroscopy (NIRS) over the head during bypass surgery, but would require the NIR OLEDs to have a longer wavelength and this procedure is still considered experimental.

1. **How do you currently use pulse oximetry?**

   Finger probes - disposable and non-disposable In hospital: less critically ill patients pulse ox is measured about once every 4 hours: nurse measures pulse ox, writes, down saturation percentage, puts machine away, one machine per x patients. Don't measure continuously because you dont have enough resources to react if oxygen suddenly decreases. Only react if low pulse ox over longer period of time.

   In intensive care unit, one nurse per patient, monitor pulse ox continuously, on finger constantly.

   For these uses, our patch isn't a huge edge over the current system for standard patient pulse ox care in hospital/during surgery. Pulse oximeters cost nothing to a hospital. "No point in getting into space."

2. **What (if any) limitations does a conventional pulse oximeter have in your work?**

   Blood flow to fingers is often reduced.

3. **If you could perform pulse oximetry anywhere on the body, where would you perform it?**

   Back, mouth, inner throat.

4. **If you could perform pulse oximetry during any procedure, when would you perform it?**

   During surgery.

5. **How often would you like to perform an oxygenation measurement and over what period of time?**

   For less critically ill patients in hospital, pulse ox is measured about once every 4 hours. For critically ill patients, measure constantly.

6. **How reliable do you consider conventional pulse oximeters?**

   It's ok, but we've had it for so long that we deal with it. Hard part is convincing [the physicians] that it isn't that good. It'd be great to have pulse ox in breathing tube. Blood flow to fingers is often reduced. Or in the mouth, but away from the body where everything can go wrong. With larger arrays, can get better SNR.

7. **Looking at our current reflectance oximeter array prototype, what do you like about it? Do you foresee any limitations of its current design?**

   Maybe make it smaller, be able to reconfigure for each application. Currently ECOG electrodes are used on the brain surface. If we put a pulse ox array there, what info can we get? This is more of a science question, physicians dont know what pulse ox in the brain means.

8. **How would you like to see the information provided by the pulse oximeter?**

   Now, at bedside plugged into machine. Always look at waveform, if waveform is bad, ignore the number. Make sure good waveform. One monitor has all readings. GE makes the monitors now.

   Other Notes:

   On current wearables, pulse ox on back of wrist doesn't work accurately. Ours could work better because it could be less sensitive to motion artifacts if secure and immobile against skin.

   Pulse ox would ideally be wireless, but wired is OK.

Definitely look into using our patch for tissue graft perfusion monitoring. Do it in five patients, see how it works, do it in another five. Avg. tissue graft is on the order of the size of our current sensor, maybe a little bigger.

Another possible application is near infrared spectroscopy (NIRS) - is a nascent field and it's still hotly debated if they are getting brain penetration with current devices. Helmet type array maybe it works better than NIRS, maybe it's more robust. Dept. Chair at Northwestern uses NIRS during cardiac bypass to adjust bypass settings. Medtronic makes one, big bulky, rack of equipment is wheeled out to be able to use it.

Potentially look into building a pulse ox array into wall of breathing tube for intubated patients. Tube is 1 mm thick, if on outside of tube, mucosal surface (mouth, windpipe, inside stomach) is much closer to blood vessels. Breathing tubes at home get clogged, causing O_2 levels to go down. A lot of time these are kids, they can't speak.

It'd be great if we could measure CO as well. Currently they measure gas concentrations optically in the operating room with a machine lots of tubes coming in and out. It would be very useful to measure CO on/in the person with a simpler device. Currently for doctors, measuring CO concentration in the blood is useful but is ungainly to do if not in operating room because it requires a large machine.

To vet each application area, run "small" clinical study 20-30 patients.

.4 Dr. Mary D. Jones, Pediatrician Rett Syndrome Clinic, UCSF Benioff Childrens Hospital Walnut Creek Campus

Interview Summary:

A single pixel reflectance pulse oximetry patch is extremely valuable for children with autonomic nervous system disorders. Caregivers want to have a constant reading of heart rate and oxygenation so they can be aware of oncoming seizures of episodes of respiratory distress. Conventional pulse oximeters are incapable of serving this purpose because the children have poor peripheral circulation and impaired motor control of their hands.

1. **How do you currently use pulse oximetry?**

   Want to measure SpO_2 and heart rate.

2. **How do you currently measure tissue oxygenation?**

   Don't.

3. **What (if any) limitations does a conventional pulse oximeter have in your work?**

   Rett Syndrome is an autonomic nervous system disorder - patients "hand wash" which knocks a pulse oximeter off of hands, sweat makes EKG probes hard to adhere, uncontrolled movement disrupts sensors. Some parents try using wrist-worn pulse oximeter from REI, but it just falls off and gives unreliable readings.

4. **If you could perform pulse oximetry anywhere on the body, where would you perform it?**

   Somewhere that the patient won't pull or knock it off. On the back, maybe upper arm. Not on the leg because patients can't control bladder.

5. **How often would you like to perform an oxygenation measurement and over what period of time?**

   Continuous monitoring would be good. The patients can suffer from seizures, poor skin temperature regulation, apnea (while awake), hyperventilation, and it would be good to monitor and maybe predict these conditions.

6. **How reliable do you consider conventional pulse oximeters?**

   They don't work well for these patients - no good finger access, unreliable movement, sometimes bad circulation to hands and feet.

7. **Would creating a 2D map of relative tissue oxygenation be beneficial to your work?**

   Not necessarily.

8. **Looking at our current reflectance oximeter array prototype, what do you like about it? Do you foresee any limitations of its current design?**

   It looks good. Also like the ringed reflection probe (4 OPD pixels, 2 OLED pixels). Set up follow up appointment with a patient to see how the different probes fit, how the geometry could be changed, how they could be attached.

9. **How would you like to see the information provided by the pulse oximeter?/ How can patients use pulse oximetry on their own to monitor their health?**

   An alert to parents would be good if SpO_2 drops too low, or if there is heart rate instability. Some children with Rett Syndrome hold their breath too long and can die without intervention. The doctors at the clinic would also like to collect SpO_2 data, HR, and pulse waveforms.

10. **How would our technology aid you in your day to day working practices, decision making processes, the added level of information that you would gain when liaising with patients?**

    It would enable the collection of new data that could help doctors find changes or trends in SpO_2 and heart rate that correspond to seizures, breath holding, etc, which in turn could improve patient care.

11. **What are the other technology solutions that are being trialled or considered and what is/are the advantage(s) of our technology if our solution was to work?**

    Commercially available wrist oximeters for fitness monitoring dont stay on patients with Rett Syndrome.

12. **Would you recommend our technology to be implemented as a tool for your working practices and explain the reasons why so (or not)?**

    Yes. There is a demand in the Rett Syndrome community for next generation sensors to better monitor and improve children's health.

13. **What (if any), may be the barriers to adoption of this technology from the doctors' point of view? For example including aspects such as the costs of the technology, what would be the maximum acceptable pricing for such a product?**

    Not very many barriers. The patient community is very receptive of anything new that can help.

14. **What is the minimum number of patients that would need to be included in a clinical test in order for the results to be sufficient to justify further more extensive trials?**

    7; sign up 10 patients hoping for 7 good tests.

15. **In a clinical trial, how frequently would the devices need to be changed and could the devices be re-used? Would they need changing (and why?) What would be the typical operational and storage life-times? What would be the power requirements (battery, mains/PSU connection?)**

    Previous heart rate variability trials conducted with ECG had continuous monitoring for four hours. Can reuse devices, clean with IPA in between use.

.5 Dr. Kristen Kester, Pediatrician, Columbia University Medical Center, New York, New York

Interview Summary:

Respiratory problems are to blame for the majority of pediatric hospitalizations and infant mortality, and oximetry is essential for diagnosing and monitoring pediatric patients. However, conventional transmission mode pulse oximeters don't fit infants well. The small probes are placed on infants feet, where they often fall off and sometimes require heating pads to generate enough blood circulation to get a measurement. A larger area sensor than can be attached securely would improve infant oxygenation monitoring. Outside of the hospital, at-home oximetry would help pediatricians decide whether or not a patient should be brought in, just as thermometers are used to measure a childs temperature. Commercially available finger probe oximeters do not fit on pediatric patients' fingers, but parents could use a disposable reflection oximeter patch.

1. **How do you currently use pulse oximetry?**

    As a pediatrician, use it more than on adults because kids number one problem is respiratory problems. Most children die from respiratory issues - highest infant and young toddler mortality are from respiratory functions. Heart it fine, it's the lungs that are small - virus, drowning, choking. Use oximetry all the time.

Over 50% of pediatric complaints in ER are respiratory, rely on pulse ox all the time. Ox sat will determine if someone is admitted to hospital or not, ex: bronchiolitis.

2. **How do you currently measure tissue oxygenation?**

Is tissue along edge of wound viable, living? No way to tell now, keep taking dressing off of skin to see if it's viable. Want to see perfusion of near surgical wounds. Vital signs every 4 hrs on the floor, every 1 hr in ICU. Would want to monitor every 1-4 hrs or on demand.

3. **What (if any) limitations does a conventional pulse oximeter have in your work?**

Only small ones available. Want something larger to put on an area it's more likely to stay on. Too big for toe, too small for foot. Very limited in terms of sizing. Larger surface area would be more helpful - for kids used band-aid like oximeter but put it around hand, toes, but trying to keep it around a baby's toe is difficult. If something is larger that can fit around the entire foot or lower leg, itd be much better.

Kids who are sick, have poor perfusion, toes get worst perfusion, put heat packs on to keep pulse ox in, but can't put pulse ox anywhere else because the transmission sensor can't take a measurement through more than 1 cm thick tissue. Can you build in warming device? Heat area to body temperature.

4. **If you could perform pulse oximetry anywhere on the body, where would you perform it?**

On the leg, or thigh for even smaller children.

5. **If you could perform pulse oximetry during any procedure, when would you perform it?**

On incoming patients in ER, constant monitoring in ICU. Would be good if parents could measure reliably at home to give data points to doctor when calling about a sick child.

6. **How often would you like to perform an oxygenation measurement and over what period of time?**

At will or once every 1-4hrs.

7. **How reliable do you consider conventional pulse oximeters?**

   Fairly reliable if you can get it to stay on. In medicine, rely on oxygen a lot. The new trend is to measure CO as well.

8. **Would creating a 2D map of relative tissue oxygenation be beneficial to your work?**

   Surgically useful. Every now and then someone has septic shock - worry about tissue perfusion and oxygenation. Usually hands and feet god first. This isn't as useful in regular floor setting but in ER, OR and ICU.

9. **If so, where on the body would you take the measurement, over how much area, and with what resolution?**

   Put something over hand and foot 4 x 4 cm, 6 x 6 cm, to see if there is perfusion. Probably wouldn't need fine resolution, but vascular surgeons and trauma surgeons would want better to see what's still alive and decide how far they'd go to save something.

10. **Looking at our current reflectance oximeter array prototype, what do you like about it? Do you foresee any limitations of its current design?**

    "This is huge!" With current pulse oximeters, it's hard to get them to wrap around equally for transmission measurements. To be able to put it on one side is huge. All babies wear them continuously. If it's not more expensive to do more pixels than one, do more. The more adhesive the better, especially in kids, or else they rip it off. A lot of people are allergic to tegaderm adhesive, but it's what's most often used. Often people are sweaty, adhesive comes off, so more adhesive the better, but not so adhesive that itd rip off fragile skin. Tegaderm is most used, usually reinforce with medical tape, not great solution to keeping things on in sweaty patients.

11. **How would you like to see the information provided by the pulse oximeter?**

    Need SpO_2, pulse waveform, and heart rate. If you can do CO, there is a waveform. Color on monitor is important. Pulse ox is in blue, CO is yellow, heart rate and pulse

are red.

12. **How can patients use pulse oximetry on their own to monitor their health?**

Usually patients with chronic cardiac or respiratory problems which are very common. All babies born premature, with syndromes, any congenital cardiac problem, arrhythmia. Probably at least 1 in every 5,000-10,000 live borns if not more common. And kids with asthma - check pulse ox to decide who gets admitted. Biggest problems when kids are sleeping. Doctors strongly discourage continuous use of pulse ox at home because current pulse ox don't stay on in the perfect location, it's overly sensitive, constant dips, which drives parents crazy. Pulse ox is more important than a thermometer in pediatrics.

13. **How would our technology aid you in your day to day working practices, decision making processes, the added level of information that you would gain when liaising with patients?**

If a parent can tell the doctor the temperature, HR, and SpO_2 from one device over the phone, the doctor can make more informed decisions on whether or not the child needs to be brought in.

It would make placement and continuous measurement of SpO_2 in patients much more user-friendly to have a large area reflectance patch wrapped around the leg.

14. **What are the other technology solutions that are being trialled or considered and what is/are the advantage(s) of our technology if our solution was to work?**

Nothing that she knows of.

15. **Would you recommend our technology to be implemented as a tool for your working practices and explain the reasons why so (or not)?**

Yes. Would recommend buying at-home patches that measure SpO_2, HR, and temperature to all parents.

16. **What (if any), may be the barriers to adoption of this technology from the doctors' point of view? For example including aspects such as the costs of**

the technology, what would be the maximum acceptable pricing for such a product?

Right now pulse ox fits into pre-existing monitors - need to connect to standard monitors. Would be good to wirelessly automatically sync with electronic medical record (EMR) and an app on physician's phone. A Pulse ox that stays on would be great. Don't know the price, what they cost. In healthcare, most physicians have no idea how much things cost.

.6 Dr. Jean-Gabriel Coignet, U.S. Air Force Flight Surgeon, Hurlburt Field, Florida

Interview Summary:

Our reflectance oximeter array would be a vast improvement on current pulse oximetry technology for military trauma surgeons. The flat form factor, ability to be attached to each patient, ability to be attached to different body parts, and multi-pixel redundancy are highly desirable.

1. **How do you currently use pulse oximetry?**

   When not deployed, monitors vital signs, temp, blood press, pulse ox. Healthy population, "more of a formality."

   When deployed, casualty evacuation. No time for blood pressure or EKG, only pulse ox. Use pulse ox on finger - "they suck." Blast injuries, no fingers, no skin, or everything is so dirty/bloody the pulse oximeter falls off. Patients transported in non-pressurized aircraft - need to tell if they're hypoxic during evacuation. Pulse ox is very important, but currently military doctors don't have a reliable sensor.

2. **How do you currently measure tissue oxygenation?**

   In ideal situation, if there are four limbs it's good to check arm vs. leg, a difference between the two could indicate massive internal bleeding. Right now, physician can only feel for a pulse - femoral, petal, on a moving helicopter or check if feet are cold (but could be flying in cold mountains), to determine if there is blood flow in an extremity. "It would be amazing to have something" that would tell him the oxygenation of different parts of the body.

Need one reliable data point for pulse ox in any situation.

3. **What (if any) limitations does a conventional pulse oximeter have in your work?**

   Battery life! Need 72 hrs. Oximeter doesnt stay on - falls off during patient transport or due to sweat, dirt, blood.

4. **If you could perform pulse oximetry anywhere on the body, where would you perform it?**

   Sternum because EKG leads go there if time to apply so it's already going to be exposed. Ear not practical either because patients are often treated in the dark with night vision (hard to see) and it also falls off.

5. **If you could perform pulse oximetry during any procedure, when would you perform it?**

   From the get go, first thing you get from the patient, check often.

6. **How often would you like to perform an oxygenation measurement and over what period of time?**

   It depends. If bad trauma, every minute. If stable patient, every hour or two. Know if patients need a blood infusion - pulse ox is deciding factor. Especially with trend in pulse ox. Pulse ox lags behind blood loss. Once you see it drop, you're already behind the curve. If over 6 hr flight pulse ox drops, there is something slower going on that needs treatment.

7. **How reliable do you consider conventional pulse oximeters?**

   "Not."

8. **If an oximeter consisted of multiple pixels that each gave their own measurement, would you consider the oximeter to be more reliable than a conventional pulse oximeter?**

Yes.

9. **If so, how many pixels would you like?**

12 lead EKG in hospital, 4 lead in the field. Pulse ox is usually one, if you can have 4, why not. 4 sounds good because of local variance in tissue.

10. **Would creating a 2D map of relative tissue oxygenation be beneficial to your work?**

Not in this setting.

11. **Looking at our current reflectance oximeter array prototype, what do you like about it? Do you foresee any limitations of its current design?**

Looks good, no foreseeable limitations. Doctors carry IFAC immediate action trauama kit with pockets to hold gear (27 pockets holding 127 items). Likes that it's a flat tool fits in pack, no tangled wires. "Flat is amazing." Ease of storage, transport, flexibility are important. When currently used pulse oximeters are dropped, the battery pops out. The fewer separate components the sensor has, the better it is. "I love the idea of it being flat."

12. **How would you like to see the information provided by the pulse oximeter?**

Currently use Tiny screen gives heart rate, pulse ox (if it works) like in hospital. There are wires everywhere, easy to get pulled off. If data was on the chest with display on the patch with the heart rate and oxygen saturation that would be ideal. Fewer wires the better. For the display, use colors compatible with night vision: red or green. Red is best, not security risk.

13. **How can patients use pulse oximetry on their own to monitor their health?**

A lot of people get hurt at once, planes and helicopters are loaded up like sardines. It would be great to strap a pulse oximeter it to patient, patient keeps track of their pulse and SpO_2 levels, tells doctor if something changes.

Other Notes:

For attachment to the patient, the pulse oximeter could be stapled in place in trauma situation, tape doesn't work on blood and sweat.

If the sensor costs a dollar, stick on patient, leave it to follow the patient to end of line. Right now each doctor has one pulse oximeter, sometimes kept on a lanyard, and has to move from patient to patient to take a measurement, so there is no continuous monitoring of patients and the pulse oximeter usually falls off.

Right now go through every instrument to set alarm. Would be ideal if they all transmitted data to a single hand-held device for the doctor. But need battery life that for 72 hrs.

Doctors carry 2 backpacks - trauma and gear, sensors are kept in the gear backpack. They need to prep all parts of sensors, so if everything is one package, it's better. Fewer steps to get ready from package to patient taking data, the better.

Air Force trauma surgeons do training exercises monthly with 2 or 3 patients, 5 or 6 providers on different aircraft commonly use non-FDA approved devices.

.7 Dr. Jade Hiramoto, Vascular and Endovascular Surgeon, Associate Professor of Surgery, Division of Vascular and Endovascular Surgery, UCSF Medical Center, San Francisco, California

Research interests: Spinal perfusion after endovascular thoracoabdominal aortic aneurysm repair

Interview Summary:

We have a potential partner for a clinical study of the reflectance oximetry array using the current array geometry. It would need to take continuous measurements during surgery for 6-7 hours, and ideally would take intermittent measurements for up to 3 days after surgery. While we wouldn't have to edit the array geometry, we would need to find a way to make it softer when it is applied to a patient's skin.

The detailed information on this potential partnership is as follows:

Dr. Jade Hiramoto, a vascular surgeon and surgery professor at UCSF. She is interested in using our reflectance oximetry array to map tissue oxygenation on a patient's back, over the psoas muscle, during multibranched thoracoabdominal stent-graft aneurysm repairs. The surgery, while successfully treating an aortic aneurysm, has a 10-20% chance of leaving the patient paralyzed from the waist down. UCSF is one of the few hospitals in the country to

perform the procedure endoscopically, which reduces the risk of paraplegia to 5-10%, but the surgeons still don't know why some patients are paralyzed by the procedure. Dr. Hiramoto would like to use our oximetry array to monitor tissue oxidation near the spine, to see if there are any changes during the procedure to indicate an increasing risk of paralysis.

She would like the sensor to look like the current array, and would maybe like to use two at a time to look at a larger area on the back, so we don't need to make changes to the current mask design. A ribbon cable connection like the one on the reflectance pulse oximetry single pixel sensors CDT made is an acceptable connector for the devices during this procedure. The one thing that Dr. Hiramoto said we would need to change is that we need to make the sensor softer; that in it's current state it could cause a pressure ulcer while the patient is lying on it in surgery. I showed her a sensor coated in a Kapton adhesive, and she said that was better, but it still needs to be softer, and we need to be able to prove to the doctors that there is no risk of causing a pressure ulcer before they would use it in a study. I tried to find out how "soft enough" could be quantified, and Duoderm was recommended as a comparison. If we could attach a thin but soft hydrocolloid dressing between the sensor and the patient without disrupting the optical signal, then Dr. Hiramoto will invite us before her research group to demonstrate the oximetry array. If enough of the group approves of its use, they will be able to test it in patients.

Dr. Hiramoto's group already has an IDE and IRB in place with UCSF and FDA approval to perform experimental procedures during the endoscopic multibranched thoracoabdominal stent-graft surgery, which would cover the study of the oximetry array in surgery. So the main approval that we would need for the study is from Dr. Hiramoto's colleagues.

I also asked Dr. Hiramoto about the potential of using the oximetry array to monitor perfusion in diabetic patients' feet, but she said that their skin can be so sensitive that applying a sensor with any sort of adhesive to it could cause damage. She said maybe the sensor could be attached with ultrasonic gel, but in general she didn't consider it a strong application of the device.

.8 Dr. Jackie Wong, OBGYN, Northwestern University Medical Center, Chicago, Illinois

Interview Summary:

In a clinical setting, a tissue oxygenation array applied to internal organs and tissue during obstetric or gynecological surgery would help physicians evaluate perfusion. There is no quantitative measurement for internal perfusion, just a qualitative judgement by the physician based on the tissues physical appearance. In a mobile setting, pregnant women whose doctors deem their oxygen physiology at risk could use a single pixel oximeter patch to monitor their oxygen saturation level. If it consistently stands below 94%, they would be instructed to call their physician.

1. **How do you currently use pulse oximetry?**

   For vital signs monitoring continuously while patients in surgery, intermittently on floor, continuous in ICU.

2. **How do you currently measure tissue oxygenation?**

   Not quantitively. Sometimes look at narcrotic vs. healthy. Any gynocologic tissue, internal organs.

3. **What (if any) limitations does a conventional pulse oximeter have in your work?**

   Nail polish - gel nail polish, thick, can't enough signal through. Patients take it off a lot, people use their hands a lot, it annoys patients. It's usually on fingers, sometimes toes. The finger is the most annoying place to put something that measures vital signs.

4. **If you could perform pulse oximetry anywhere on the body, where would you perform it?**

   The chest - somewhere out of the way, where obesity won't matter.

5. **How reliable do you consider conventional pulse oximeters?**

   Pretty reliable. Sometimes you see how reliable the measurement/waveform is on the machine, with number of stars, telling you how clear the waveform is.

6. **How would you like to see the information provided by the pulse oximeter?**

   As small and accurate as possible.

7. **How can patients use pulse oximetry on their own to monitor their health?**

   In pregnancy, physiological changes, shortness of breath, oxygen physiology changes. Would be good to know if women are shorter breath at home, if SpO_2 is over 94%,

theyre ok, but if lower, they should come in to hospital. Almost everyone gets it during pregnancy.

8. **What type of approval process(es) would need to be gained before such a technology could be used (assuming that of all the technical targets/goals would be met).**

Gold standard and then your implementation. Every patient would need to routinely take pulse ox. Our device vs. gold standard. IRB approval. Copy something already approved and change to our style. For patient population need a big enough number of patients for the outcome I'm looking at accuracy of pulse ox in relation to standard pulse ox. Power estimate less than 5% chance of error given sample size tells you how many patients to enroll in order to have effective outcome. Make everything as binary as possible. Need baseline patient demographics - age, gender, race/ethnicity, circle boxes, not square, is a not easier to code things by number.

Other notes:

Want to measure all hemoglobin species. Methemoglobanemia is showing false adequate oxygenation, met hemoglobin cant carry oxygen, but it will show up on pulse ox but you cant tell the difference. It's very rare, usually when patients have oxidative stress from chemical, medication exposure.

.9 Dr. Eric Dong, anesthesiologist, Baylor Scott and White Memorial Medical Center, Austin, Texas

Interview Summary:

We shouldn't try to replace the currently available pulse oximeters that are working fine/well enough for generally "healthy" patients in the average American hospital setting. Its the "unhealthy" patients in non-standard settings where conventional pulse oximeters don't work well that our technology will best fit. Anesthesiologists want a sensor that can measure pulse ox more than oxygenation and pulse - CO, hemoglobin concentration, and cardiac output - there isn't a simple way to do this yet.

1. **How do you currently use pulse oximetry?**

Number 1 sign of oxygenation in blood, by proxy in the lung. Need to know all the time because most of the time you are impairing the patient's ability to breathe somewhat or completely.

Secondarily, determine rhythm. EKG is electrical and there is way more electrical than optical interference.

2. **How do you currently measure tissue oxygenation?**

Expect suboptimal tissue perfusion in skin graft, pressure ulcer. So you might not use oxygenation as a marker. In terms of perfusion, use a combination of things - blood pressure, pulse ox, partial pressure O_2 in arteries, ECG all together. As an anesthesiologist, don't care about tissue as much as vital organ perfusion. Sometimes more invasively measure cardiac output with a gas analyzer outside body.

3. **What (if any) limitations does a conventional pulse oximeter have in your work?**

MRI. Number one. Electronics to make it MRI proof distort the waveform a lot. Specialized pulse ox for MRI is wireless, the MRI interferes with the signal. Pulse ox is most valuable single monitor and it's not reliable in the MRI - 2 to 3 minutes away from accessing patient. InVivo supplies MRI compatible things, but you can't halfway get rid of artifacts from RF jamming.

4. **If you could perform pulse oximetry anywhere on the body, where would you perform it?**

Fingertips, ear, in the nose/nostril, lip, tongue - thin enough to fit device. If it was in breathing tube? - "Why would you?" Just adding more foreign material into the body when already there is a reliable, cheap, noninvasive way to do it outside the body. Would be getting the same numbers.

5. **If you could perform pulse oximetry during any procedure, when would you perform it?**

During every surgical procedure.

6. **How often would you like to perform an oxygenation measurement and over what period of time?**

Continuous pulse oximetry in surgery. Sometimes there is a difference between what the doctors think and what is, so they get direct measurement with arterial blood - not commonly, but sometimes, do it intermittently.

7. **How reliable do you consider conventional pulse oximeters?**

Only accurate down to 70%. When things get to 85-90% it doesn't matter, it's just the trend, they don't reach the point where it becomes physically unreliable. We prevent that from getting that low. 91-92% get nervous, start to fix it.

8. **If an oximeter consisted of multiple pixels that each gave their own measurement, would you consider the oximeter to be more reliable than a conventional pulse oximeter?**

Not necessarily useful to have multiple channels because all data is based off of blood flow to places as close together as pixels. There is no physiologic difference in the flow that close. But if signal is poor in one pixel, you can integrate all pixels. Multi-channel pulse oximetry would be helpful because there are instances where we fidget with pulse oximeter and it still doesn't get a good signal.

9. **Would creating a 2D map of relative tissue oxygenation be beneficial to your work?**

No.

10. **Looking at our current reflectance oximeter array prototype, what do you like about it? Do you foresee any limitations of its current design?**

The size it is is probably useful for measuring differentials in oxygenation across a skin graft because it's roughly the size of critical skin graft size. Right now one of the most dicey grafts is wrist, leg, or thigh tissue formed into a tongue. If you can put perfusion monitor on tongue, right now what they do if put conventional pulse ox on tongue - one channel, one point. If you can get a picture, great. Measure differences in channel detection. In a normal healthy person, multi-channel doesn't add very much, most

healthy people dont have a difference. More value is to find people with a stake in knowing this data. Want to know tissue is losing perfusion somewhere, where. Plastics for skin graft/ulcer, anyone who deals with expected changes in organ perfusion.

anesthesiologist care about entire organ system, dont need differential.

Co-oximetry - want to know O_2 in presence of CO, abnormal hemoglobin, hemoglobin concentration. Currently use different devices but all optical. If that is all one one sensor, you have a winner. If one thing generates CO, O_2, and hemoglobin concentration are important in everyday use, healthier patients.

11. **How would you like to see the information provided by the pulse oximeter?**

On standard monitors.

12. **How can patients use pulse oximetry on their own to monitor their health?**

Multi-channel integration should be an improvement over current things patient's buy for $20 on Amazon. People with high blood pressure or diabetes, measure blood pressure and blood sugar at home because there's something to do about it, but if youre low on oxygen, you dont need a number to tell you, there's only one solution which is to breathe more. Every relatively severe lung disease is progressive, even if you know your oxygen is low, people live at low O2 slowly over time the pulse ox goes down. The sliding to the number that feels low slides lower. Dont measure pulse ox for how bad the lung disease is, measure how much extra oxygen they're carrying around.

Other Notes:

Multi-channel integration "blows my mind," thought it already was that way.

Make the patch smaller. If it's big, it's liable to be messed around, ripped off. Closer to the size of the penny. But for integrating multiple measurements as a new device, any size.

Hot thing: Look into optical hemoglobin measurement/extrapolation. Gold: Even more fledgling - if you can deduce velocity in blood flow over time, if you integrate velocity you get displacement, displacement is cardiac output - that is gold. The difference between invasive and non-invasive is so large. To measure it continuously right now, is very invasive. Can calculate with repeated measurements at single time points requires chemistry, not instantaneous measurement.

.10   Dr. Ben Kester, Orthopedic Surgeon, Columbia University Medical Center, New York, New York

Interview Summary:

Orthopedic surgeons are concerned with whether or not injured/repaired limbs are receiving adequate blood flow. For example, if a patient had reconstructive hand surgery, physicians will use hand-held doppler ultrasound device to listen to blood flow in each finger. There is a different sound for venous and arterial blood flow that the physicians listen to and qualitatively compare the strength of. Clinicians will perform this test every 1-2 hours for up to 14 days. A visual map of oxygenation would be useful to replace doppler sonography, which is subject to user error. Before a reflectance oximetry array would be used by physicians, the relationship between mapped oxygenation and prognosis would need to be thoroughly studied and understood.

1. **How do you currently use pulse oximetry?**

   Use pulse ox to monitor global SpO_2.

2. **How do you currently measure tissue oxygenation?**

   Looking at visual perfusion - hand-held doppler signal ultrasound on each finger to look for perfusion. Listen for arterial vs. venous signal in signal. Look for arterial pump in finger. Listen to sound of artery/vein.

3. **How often would you like to perform an oxygenation measurement and over what period of time?**

   Once every hour/ 2 hrs do doppler. Monitor over days, up to 14 days.

4. **How reliable do you consider conventional pulse oximeters?**

   Very.

5. **Would creating a 2D map of relative tissue oxygenation be beneficial to your work?**

A 2D map of tissue oxygenation would be useful. Never thought of it before. What is correlation between tissue perfusion and arterial perfusion? How does this data correlate to survival of extremity.

6. **If so, where on the body would you take the measurement, over how much area, and with what resolution?**

   On hands and fingers. Not sure about the resolution. Would need to know the correlation between tissue perfusion and arterial perfusion, and how this data correlates to survival of extremity.

7. **How would you like to see the information provided by the pulse oximeter?**

   Would like an alarm when lack of perfusion is sensed.

8. **How would our technology aid you in your day to day working practices, decision making processes, the added level of information that you would gain when liaising with patients?**

   Need to know more about it - how data given by tissue O_2 map correlates to the patient's actual status.

9. **What are the other technology solutions that are being trialled or considered and what is/are the advantage(s) of our technology if our solution was to work?**

   Doppler ultrasound sonography is currently used to check for perfusion in extremities. The physician listens for the sound of blood pumping. The current advantage is that ultrasound sonography has proven accuracy for sensing the presence of adequate perfusion. The drawbacks of ultrasound sonography include:

   There is a learning curve for its accurate use.

   Different devices work different, if doctors move around hospitals they have to figure out how to use each new device.

   Most hospitals only have one or two in supply, so it can take time finding it.

   If perfusion is questionable, it can be hard to pick up the signal. For example, a finger can be perfused but the doctor has a hard time hearing the blood flow.

It doesn't say how well perfused the tissue is.

Advantages of our technology include availability, disposability, and ease of use.

10. **Would you recommend our technology to be implemented as a tool for your working practices and explain the reasons why so (or not)?**

    It needs to be tested, with clear lines drawn between the data collected by our device and actual perfusion and patient outcomes. And it needs to be a lot better than the ultrasound sonography currently in use.

11. **What (if any), may be the barriers to adoption of this technology from the doctors' point of view? For example including aspects such as the costs of the technology, what would be the maximum acceptable pricing for such a product?**

    Doctors want to use the nearest, proven, most convenient and easy to use device. Many doctors work in four different hospitals, so if a new device isn't completely groundbreaking, doctors wont fight to make it available in hospital.